Natural Resources Canada | Ressources naturelles Canada

GEOLOGICAL SURVEY OF CANADA
OPEN FILE 9248e

ID-TIMS and SHRIMP U-Pb geochronology of volcanic, sedimentary, and intrusive rocks from the Chibougamau, Val-d'Or, Malartic, Amos, and Rouyn-Noranda areas, Abitibi greenstone belt, Quebec

P. Mercier-Langevin, N. Wodicka, V. McNicoll, J. Goutier, P. Pilote, F. Leclerc, and B. Dubé

2025

Canada

GEOLOGICAL SURVEY OF CANADA
OPEN FILE 9248e

ID-TIMS and SHRIMP U-Pb geochronology of volcanic, sedimentary, and intrusive rocks from the Chibougamau, Val-d'Or, Malartic, Amos, and Rouyn-Noranda areas, Abitibi greenstone belt, Quebec

P. Mercier-Langevin[1,2], N. Wodicka[3], V. McNicoll[3]*, J. Goutier[4]*, P. Pilote[5]*, F. Leclerc[6], and B. Dubé[1]*

[1]Natural Resources Canada, Geological Survey of Canada, 490, rue de la Couronne, Québec, Quebec G1K 9A9
[2]Current address: Agnico Eagle Mines Ltd., 145 King Street East, Toronto, Ontario M5C 2Y7
[3]Natural Resources Canada, Geological Survey of Canada, 601 Booth Street, Ottawa, Ontario K1A 0E8
[4]Ministère des Ressources naturelles et des Forêts, 70, avenue Québec, Rouyn-Noranda, Quebec J9X 6R1
[5]Ministère des Ressources naturelles et des Forêts, 201, avenue du Président-Kennedy, Montréal, Quebec H2X 3Y7
[6]Ministère des Ressources naturelles et des Forêts, 5700, 4[e] Avenue Ouest, Québec, Quebec G1H 6R1
*Retired

2025

© His Majesty the King in Right of Canada, as represented by the Minister of Natural Resources, 2025

Information contained in this publication or product may be reproduced, in part or in whole, and by any means, for personal or public non-commercial purposes, without charge or further permission, unless otherwise specified.
You are asked to:
- exercise due diligence in ensuring the accuracy of the materials reproduced;
- indicate the complete title of the materials reproduced, and the name of the author organization; and
- indicate that the reproduction is a copy of an official work that is published by Natural Resources Canada (NRCan) and that the reproduction has not been produced in affiliation with, or with the endorsement of, NRCan.

Commercial reproduction and distribution is prohibited except with written permission from NRCan. For more information, contact NRCan at nrcan.copyrightdroitdauteur.rncan@canada.ca.

Recommended citation
Mercier-Langevin, P., Wodicka, N., McNicoll, V., Goutier, J., Pilote, P., Leclerc, F., and Dubé, B., 2025. ID-TIMS and SHRIMP U-Pb geochronology of volcanic, sedimentary, and intrusive rocks from the Chibougamau, Val-d'Or, Malartic, Amos, and Rouyn-Noranda areas, Abitibi greenstone belt, Quebec; Geological Survey of Canada, Open File 9248e, 1 .zip file. https://doi.org/10.4095/p4g25xxmz0

Publications in this series have not been edited; they are released as submitted by the author.

ISSN 2816-7155
ISBN 978-0-660-77031-4
Catalogue No. M183-2/9248E-PDF
https://doi.org/10.4095/p4g25xxmz0

ID-TIMS and SHRIMP U-Pb geochronology of volcanic, sedimentary, and intrusive rocks from the Chibougamau, Val-d'Or, Malartic, Amos, and Rouyn-Noranda areas, Abitibi greenstone belt, Quebec

Patrick Mercier-Langevin[1,2], Natasha Wodicka[3], Vicki McNicoll[3]*, Jean Goutier[4]*, Pierre Pilote[5]*, François Leclerc[6], and Benoît Dubé[1]*

[1] Natural Resources Canada, Geological Survey of Canada, 490 rue de la Couronne, Québec, Québec G1K 9A9
[2] Current address: Agnico Eagle Mines Ltd., 145 King Street E., Toronto, Ontario, M5C 2Y7
[3] Natural Resources Canada, Geological Survey of Canada, 601 Booth Street, Ottawa, Ontario K1A 0E8
4 Ministère des Ressources naturelles et des Forêts, 70 avenue Québec, Rouyn-Noranda, QC J9X 6R1
5 Ministère des Ressources naturelles et des Forêts, 201 avenue du Président-Kennedy, Montréal, QC H2X 3Y7
[6] Ministère des Ressources naturelles et des Forêts, 5700, 4e Avenue Ouest, Québec, Québec G1H 6R1
*retired

ABSTRACT

The Abitibi greenstone belt is exceptionally well endowed in precious, base, and critical metals. It, however, has a complex geological and metallogenic history. Rocks are generally well preserved but local major deformation complicates the understanding of the belt's evolution and metallogenesis. Ore deposits were formed at different, and in most cases, specific times in the belt's evolution, and knowing the age of these deposits is essential in linking ore genesis with key controlling geological factors. Precise geochronology and relative timing relationships are thus key in deciphering the belt's evolution.

This report presents U-Pb geochronological results from isotope dilution-thermal ionization mass spectrometry (ID-TIMS) and sensitive high-resolution ion microprobe (SHRIMP) dating of zircon, titanite, and/or baddeleyite from volcanic, sedimentary, and intrusive rocks from major mining areas (Chibougamau, Val-d'Or, Malartic, Amos, and Rouyn-Noranda) in the Abitibi greenstone belt. The ages (n=21) document the evolution of the Abitibi greenstone belt through time and constrain the timing of ore-forming events within the Abitibi.

In the Chibougamau area, samples from the Blondeau and Stella formations gave ages of <2721 ± 3 Ma and <2704 ± 2 Ma, respectively, whereas an intermineral dyke yielded an age of 2715.2 ± 0.7 Ma, helping further constrain the volcanic and sedimentary evolution, timing and duration of magmatism, and timing of mineralization in Chibougamau. A leucotonalite south of Chibougamau yielded an age of 2701 ± 0.7 Ma, similar to other intrusive bodies in the region, indicating that magmatism in the area spans a significant period of time. A series of samples from the Dubuisson, Lanaudière and Deguisier volcanic and volcaniclastic units forming part of the stratigraphy in the Val-d'Or-Malartic-Amos area gave ages of 2708.0 ± 1.5 Ma, ~2705 ± 3 Ma, 2716.2 ± 0.8 Ma, 2718.5 ± 1.1 Ma, 2719.0 ± 1.0 Ma, and 2719.4 ± 1.0 Ma. The La Pause Pluton, situated in the

same area, is dated at 2709.8 ± 1.0 Ma, coeval with the Dubuisson Formation. Titanite at 2656.4 ± 9.3 Ma in the La Pause Pluton probably represent the age of metamorphism. A 2718.5 ± 0.8 Ma tonalitic dyke that cuts mafic volcanic rocks considered to be part of the ~2708-2705 Ma Dubuisson Formation suggests that the volcanic rocks of this area may be older than expected, implying further structural complexities (tectonic imbrications and or juxtapositions) in the region. The Caste Formation conglomerate gave an age of <2697 ± 3 Ma. These ages help to better constrain the evolution of this complex area. Five samples from mafic to intermediate intrusive units in the Rouyn-Noranda area (Blake River Group), and one sample from a rhyolite intercalated with the tuff units of the Stadacona member in the southern part of the town of Rouyn-Noranda yielded ages varying between ~2700.2 ± 0.9 Ma and 2695.0 ± 1.0 Ma, helping refine the magmatic evolution in the Blake River. Finally, a detrital zircon age (<2672 ± 2 Ma) from a conglomerate south of the Doyon-Bousquet-LaRonde camp helped identify a new occurrence of Timiskaming rocks.

INTRODUCTION

The Abitibi greenstone belt, extending from northeastern Ontario to northwestern Québec (Fig. 1), is the largest and one the best-preserved belt of Neoarchean supracrustal rocks on the planet. It is also one of the richest in terms of base and precious metals.

As most major greenstone belts, the Abitibi belt has a complex geological history and comprises several sequences of volcanic and sedimentary rocks, which are generally oriented east-west, folded, and intersected by several faults and intrusive bodies (Fig. 1). The primary characteristics of these rocks are generally well preserved despite the deformation and the low to moderate metamorphism affecting the entire belt (e.g., Dimroth et al., 1982, 1983; Daigneault et al., 2002; Goutier et al., 2010; Monecke et al., 2017b and references therein). Significant east-west, northeast-southwest, and northwest-southeast corridors of ductile to brittle faults intersect the rocks of the belt and complicate the understanding of the belt's evolution and reconstruction. During this complex and protracted geological history, an exceptional wealth of mineral resources was created and is expressed through the large diversity of styles of deposits found in the Abitibi (e.g., Card and Poulsen, 1998; Dubé and Mercier-Langevin, 2020; Mercier-Langevin et al., 2022, 2023 and references therein). These deposits formed at specific times in the belt's evolution and knowing the exact timing of these deposits is essential in linking ore genesis with key controlling geological factors, a key ingredient of efficient exploration guides.

Thus, precise geochronology and relative timing relationships is required to decipher the belt's geology and evolution. In the last few decades access to geochronological data has become a key component in mapping, research, and exploration programs, by providing key constraints and anchor points in the belt's geological and metallogenic history.

The objective of this report is to present and very briefly discuss critical ages that help constrain the geological evolution of the Abitibi greenstone belt, including the timing of several ore deposits within the belt. The U-Pb ages presented here were never formally published, therefore precise information about the samples, including their location, composition, and complete analytical data are provided in this report. Unsuccessful attempts at dating key units through the TGI-3 Abitibi

and Plan Cuivre projects are also reported. Specifically, this report presents U-Pb geochronological results from isotope dilution-thermal ionization mass spectrometry (ID-TIMS) and sensitive high-resolution ion microprobe (SHRIMP) dating of zircon, titanite, and/or baddeleyite from volcanic, sedimentary, and intrusive rocks of the Abitibi greenstone belt. These samples comprise material from the Chibougamau, Val-d'Or, Malartic, Amos, and Rouyn-Noranda areas (Figs. 1 and 2). The U-Pb ages reported here were, except for one sample (KQ-91-7, sampled in 1991), obtained between 2006 and 2010 through the joint Targeted Geoscience Initiative (TGI) Abitibi (TGI-3: 2005-2010) and Plan Cuivre (2006-2010) projects of the Geological Survey of Canada (GSC), the Ministère des Ressources naturelles et de la Faune (MRNF, now Ministère des Ressources naturelles et des Forêts), and the Ontario Geological Survey (OGS). This work was done in collaboration with industry and academia through several projects and studies that are now completed.

ANALYTICAL METHODS

U-Pb geochronology was conducted at the Geochronology Laboratories at the Geological Survey of Canada (Ottawa, Ontario). Heavy minerals were concentrated from plutonic, volcanic, and detrital samples using standard crushing, grinding, and separation on a Wilfley™ table and by heavy liquid techniques. Mineral separates were sorted by magnetic susceptibility using a Frantz™ isodynamic separator and hand-picked using a binocular microscope.

ID-TIMS U-Pb zircon geochronology analytical methods

High-precision U-Pb dating of zircon and baddeleyite was carried out by ID-TIMS using analytical methods modified after Parrish et al. (1987), including addition of an in-house ^{205}Pb-^{233}U-^{235}U spike, dissolution, column chemistry, and analysis on a Triton thermal ionization mass spectrometer for all samples except for sample KQ-91-7, which was analyzed on a Finnigan-MAT 261 mass spectrometer. Analytical methods for ID-TIMS U-Pb analyses of titanite are summarized in Davis et al. (1997). Titanite and baddeleyite were not abraded, however zircon fractions were either air abraded (Krogh, 1982) or chemically abraded following the techniques of Mattinson (2005) prior to dissolution. Chemically abraded grains were annealed for 48 h at 1000°C then leached with HF at 180°C for varying lengths of time. The isotopic ratios were corrected for the presence of initial common Pb above the laboratory blank using the Pb composition predicted by the model of Cumming and Richards (1975) using the age of the sample. Data reduction and error propagation follow methods outlined in Roddick (1987). Interpreted age summaries for all samples are given in Table 1. U-Pb ID-TIMS analytical results are presented in Electronic Table 2 with uncertainties reported at the 2σ level. Details of zircon, titanite, and baddeleyite morphology, quality, and physical or chemical abrasion times, where applicable, are also summarized in Electronic Table 2.

SHRIMP U-Pb zircon geochronology analytical methods

Four detrital samples (OVB-1, OVB-3, KI-07-09, and LAPL-2008-011) and one felsic volcanic rocks sample (PBA06-385A) dated using the ID-TIMS method were also analyzed on a SHRIMP II (Sensitive High Resolution Ion Microprobe) instrument. SHRIMP analytical procedures

followed those described by Stern (1997), with reference materials and U–Pb calibration methods following Stern and Amelin (2003). Zircon were cast in three separate, 2.5 cm diameter epoxy mounts (IP433 for PBA06-385A; IP511 for OVB-1 and OVB-3; IP530 for KI-07-09 and LAPL-2008-011), together with reference materials. Zircon z6266 was used as the primary reference material ($^{206}Pb/^{238}U$ age = 559 Ma; Stern and Amelin, 2003) and zircon z1242 as the secondary reference material for mounts IP511 and 530 only ($^{207}Pb/^{206}Pb$ age = 2679.7 Ma; Davis et al., 2019). Both reference materials were analysed under the same conditions as the unknowns. The midsections of the zircon grains were exposed via polishing using 9, 6, and 1 μm diamond compound, and the internal features (such as zoning, structures, alteration, etc.) were characterized with backscattered electrons utilizing a Cambridge Instruments scanning electron microscope. The zircon images annotated with the SHRIMP spot location are included in this Open File report as separate pdf files (Electronic Appendices A−E). Mount surfaces were evaporatively coated with 10 nm of high purity Au. Analyses were conducted using an $^{16}O^-$ primary beam, projected onto the zircon at 10 kV. The count rates of ten isotopes of Zr^+, U^+, Th^+, and Pb^+ in zircon were sequentially measured over six (IP433 and IP511) or five (IP530) scans with a single electron multiplier and a pulse counting system with a deadtime of 23 ns (IP433), 24 ns (IP511), or 8 ns (IP530). Offline data processing was accomplished using customized in-house software for IP433 and SQUID2 (v. 2.22.08.04.30, rev. 30 Apr 2008; Ludwig, 2009) for IP511 and 530. The 1σ external errors of $^{206}Pb/^{238}U$ reported in the data table (Electronic Table 3) incorporate the error in calibrating the primary zircon reference material (see Stern and Amelin, 2003). Analyses of the secondary reference material z1242 were interspersed between the sample analyses to monitor accuracy of the measured $^{207}Pb/^{206}Pb$ ratios and correct for any instrumental mass bias. Intra-element mass fractionation corrections of 1.003 and 1.006 were applied to all samples on mounts IP511 (session 2 only) and IP530, respectively. The Pb composition of the surface blank was used to correct for ^{204}Pb following the methods of Stern (1997). Errors reported in Electronic Table 3 are given at the 1σ confidence interval. Further details of analytical conditions for all four samples are provided in the footnotes to this electronic table.

For both ID-TIMS and SHRIMP results, age calculations were done using a present-day $^{238}U/^{235}U$ ratio of 137.88 as recommended by Steiger and Jäger (1977) and decay constants of 1.55125×10^{-10} yr^{-1} and 9.8485×10^{-10} yr^{-1} for ^{238}U and ^{235}U, respectively, from Jaffey et al. (1971). The program ISOPLOT v. 4.15 (Ludwig, 2012) was used to generate concordia plots and derive ages. Probability density distribution plots were calculated using AGEDISPLAY (Sircombe, 2004). With the exception of the detrital samples, ages calculated are based on either a weighted average of $^{207}Pb/^{206}Pb$ dates or regressions using a modified version of York (1969) to calculate upper and lower concordia intercept ages. The error ellipses on the concordia diagrams and all age uncertainties reported in the text are at the 95% confidence level. The concordia curve in all ID-TIMS plots is shown as a band incorporating uncertainties in the ^{235}U and ^{238}U decay constants.

SAMPLE DESCRIPTIONS AND RESULTS

Twenty-one samples were selected to document the evolution of the Abitibi greenstone belt and provide further constraints on the timing of ore-forming events within the greenstone belt. The dated samples come from the Chibougamau, Amos, and Rouyn-Noranda general areas (Figs. 2−5).

Descriptions for each sample are given below, followed by a description of the dated minerals and interpreted ages, and a brief discussion of the results and their implication.

Chibougamau area

The Chibougamau area represents one of the major mining camps of the Abitibi greenstone belt with numerous styles of syngenetic and epigenetic deposits (Guha et al., 1988, 1990; Pilote and Guha, 1995; Leclerc et al., 2012 and references therein), including volcanogenic massive sulphide deposits (e.g., Lemoine: Mercier-Langevin et al., 2014b), synmagmatic Fe-Ti-V deposits (Allard, 2002), magmatic Ni-Cu prospects (Leclerc et al., 2012), synmagmatic "epithermal" polymetallic vein systems (e.g., Lac Berrigan: Pilote, 1987, and Brosman: Côté-Mantha et al., 2012, and Lac Berrigan: Pilote, 1987), Chibougamau-type Cu-Au sulphide vein systems and porphyry-type Cu-Mo deposits (e.g., Main mine, Copper Rand: Pilote et al., 1996; Magnan et al., 1998, and Lac Clark: Sinclair et al., 1994; Leclerc et al., 2012), and orogenic gold deposits (e.g., Norbeau: Dubé et al., 1989, Cooke: Dubé and Guha, 1992, and Joe Mann: Dion and Maltais, 1998). Four dated samples included in this report are from the Chibougamau area (Figs. 2, 3) and help further constrain its geological and metallogenic evolution.

Sample 06-PR-246-A (Leucotonalite, Baie Queylus; z9418) is from a quartz-phyric trondhjemite (or leucotonalite; 68.9 wt.% SiO_2, 15.4 wt.% Al_2O_3, 80 ppm Zr: Electronic Table 4) intrusive rock sampled southwest of Lac Doré near Chibougamau, on an outcrop a few hundred metres west of Highway 167 (Figs. 3, 6A). The sampled intrusive unit has up to 10 vol.% quartz phenocrysts up to 6-7 mm in size, with minor biotite, muscovite, epidote, carbonate, and apatite in a fine-grained quartz-feldspathic matrix (Fig. 7A).

This sample of leucotonalite contains abundant high-quality zircon including pale brown, euhedral, subequant grains and stubby to elongate prismatic crystals (aspect ratios of 2:1 to 5:1) (Fig. 7B). Seven single grains were analyzed and range from 3.5 to -0.4% discordant (Electronic Table 2; Fig. 7C). A linear regression including all 7 analyses has an upper intercept of 2701.7 ± 0.7 Ma and a lower intercept of 450 ± 83 Ma (MSWD = 0.58, probability of fit = 71%). The 2701.7 ± 0.7 Ma age (first reported in McNicoll et al., 2008) is interpreted as the crystallization age of the leucotonalite (Table 1).

At 2701.7 ± 0.7 Ma, the leucotonalite is approximately 13 million years younger than the main dioritic and tonalitic phases of the Chibougamau Pluton, which were emplaced between 2718 ± 2 Ma and 2714 +3/-2 Ma (Krogh, 1982; Pilote, 1995; Pilote et al., 1997; Joanisse, 1998). The significant time gap between the emplacement of the early phases of the Chibougamau Pluton and the crystallization age of the leucotonalite in the Baie Queylus area indicates either very long-lived magmatic activity centered on the Chibougamau pluton, or, alternatively and more plausibly, a series of magmatic events in the Chibougamau region as suggested by nearby intrusions having similar ages to the leucotonalite. For example, the Muscocho Pluton, a foliated granodioritic intrusion about 15 kilometres southeast of the Baie Queylus area is dated at 2701.2 +1.7/-1.3 Ma (Mortensen, 1993a). Other intrusive rocks associated with the Chibougamau Pluton that were dated in the region include syn-mineralization dykes (e.g., 2715.2 ± 0.7 Ma: Pilote et al., 1997, 2006), 2705.1 +1.7/-1.2 Ma dykes (David et al., 2011), and the Line Lake satellite intrusion

(2707.6 ± 1.4.Ma: Côté-Mantha et al., 2012), which suggest distinct magmatic pulses possibly associated with the first episodes of deformation (local D_1 and early D_2: Daigneault et al., 2004).

Sample OVB-1 (Blondeau Formation, sandstone; z9678) is from a feldspathic to quartzitic sandstone that forms part of the Blondeau Formation northeast of the town of Chibougamau along Highway 167 (Figs. 3, 6B), on the northern flank of the Chibougamau syncline. The Blondeau Formation consists of volcanic-derived metasedimentary rocks, felsic volcaniclastic rocks, and minor rhyolite and basalt. This forms one of the youngest units of the Roy Group and represents the volcanic construction in the northeastern part of the Abitibi belt (Leclerc et al., 2012 and references therein). The sampled sandstone is part of a fining-upward, southward younging sequence including siltstone and mudstone (Fig. 8A) that locally contains pyrite. The sandstone is probably hydrothermally altered with 4.85 wt.% loss-on-ignition and 6 wt.% CaO, suggesting the presence of secondary carbonate (Electronic Table 4).

The ID-TIMS and SHRIMP ages reported here for samples OVB-1 and OVB-3 were presented in Leclerc et al. (2012), however, the electronic appendices that originally accompanied that paper are no longer available, explaining why the data are presented herein. Although the original data were verified and calculations remade for this report, the following is largely taken from Leclerc et al. (2012). The detrital zircon population from this sandstone consists of light brown stubby prisms that are characteristic of an igneous origin (Figs. 8B, 9A). Few grains show evidence of rounding by mechanical abrasion, suggesting a proximal source. A cluster of five single grain ID-TIMS analyses (A1, B2, B3, B4, and B5) are concordant to 0.7% discordant (Fig. 8C; Electronic Table 2). A maximum age of deposition of 2721 ± 3 Ma (Table 1) is based on the $^{207}Pb/^{206}Pb$ date of concordant analysis (B4), which is consistent with a 2717 ± 1 Ma minimum age determined on zircon from a crosscutting quartz-bearing ferrodiorite sill of the Cummings Complex (Mortensen, 1993a). Analysis B1 yields a significantly younger $^{207}Pb/^{206}Pb$ date of 2711.4 ± 1.9 Ma. However, this analysis corresponds to a tabular grain with simple pyramids and sharp edges that is atypical of the general population.

Seventy SHRIMP $^{207}Pb/^{206}Pb$ dates from sample OVB-1 of the Blondeau Formation are clustered with an age range from 2737 ± 14 to 2687 ± 26 Ma (Fig. 9B, inset; Electronic Table 3). A probability density distribution plot shows a single population with a peak at 2712 Ma. This age peak coincides, within uncertainty, with the 2717 ± 1 Ma age for the Bourbeau sill, which is the uppermost part of the Cummings Complex that intrudes the Blondeau Formation. It also coincides with the 2712 +9/-7 Ma age for a quartz and feldspar porphyritic sill intruding the Bruneau Formation (Mortensen, 1993a) and thus strengthens the idea previously based on field observations that such sills may represent feeders to the overlying Blondeau Formation effusive volcanic rocks (Bélanger, 1979). The data indicate a single zircon population, derived from proximal igneous sources, indistinguishable in age from the time of deposition. The age distribution is consistent with igneous zircon morphology and general absence of rounding.

In addition to the comments made in Leclerc et al. (2012), the age of the Blondeau Formation is now further constrained by an age of 2724.4 ± 1.2 Ma for a lapilli tuff from the underlying Bruneau Formation (Davis et al., 2014) and an age of 2716.4 ± 1.0 Ma for a lapilli tuff in the overlying Scorpion Formation in the Chapais area (David et al., 2012).

Sample OVB-3 (Stella Formation, conglomerate; z9679) is from a clast- to matrix-supported polygenic conglomerate unit that forms part of the Stella Formation southwest of the town of Chibougamau, south of Highway 113 a few kilometres east of the town of Chapais (Figs. 3, 10A). The Stella Formation consists of conglomerate, sandstone, and argillite. It is part of the sedimentary-dominated Opémisca Group that overlies the volcanic-dominated Roy Group (Daigneault and Allard, 1990; Leclerc et al., 2012 and references therein). The sampled conglomerate has well-rounded clasts of varying size (≤10 cm, 1-3 cm on average) and composition (clasts of volcanic, intrusive, and sedimentary rocks), although tonalitic clasts dominate in the sample (Fig. 11A, B). The sample was not analyzed for whole-rock lithogeochemistry. The Stella Formation is overlain by the sedimentary rocks of the Haüy Formation, dated at <2691.7 ± 2.9 Ma (David et al., 2007) a few kilometres southeast of sample OVB-3 location.

Although the original data were verified and calculations remade for this report, the following is largely taken from Leclerc et al. (2012). Zircon from this conglomerate are light brown prisms of igneous origin that are slightly more elongate and also slightly more round than those from the Blondeau Formation (Figs. 11C, 12A). Six single grain ID-TIMS analyses from the Stella conglomerate are concordant to 0.8% discordant (Electronic Table 2; Fig. 11C), with $^{207}Pb/^{206}Pb$ dates ranging from 2720.2 ± 2.6 to 2702.1 ± 2.1 Ma. A 2704 ± 2 Ma maximum age of deposition is based on concordant analysis A3 (Table 1).

The majority of SHRIMP $^{207}Pb/^{206}Pb$ dates (56 concordant analyses out of 60; Electronic Table 3) from sample OVB-3 of the Stella Formation are clustered about a well-defined peak at 2701 Ma (Fig. 12B). A few grains reveal a small peak at 2736 Ma. While a single 2791 ± 14 Ma zircon reflects input from older rocks, the main zircon population is derived from igneous sources indistinguishable in age from the time of deposition.

The Stella Formation also occurs on the south flank of the Chibougamau Pluton, where a basal conglomerate marks an angular unconformity. This conglomerate contains a large number of clasts derived from the Doré Lake complex and Chibougamau pluton intrusive bodies. The relative timing relationships exposed on this outcrop have contributed much to the understanding of the regional stratigraphy. The implications of this angular unconformity at regional scale between the Roy Group and the Opemisca Group are discussed in Cimon and Gobeil (1976), Cimon (1979, in Allard et al., 1979) and Allard et al. (1990). The ~10−15 Ma age difference in depositional ages between the Stella Formation and the underlying Blondeau Formation, as well as the ~23 Ma age difference between the Stella Formation and the upper part of the Doré Lake Complex likely reflect the transition from volcanic construction (Roy Group) to major crustal uplift, and to the development of sedimentary basins in the northern part of the Abitibi greenstone belt. This inference, consistent with the Chibougamau stratigraphy (Cimon and Gobeil, 1976; Leclerc et al., 2009), would imply that the Stella Formation is at least 12 Ma older than the <2700–2685 Ma Porcupine-age turbidite of the southern part of the Abitibi greenstone belt, including the Porcupine equivalents in Quebec such as the ≤2685 Ma Cadillac and Kewagama groups (Davis, 2002; Lafrance et al., 2005; Mercier-Langevin et al., 2007). The Porcupine assemblage, which postdates the last large scale volcanic activity (Blake River Group) by approximately 5 million years (e.g.,

LaRonde mine area: Mercier-Langevin et al., 2007) in the southern part of the Abitibi belt, seems to have no time equivalent in the north-eastern segment. The Stella Formation sedimentary succession could represent a similar stage in the tectonic evolution of the northern part of the belt, albeit slightly earlier than in the southern Abitibi belt, in agreement with previous interpretations (e.g., Daigneault et al., 1990, 2002, 2004; Chown et al., 1992; Dubé and Mercier-Langevin, 2020).

Sample KQ-91-7 (Pyritic quartz-feldspar-biotite porphyry; z3611) is from a quartz and feldspar phyric felsic dyke (Fig. 13A, B) in the Lac Clark area in the central Chibougamau camp a few kilometres south of the town of Chibougamau (Figs. 3, 10B). The Lac Clark prospect has been interpreted as a Cu-Mo porphyry-type deposit hosted in the granophyre and gabbroic anorthosite phases of the ca. 2728 Ma Doré Lake Complex (Kirkham, 1972; Ford, 1974; Sinclair et al., 1994; Pilote, 1995; Pilote et al., 1996). The host rocks are cut by numerous sets of dykes, including porphyritic (quartz and feldspar) dykes that are considered intermineral (Robert, 1994; Sinclair et al., 1994). These dykes cut sulphidic and alteration veins but are also cut by some of these veins. One of these was sampled in 1991 for geochronology. Although the rounded age (2715 ± 1 Ma) was reported numerous times in various publications and studies (e.g., Pilote et al., 1996, 1997, 2006; Leclerc et al., 2012), the original data, concordia diagram, and detailed information were never formally published, despite the importance of this age in the understanding of the metallogenic evolution of the Chibougamau camp and entire Abitibi belt.

Zircon in this porphyry sample are dominated by pink, sharply facetted prisms ranging from sub-equant to elongate (4:1). Three multigrain fractions were analyzed all of which plot slightly above concordia (-0.4 to -1.0% discordant) with $^{207}Pb/^{206}Pb$ dates clustered between 2715.5 ± 0.9 Ma and 2714.1 ± 2.5 Ma (Electronic Table 2; Fig. 13). The reverse discordance is thought to be real, resulting from strong physical abrasion (34.5 and 52 hours; Electronic Table 2) and removal of U-rich outer rims to most of the crystals (R. Parrish, written communication, 1994). A linear regression containing all three analyses and a lower intercept at the origin yields an upper intercept of 2715.2 ± 0.7 Ma (MSWD = 0.54; probability of fit = 58%). This age is interpreted as the time of crystallization of the intermineral pyritic quartz-feldspar-biotite porphyry dyke (Table 1).

The age of sample KQ-91-7 provides a very precise age constraint on the timing of porphyry-style mineralization in the Chibougamau camp and indicates that the pre-main-deformation magmatic-hydrothermal system was contemporaneous with the early tonalitic phases of the Chibougamau Pluton (2718–2714 Ma) and cycle 2 volcanism (2724–2716 Ma) in the region (Pilote and Guha, 1995; Pilote et al., 1996; David et al., 2011; Davis et al., 2012). A foliated, 1 m-thick feldspar and quartz-phyric felsic dyke that intruded a shear zone at the contact between an ore vein and the host anorthosite at the Copper Rand mine gave an age of 2705.1 +1.7/-1.2 Ma (Joanisse, 1998; David et al., 2011). This dyke provides a minimum age for the Chibougamau-type Cu-Au mineralization and further indicates that the main deformation is younger than the mineralization.

Val-d'Or-Amos-Malartic area

The Val-d'Or-Amos-Malartic area, including the area northeast of the large Preissac-La Corne plutonic suite (Figs. 1, 2; Boily et al., 1989; MERN, 2018), comprises volcanic, sedimentary, and intrusive rocks of various compositions (Fig. 4). The rocks present in these areas are associated

with a rich metallogenic history and potentially include volcanogenic massive sulphide deposits, komatiite-associated Ni-Cu-(PGE) deposits (e.g., Marbridge: Lafrance, 2015), molybdenum deposits (e.g., Cadillac Moly: Taner et al., 1998), and lithium pegmatites (e.g., North American Lithium: Boily et al., 1989). Nine dated samples included in this report are from the Amos-Preissac-Lac Caste area (Figs. 2, 4).

Sample PP-06-89 (Dubuisson Formation, felsic tuff; z9341) is from a felsic tuff in the Dubuisson Formation in the central part of the Malartic Group. The sample was taken from an outcrop in the central part of a thick succession of dacitic and felsic volcaniclastic rocks near forest roads east of the Kinojévis River (Figs. 4, 14A). The tuff is homogeneous with a white patina (Fig. 15A, B) with lapilli-sized clasts in a fine-grained quartzo-feldspathic matrix. The sampled rock has an intermediate composition that seems relatively fresh, except perhaps for a weak sericite alteration (Electronic Table 4). The tuff has a calc-alkaline magmatic affinity based on a Zr/Y ratio of ~20.7 (Electronic Table 4).

Most zircon grains in this sample are of good quality, forming dominantly colourless, well-faceted, clear, short to elongate prisms with aspect ratios ranging from 2:1 to 5:1 (Fig. 15C). Few subequant crystals are also present. Nine single zircon grains were analyzed, five of which (A1, A2, B1, B3, and C1) yield highly colinear results ranging from concordant to 2.6% discordant and give an upper intercept of 2708.0 ± 1.5 Ma and a lower intercept of 1089 ± 94 Ma (MSWD = 0.87; probability of fit = 46%) (Electronic Table 2; Fig. 15C). The 2708.0 ± 1.5 Ma result is interpreted as the crystallization age of the felsic tuff (Table 1), whereas the ca. 1089 Ma lower intercept suggests Grenvillian isotopic disturbance. Discordant fractions B4 and C2 (latter not included in Fig. 15C), which plot above the discordia line, could reflect more ancient Pb loss compared to the colinear analyses. A subequant crystal (A3), with a distinctly older concordant $^{207}Pb/^{206}Pb$ date of 2718.0 ± 2.9 Ma, may contain an inherited component. The significance of the slightly reversely discordant analysis B2 is unclear but could indicate an analytical artefact.

The 2708.0 ± 1.5 Ma age of the felsic tuff is similar to the age of the nearby La Pause tonalitic Pluton (see sample PP-06-64A below) and indicates that they are both part of the same felsic event in the Dubuisson Formation. This age is broadly equivalent to the uppermost part of the Kidd-Munro Assemblage (2719−2711 Ma), or the lowermost part of the Tisdale Assemblage (2710−2704 Ma). The Kidd-Munro Assemblage hosts the giant Kidd Creek volcanogenic massive sulphide deposit in Ontario (Hannington et al., 1999) and other smaller occurrences in tholeiitic volcanic successions, whereas the Tisdale Assemblage hosts volcanogenic massive sulphide deposits in the Amos and Val-d'Or area to the east in different volcanic settings (Mercier-Langevin et al., 2023 and references therein). The Tisdale Assemblage is also associated with mafic-ultramafic magmatic sulphide systems (Houlé et al., 2017; Mercier-Langevin et al., 2023 and references therein).

Sample PP-06-117A (Dubuisson Formation, felsic tuff; z9084) is from a felsic volcaniclastic unit located in the Dubuisson Formation in the western part of the Malartic Group. The sample was taken from an outcrop in the central part of a thick succession of dacitic and felsic volcaniclastic rocks near forest roads east of the Kinojévis River, approximately 400 m SW of sample PP-06-89 (Figs. 4, 14B). The volcaniclastic rock is homogeneous with a white to slightly greenish patina

(Fig. 16A, B) with block-sized subangular to angular clasts in a fine-grained, weakly foliated quartzo-feldspathic matrix. The sampled rock has an intermediate composition (dacitic) that seems relatively fresh (Electronic Table 4). It has a calc-alkaline magmatic affinity based on a Zr/Y ratio of ~12.1 (Electronic Table 4).

This sample yielded a modest amount of zircon that display somewhat diverse morphologies including short to elongate prisms, rounded grains, and subhedral to anhedral fragments (Fig. 16C). Six of the seven single-grain analyses comprising mostly stubby prisms and fragments yielded a cluster of concordant to near-concordant $^{207}Pb/^{206}Pb$ dates between 2723.8 ± 4.7 and 2716.3 ± 2.6 Ma, whereas a euhedral prismatic grain (fraction A1) gave a distinctly younger concordant date of 2705.0 ± 2.9 Ma (Electronic Table 2; Fig. 16C). The 2705 ± 3 Ma result, which is slightly younger but within error of the 2708.0 ± 1.5 Ma age for felsic tuff sample PP-06-89 from the same formation, is interpreted to approximate the time of crystallization of felsic tuff PP-06-117A. Like for sample PP-06-89, the older zircon analyses are regarded as inherited, xenocrystic grains.

Sample PP-06-118A (Lanaudière Formation, rhyolite; z9085) is from a felsic volcanic rock between D'Aiguebelle Road and Caste Lake. This felsic unit forms a small (~1 kilometre long and <500 metres thick) lens intercalated in a succession of mafic volcanic units of the Lanaudière Formation (Figs. 4, 17A). The sampled unit is felsic (rhyolitic) with 77.8 wt.% SiO_2 and 0.1 wt.% TiO_2. This rhyolite is tholeiitic with 306.9 ppm Zr and a Zr/Y ratio of ~1.4 (Electronic Table 4). The rhyolite is massive, weakly foliated, and shows locally preserved flow-banding (Fig. 18A).

Colourless, sharply faceted, prismatic crystals were retrieved from this rhyolite (Fig. 18B). Five single grain zircon fractions were analyzed, four of which overlap each other and are <0.4% discordant (Electronic Table 2; Fig. 18C). A weighted average $^{207}Pb/^{206}Pb$ age for these analyses (excluding highly reversely discordant analysis A2) is 2716.2 ± 0.8 Ma (MSWD = 0.26; probability of fit = 85%), which is interpreted as the crystallization age of the Lanaudière Formation rhyolite PP-06-118A (Table 1).

This age is similar to that of the tholeiitic felsic rocks of the Kidd-Munro Assemblage (2719-2710 Ma), and more particularly to that of the rhyolite hosting the giant Kidd Creek Zn-Cu deposit in Ontario (Bleeker et al., 1999). It is also similar in age to the host units of the Gonzague-Langlois Zn-Cu deposit (2718.2 ± 2.1 Ma) in Lebel-sur-Quévillon in northwestern Abitibi (Théberge et al., 1999; Davis et al., 2005).

Sample PP-07-144 (Lanaudière Formation, rhyolite; z9439) is from a narrow rhyolite band in the northern part of the Lanaudière Formation (Fig. 3) approximately 10 kilometres east-northeast of sample PP-06-118A, north of Kinojévis River. This area has a complicated geology with a complex intercalation of andesite, komatiite, basalt, and rhyolite cut by gabbro and tonalite, and by much younger (Proterozoic) diabase dykes (Fig. 17B; Pilote et al., 2018, 2019). The sampled unit is felsic (rhyolitic) with 76.4 wt.% SiO_2 and 0.21 wt.% TiO_2. This rhyolite is tholeiitic with 238.5 ppm Zr and a Zr/Y ratio of ~2.2 (Electronic Table 4). The rhyolite is massive, weakly to moderately foliated, and is intercalated with strongly foliated felsic volcaniclastic rocks (Fig. 19A).

This rhyolite sample predominantly contains colourless, well-faceted prisms (aspect ratios of 2:1 to 3:1) (Fig. 19B). Sub-rounded prisms were also retrieved but were not analyzed owing to potential inheritance. Eight single grains and one multigrain fraction were analyzed and range from 2.1 to -1.5% discordant (Electronic Table 2; Fig. 19C). A linear regression through six of the nine analyses (A2, A3, A4, A6, A8, A9) and a lower intercept at the origin gives an upper intercept of 2719.1 ± 1.0 Ma (MSWD = 1.3; probability of fit = 27%), interpreted as the crystallization age of the Lanaudière Formation rhyolite PP-07-144 (Table 1). Fractions A1, A6, and A7 overlap concordia but have slightly older $^{207}Pb/^{206}Pb$ dates (2721.2 to 2722.1 Ma) likely reflecting minor inheritance and (or) the large common Pb correction required for analyses A1 and A7. These analyses, along with highly reversely discordant analysis A5, were excluded from the age calculation.

This sample is of similar age to its lateral equivalent, the rhyolite sample PP-06-118A in the upper part of the Lanaudière Formation, as well as the rhyolites that host significant base metal deposits along the Kidd-Munro Assemblage (2714.3 ± 1.2 Ma and 2716 +/- 0.6 Ma; Bleeker and Parrish, 1996; Bleeker et al., 1999). The fact that both rhyolite lenses dated with samples PP-06-118A and PP-07-144 are relatively small and discontinuous suggest isolated vents, partial preservation, and/or complex structural modification(s) to the stratigraphy, in agreement with the presence of the Manneville Thrust Zone (see below) and Matissard corridor in this area (Mueller et al., 1996; Daigneault et al., 2002; Pilote et al., 2018, 2019).

Sample P8-6-D (Deguisier Formation, intermediate lapilli to blocky tuff; z9630) is from an intermediate, polymictic block and lapilli tuff in the central part of the Deguisier Formation exposed on a roadside outcrop along Highway 395 (Figs. 4, 20A). The tuff is well preserved and weakly foliated, the clasts showing a moderate degree of flattening into the east-west foliation. Although part of a dominantly felsic unit, the sample bulk composition has low SiO_2 content and slightly elevated CaO and $Fe_2O_3^T$ values (Electronic Table 4), suggesting minor alteration, or more likely clast populations with both mafic-intermediate and felsic compositions, in agreement with the overall polymictic aspect of the sampled rock (Fig. 21A). The Deguisier Formation, which is at the base of the Kinojévis Group, has not been dated before and samples P8-6-D and P8-41-C2 (see below) are the only available ages for this formation. The age of sample P8-6-D has been divulgated in presentations and extended abstracts (Pilote et al., 2009) but has never been formally published with the supporting data.

Zircon retrieved from this intermediate lapilli to blocky tuff include mostly colourless, euhedral, stubby prismatic grains (Fig. 21B). Six single grain zircon fractions were analyzed, all of which are concordant to slightly discordant (up to 0.6%) with $^{207}Pb/^{206}Pb$ dates ranging from 2720.9 ± 4.7 Ma to 2717.0 ± 1.6 Ma (Electronic Table 2; Fig. 21C). Fractions A2S, B1, B2, and C2 yield a weighted mean age of 2719.4 ± 1.0 Ma (MSWD = 0.53; probability of fit = 66%), interpreted as the crystallization age of the Deguisier Formation tuff (Table 1). Including fraction A1 with a slightly younger $^{207}Pb/^{206}Pb$ date (2717.0 ± 1.6 Ma) in the weighted mean age calculation yields a higher MSWD of 2.0, possibly indicating the presence of non-analytical scatter such as minor ancient Pb loss compared to the other analyses. The imprecise fraction C1 reflects a combination of low radiogenic Pb and relatively high common Pb.

Sample P8-41-C2 (Deguisier Formation, flow-banded rhyolite; z9629) is from a flow-banded rhyolite that is part of a narrow lens of felsic volcanic and volcaniclastic rocks that is surrounded by a large gabbro intrusion (Figs. 20B, 22A). The felsic unit is part of the Deguisier Formation and is interpreted to be located slightly higher in the formation stratigraphy than the felsic unit dated with sample P8-6-D. The dated sample (P8-41-C2) was taken near the northern contact of the unit (Fig. 20B). It is rhyodacitic to rhyolitic in composition and tholeiitic to transitional with a Zr/Y ratio of ~4.5 (Electronic Table 4). The age of sample P8-41-C2 has been divulgated in presentations and extended abstracts (Pilote et al., 2009) but has never been formally published with the supporting data.

Zircon recovered from this flow-banded rhyolite sample consist principally of colourless, euhedral, prismatic crystals (Fig. 22B). Blocky fragments are also present. Four euhedral single prismatic grains and two fragments were analyzed, and the analyses range from 6.8% discordant to sub-concordant (down to 0.4%) (Electronic Table 2; Fig. 22C). Five of the six analyses lie on a regression line with an upper intercept at 2718.5 ± 1.1 Ma and a lower intercept at 408 ± 59 Ma (MSWD = 1.05; probability of fit = 37%). Zircon grain E1, with a slightly older $^{207}Pb/^{206}Pb$ date of 2721.7 Ma, may contain a minor inherited component. The upper intercept age of 2718.5 ± 1.1 Ma is interpreted as the time of igneous crystallization of the Deguisier Formation rhyolite (Table 1).

The Deguisier Formation at the base of the Kinojévis Group is overlain by the Lanaudière Formation, although both formations are locally in structural contact (Pilote et al., 2009). Ages presented here for the Lanaudière (samples PP-06-118A and PP-07-144) and Deguisier (samples P8-6-D and P8-41-C2) formations partly overlap within uncertainty at ca. 2718 Ma (Table 1), with the Lanaudière Formation rhyolite (sample PP-06-118A) being slightly younger based on the ages obtained, in agreement with observations presented in Goutier (1997).

Sample PP-07-143 (Tonalite dyke; z9508) is from a quartz±feldspar porphyritic tonalitic dyke sampled on an outcrop situated along a dirt road parallel with the Mont-Brun gravel road where it is intruding a succession of mafic to ultramafic volcanic and volcaniclastic rocks historically attributed to the Dubuisson Formation (Figs. 4, 23A, 24). Although the sample was taken in 2007, it has been sampled on an outcrop described in 2006 (station PP-2006-20), which appears in SIGEOM. There are a series of such dykes in this area, which are oriented or elongated parallel to the WNW-ESE regional structural grain in the area. The tonalite is homogeneous, pale in colour, and well foliated (Fig. 24A, B). The rock seems to be relatively fresh geochemically with a transitional composition and a strong calc-alkaline magmatic affinity (Zr/Y ratio of ~14.9: Electronic Table 4).

This tonalite dyke sample predominantly contains colourless, euhedral, prismatic (aspect ratios of 2:1 to 4:1) to subequant zircon crystals (Fig. 24C). Six single grain fractions were analyzed, all of which are concordant to sub-concordant (up to 0.3%) with $^{207}Pb/^{206}Pb$ dates ranging from 2722.0 ± 2.9 and 2717.6 ± 1.8 Ma (Electronic Table 2; Fig. 24C). Five of the six fractions (A1, A2, A3, A4, and C2) give a weighted mean age of 2718.5 ± 0.8 Ma (MSWD = 0.43; probability of fit = 79%). Based on the relatively uniform morphology of zircon in the sample and coherent U-Pb results, the 2718.5 ± 0.8 Ma age is interpreted as the time of igneous crystallization of the tonalite

dyke. The oldest analysis B1, with a $^{207}Pb/^{206}Pb$ date of 2722.0 ± 2.9 Ma, likely contains a small amount of inheritance.

The volcanic rocks that are cut by sample PP-07-143 tonalitic dyke are considered to be part of the Dubuisson Formation, which is however significantly younger than the age obtained from sample PP-07-143. The dated tonalitic dyke indicates that the host mafic to ultramafic volcanic rocks are older than 2717.7 Ma, and perhaps as old as 2719.3 Ma, which is in the range of ages of the Lanaudière or Deguisier formations. This would imply major structural imbrication and/or juxtaposition of distinct stratigraphic segments in that area, which is in the west-northwest continuation of the regional-scale Rivière-Héva Shear Zone. This shear zone juxtaposes, on the southwestern side of Malartic Lake, the ca. 2698 Ma felsic rocks of the Héva Formation to the north to the older mafic to ultramafic rocks of the Dubuisson Formation to the south (Guay et al., 2018). This probably means that a major shear zone runs in the area where sample PP-07-143 was taken, maybe analogous to the Rivière-Héva Shear Zone (or a splay), which may have significant implications on the geology of the area. More work would be necessary to confirm this hypothesis, but the potential implications on the regional geology are considerable.

Sample PP-06-64A (La Pause Pluton, tonalite-granodiorite; z9086) is from a quartz and feldspar porphyritic tonalitic to granodioritic intrusive unit that cuts the volcanic rocks of the La Motte-Vassan Formation. It was sampled on an outcrop along a forest road approximately 7.5 kilometres east of the Dubuisson Formation felsic tuff sample PP-06-89 (Figs. 4, 23B). The tonalite (granodirite) is homogeneous, pale in colour, weakly foliated and cut by late white quartz veins (Fig. 25A). The rock seems to be relatively fresh geochemically with a transitional to felsic composition and a strong calc-alkaline magmatic affinity (Zr/Y ratio of ~32.3: Electronic Table 4), although Y is very low at 3.6 ppm and perhaps a bit suspicious. Although the unit is called a tonalite, the composition of the dated sample is that of a granodiorite. Limited data is available for the La Pause Pluton; more work would be necessary to determine its exact composition.

Both zircon and titanite were recovered from the La Pause Pluton sample. Zircon comprise a dominant population of colourless, euhedral, elongate prisms (aspect ratios of 3:1 to 5:1) and a subpopulation of larger, pale brown or colourless, euhedral to subhedral prism fragments (Fig. 25B). Cores were observed in some grains, but these were avoided during final grain selection. Six single grain fractions of zircon were analyzed from the sample. Two of the analyses (C3 and C5) are strongly discordant (8.8 and 7.2%, respectively) owing to variable Pb loss and were not included in the age interpretation. The remaining four analyses are ≤0.3% discordant with $^{207}Pb/^{206}Pb$ dates clustered between 2710.9 ± 2.6 Ma and 2706.8 ± 2.4 Ma (Electronic Table 2; Fig. 25C). A weighted mean calculated from the three most concordant and overlapping analyses (B1, C1, and B4) from this cluster yields an age of 2709.8 ± 1.0 Ma (MSWD = 0.54; probability of fit = 58%), interpreted to date crystallization of the La Pause tonalite (Table 1). The slightly younger analysis C2 with a $^{207}Pb/^{206}Pb$ date of 2706.8 ± 2.4 Ma may have undergone minor ancient Pb loss. Titanite occurs as pale yellow, multifaceted crystals or as brown, subhedral fragments (Fig. 25B). Four multigrain fractions were analyzed, one of which is concordant with a $^{207}Pb/^{206}Pb$ date of 2658.7 ± 19.5 Ma (fraction T1A) and the other three are 0.6 to 3.8% discordant with $^{207}Pb/^{206}Pb$ dates ranging from 2659.1 ± 13.3 Ma to 2645.8 ± 28.9 Ma. Linear regression of these four analyses forced through a lower intercept at the origin gives an upper intercept at 2656.4 ±

9.3 Ma (MSWD = 0.30; probability of fit = 83%). The titanite age is significantly younger than the zircon crystallization age of the pluton, indicating the effects of a later disturbance.

The La Pause Pluton represents a synvolcanic intrusion that is the same age as the Dubuisson Formation felsic tuff dated in this study (sample PP-06-89), but younger than both the nearby Deguisier and Lanaudière formations. It is also significantly older than the 2664-2660 Ma Preissac batholith (Ducharme et al., 1997) located southeast of the La Pause Pluton, both intrusive bodies being separated by a narrow band of mafic and ultramafic rocks. The 2656 Ma age of the titanite corresponds to the time of peak regional metamorphism (2657.5 ± 4.4 Ma) in the region (Powell et al., 1995; Piette-Lauzière et al., 2019) and is similar to other titanite and rutile ages in the Abitibi (Dubé and Mercier-Langevin, 2020 and references therein).

Sample KI-07-09 (Caste Formation, conglomerate; z9920) conglomeratic sandstone is from hole KI-07-09 drilled by Cartier Resources Inc. in 2007 (Berthelot, 2008) on a property east of Highway 109 southwest of Amos (Figs. 2, 4). This hole, which was drilled to the south (N180°) at a plunge of -50°, is collared in mafic volcanic rocks but intersects a steeply dipping succession of sedimentary rocks downhole (Fig. 26A). The sedimentary band intersected begins at 59.2 m and ends at 228.4 m. This band consists of a medium-grained sandstone (wacke) containing conglomeratic beds with pebbles and contiguous blocks of mafic and felsic volcanic rocks, some with a cherty appearance, as well as porphyritic granitoid rocks. Tonalitic dykes commonly cut the sedimentary units.

The portion of conglomeratic sandstone sampled for geochronology lies within the interval extending from 140.5 m to 186.5 m depth downhole. The main conglomeratic unit extends from 153.4 m to 186.0 m. This conglomerate consists of polygenic pebbles and boulders, ranging in size from 0.5 cm to 3 cm on average, hosted in a light-green-grey wacke-type matrix of fine to medium grain size (Fig. 27A, B). The unit is chloritized and contains biotite mainly at the beginning of the conglomeratic unit, while epidote is present locally in the matrix towards the southern end. From 0.5% to locally 1% of very fine disseminated sulphides (pyrite and pyrrhotite) are found in the matrix. Pyrrhotite veinlets are locally present (Fig. 27B). This conglomerate is followed on the south side by a mudstone unit extending from 186.0 m to 228.4 m.

This east-west-trending sedimentary band is hosted in a major east-west-trending, moderately north-dipping deformation zone (30° to 45°) in-between two structural panels of volcanic rocks of the Lanaudière Formation; the north and south contacts of this sedimentary band with the adjacent volcanic units are severely deformed and sheared. There are no reliable polarity indicators in the sedimentary rocks, although coarse stratification is locally discernible in the sandstone (wacke) and mudstone. Polarity indicators in the volcanic units (Lanaudière Formation), on the other hand, are all to the south. The intensity of deformation decreases rapidly on either side of these sheared edges, in both volcanic and sedimentary units.

Zircon retrieved from this conglomerate sample display a range of morphologies from clear, colourless, well-facetted stubby prisms (Fig. 27C) to colourless or brown elongate prisms (3:1–4:1) and rare rounded grains (Fig. 28A). SEM imaging shows that most grains have sharply facetted to weakly rounded prismatic forms, many of which are characterized by igneous

oscillatory internal zonation. Fourteen single grain fractions analyzed by ID-TIMS yield $^{207}Pb/^{206}Pb$ dates ranging from 2754.3 ± 1.5 to 2697.4 ± 2.8 Ma (concordant to 0.7% discordant; Electronic Table 2; Fig. 27C). Twelve out of 14 analyses define a grouping near 2718 Ma, which is interpreted to reflect derivation from local volcanic units. The youngest concordant analysis (A10), with a $^{207}Pb/^{206}Pb$ date of 2697 ± 3 Ma, provides an estimate of the maximum age of deposition of the Caste Formation conglomerate (Table 1). SHRIMP analysis of 61 grains from this conglomerate shows a spread of $^{207}Pb/^{206}Pb$ dates between 2759 ± 74 and 2646 ± 120 Ma, and a single older, concordant analysis at 2880 ± 18 Ma (Electronic Table 3; Fig. 28, inset). On the probability density distribution plot, the majority of analyses define a bimodal grouping near 2727 and 2690 Ma, broadly consistent with the ID-TIMS results. Though the peak at 2690 Ma could be interpreted as the maximum depositional age of the conglomerate, the 2697 ± 3 Ma ID-TIMS date remains a more robust estimate given the comparatively larger SHRIMP analytical uncertainties.

The young ages obtained (<2697 ± 3 Ma by the ID-TIMS method and <2690 Ma by SHRIMP), together with the configuration of the sandstone (wacke), wedged between major deformation zones along much older volcanic rocks, imply that these faults are part of the shallowly north-dipping regional-scale thrust referred to as the Manneville Thrust Zone (MTZ; Mueller et al., 1996; Daigneault et al., 2002; Pilote et al., 2018, 2019). The MTZ can be interpreted as a folded succession, materialized in the Barraute region by a series of synclinal folds (Barraute and Figuery synclines) and anticlines, all overturned towards the south and cut by faults. The strata are overturned and stratigraphic tops commonly face south. The main foliation consists of a composite S_0/S_1 surface with a slight dip (30° to 50°) towards the north. This thrust affects the entire Kinojévis Group, the Landrienne Formation and the sedimentary rocks of the Caste Formation, which gives this structure an apparent horizontal thickness varying from 6 to 8 kilometres. The presence of these sedimentary rocks within these volcanic assemblages can be explained by transport, and/or duplication-juxtaposition of lithologies of contrasting ages and distinct origins along the various faults that make up the MTZ (Daigneault et al., 2002; Pilote et al., 2018, 2019). A polygenic conglomerate unit showing typical Timiskaming-like features hosted in the Fiedmont Formation, a few tens of kilometres to the east, has yielded a maximum U-Pb age of 2715.8 ± 4.2 Ma (Pilote et al., 2018; David, 2020).

Rouyn-Noranda area

The Rouyn-Noranda area is largely underlain by the 2704-2695 Ma (Corfu, 1993; Mortensen, 1993b; Lafrance et al., 2005; Mueller et al., 2012; McNicoll et al., 2014) Blake River Group that contains the most important concentration of volcanogenic massive sulphide deposits of the Superior Province, and of any other Archean sequence (e.g., Dubé et al., 2007a, b; Gibson and Galley, 2007; Mercier-Langevin et al., 2011a, 2014a, 2017a, 2023; Goutier, 2017; Monecke et al., 2017a, b). Approximately half of the total VMS tonnage and about 90% of the total gold hosted in VMS deposits of the Abitibi greenstone belt is found in the Blake River Group (Mercier-Langevin et al., 2009). The Horne complex (Horne and Horne 5; 166.4 Mt: Krushnisky et al., 2023) and LaRonde Penna (70.7 Mt: Mercier-Langevin et al., 2021b) together contain more than 40% of the total gold hosted in volcanogenic massive sulphide deposits of the entire Abitibi belt (Mercier-Langevin et al., 2011b). The Blake River Group volcanic and intrusive rocks host a wide spectrum of mineralization types (Couture and Goutier, 1996): 1) Cu-Zn volcanogenic massive sulphide

deposits (e.g., Ansil: Galley et al., 1995, Bouchard-Hébert: Riopel et al., 1995, Millenbach: Knuckey et al., 1982), 2) Au-rich and auriferous volcanogenic massive sulphide deposits (e.g., Quemont: Cattalani et al., 1993, Bousquet 2-Dumagami: Dubé et al., 2014), 3) intrusion-related or porphyry-style disseminated Cu mineralization (e.g., Don Rouyn: Goldie et al., 1979; Mercier-Langevin et al., 2024), 4) auriferous volcanogenic disseminated sulphides (e.g., Bousquet 1 and LaRonde Zone 5: Tourigny et al., 1992; Boily-Auclair et al., 2020, 2022), 5) intrusion-hosted auriferous quartz-sulphide vein systems (e.g. Doyon: Savoie et al., 1991; Galley and Mercier-Langevin, 2025), 6) magmatic/hydrothermal Ni-Cu-(PGE) sulphides (e.g., R.M. Nickel: Barnes et al., 1993), and 7) mesothermal (or "orogenic") quartz-carbonate and disseminated gold deposits (e.g., Astoria: Gauthier et al., 1990, Francoeur: Couture and Pilote, 1993, Silidor: Carrier et al., 2000).

The Blake River Group consists of a thick sequence of dominantly submarine volcanic rocks of mafic to intermediate composition, with minor felsic volcanic rocks and tholeiitic to calc-alkaline magmatic affinity (Goutier et al., 2007, 2009, 2011; Sterckx, 2018; Vite-Sanchez et al., 2024, and references therein). Because of its wealth in VMS deposits and the importance of understanding the volcanic stratigraphy, there are numerous U-Pb dates available in the literature. However, stratigraphy is still not entirely firmly established at regional scale due to the small extent of felsic volcanic units and structural complexities. The volcanic rocks are cut by synvolcanic to syntectonic mafic to felsic intrusions, many of which have been dated (e.g., Mortensen, 1993b; Mueller et al., 2012; McNicoll et al., 2014). Among these intrusions are numerous subvolcanic gabbro bodies intruding the volcanic rocks of the Blake River Group in the Rouyn-Noranda area (Goutier, 2017). Some of these intrusions have been studied in detail by Mueller et al. (2009), Kuiper (2010), and Goutier et al. (2011). Five dated samples included in this report are from gabbro intrusions in the Rouyn-Noranda area (Figs. 2, 5), whereas a sixth sample from the Rouyn-Noranda area is from a rhyolite lens intercalated with andesitic tuff units of the Stadacona member of the Rouyn-Pelletier Formation (Figs. 2, 5).

Sample 06-CD-3037 (R.M. Nickel gabbro; z9026) is from a coarse-grained to pegmatitic gabbro to leucogabbro phase (Fig. 29A, B) that outcrops just west of a forest road that runs south to north from the village of Arntfield to the Inmont and Four Corners prospects in the western part of the Noranda camp (Figs. 4, 26B). It is likely altered with 48.9 wt.% SiO_2 and 12.8 wt.% CaO (Electronic Table 4). It is part of the R.M. Nickel gabbro, a small (less than 2 km x 2 km) irregular body that cuts the andesite and basaltic andesite of the Duprat-Montbray Formation (Fig. 26B), less than 600 metres east-northeast of the Horseshoe gabbro (see sample 08-DK-8286 below). The gabbro has been folded and a sample taken a few hundred meters south of sample 06-CD-3037 was dated at 2695.8 ± 1.5 Ma (Mueller et al., 2009). The R.M. Nickel gabbro was previously considered to be the continuity of the Horseshoe gabbro to the southwest and of the Dasserat gabbro to the west but contrasting textures and compositions, and different U-Pb ages (see below), indicate that the three intrusive bodies consist of distinct magmatic elements that cannot be correlated (Kuiper, 2010).

This gabbro sample contains zircon with two main morphologies: anhedral fragments and prisms with aspect ratios of 2:1–4:1, both of which are colourless (Fig. 29C). Six analyzed single-grain fractions are concordant to near-concordant (-0.1 to 0.5% discordant) with $^{207}Pb/^{206}Pb$ dates

ranging from 2700.4 ± 1.8 Ma to 2693.9 ± 2.0 Ma (Electronic Table 2; Fig. 29C). The four youngest analyses overlap each other and were used to calculate a weighted average $^{207}Pb/^{206}Pb$ age of 2695.0 ± 1.0 Ma (MSWD = 0.69; probability of fit = 56%), which is interpreted as the crystallization age of the R.M. Nickel gabbro (Table 1). Fractions B1 and C5 have slightly older $^{207}Pb/^{206}Pb$ dates (2698.4 ± 2.4 Ma and 2700.4 ± 1.8 Ma, respectively), suggesting the presence of a small amount of inherited material. This age is very similar to the age reported in Mueller et al. (2012), although slightly more precise. An age of 2695 ± 1 Ma means that it was emplaced in the very last stages of the Blake River Group construction (e.g., Mobrun rhyolite at 2695.8 ± 0.8 Ma: McNicoll et al., 2014, and rhyolite in the D'Alembert tuff at 2694.5 ± 0.9 Ma: Ross et al., 2011b). An intermediate porphyry dyke at the Horne West Zone gave a similar age (2694.5 ± 0.9 Ma: Krushnisky et al., 2023).

Sample 07-PCT-014 (Dufresnoy gabbro; z9314) is from the Dufresnoy gabbro that outcrops in the southern part of the Noranda central camp (Figs. 5, 30A). The Dufresnoy gabbro has a thickness of several hundred metres. It is oriented north-northwest – south-southeast and dips moderately to the north-northeast (50º). The gabbro cuts the host sequence of the northern and southern central camp volcanogenic massive sulphide deposits. Displacement of the mineralized horizon on both sides of the gabbro suggests that an apparent reverse movement (Gibson and Watkinson, 1990) occurred in this area due to uplift of the volcanic succession on one side of the intrusion that is sub-parallel with the volcanic strata (Goutier et al., 2011; Goutier, 2017). The sampled gabbro is coarse-grained with decimetre-scale pegmatitic sections richer in quartz, feldspar, and zircon (Fig. 31A, B) and appears to be chemically fresh (60.5 wt.% SiO_2, 1.32 wt.% LOI: Electronic Table 4). This outcrop presents textures that are similar to those observed in other gabbroic bodies of the Rouyn-Noranda area (Kuiper, 2010).

This sample contains abundant high-quality, euhedral, colourless zircon ranging from stubby prismatic to elongate grains with aspect ratios of ≥4:1 (Fig. 31C). A subpopulation of tabular grains is also present. Five single-grain zircon fractions were analyzed, and the data are concordant to slightly discordant (0.3 to -0.7%) with $^{207}Pb/^{206}Pb$ dates between 2699.5 ± 2.1 Ma and 2697.3 ± 1.5 Ma (Electronic Table 2; Fig. 31C). A weighted average of the $^{207}Pb/^{206}Pb$ dates of four analyses (excluding reversely discordant analysis D2, which yielded the oldest $^{207}Pb/^{206}Pb$ date) is calculated at 2697.9 ± 0.8 Ma (MSWD = 0.39; probability of fit = 76%) and is interpreted as the crystallization age of the Dufresnoy gabbro (Table 1).

The 2697.9 ± 0.8 Ma age is similar to the age obtained for rhyolite of the central camp (e.g., Lac Turcotte dacite; 2698.3 +1.2/-1.0 Ma: David et al., 2011) and for the uppermost units of the Bousquet Formation to the east (2699-2696 Ma; Lafrance et al., 2005; Mercier-Langevin et al., 2007; McNicoll et al., 2014). The age and setting of the Dufresnoy gabbro are therefore important in constraining the minimum age of the central camp volcanogenic massive sulphide deposits (Goutier et al., 2011)

Sample 07-CD-3554C (Duprat gabbro; z9344) is from the Duprat gabbro, approximately 20 kilometres northwest of the town of Rouyn-Noranda (Fig. 5). The gabbro forms an elongated body that runs south-southeast – north-northwest and cuts the volcanic rocks of the Duprat-Montbray Formation, including a rhyolite dated at 2701.4 ± 1 Ma (McNicoll et al., 2014) a couple kilometres

north-east of sample 07-CD-3554C. The sample was taken on an outcrop on the northeast side of a gravel road, near the contact with andesite (Fig. 30B). Although the intrusive unit is mapped as a diorite, the sampled location has a mafic (gabbroic) composition with 46.6 wt.% SiO_2 (Electronic Table 4). The selected sample is from a massive part of the unit that does not seem to be foliated, with a slightly irregular texture varying from medium- to coarse-grained patches of leucogabbro (Fig. 32A, B).

Both zircon and baddeleyite were retrieved from the Duprat gabbro sample. Zircon displays varying morphologies, including colourless to pale brown, mostly broken stubby to elongate prisms, tabular grains, and subhedral fragments (Fig. 32C). Four single-grain zircon fractions yield concordant to near-concordant (0.2 to 0.4% discordant) results with $^{207}Pb/^{206}Pb$ dates ranging between 2699.3 ± 1.7 Ma and 2697.5 ± 1.5 Ma. The three most concordant and overlapping analyses (A2, B1, and B2) yield a weighted average $^{207}Pb/^{206}Pb$ age of 2698.0 ± 0.8 Ma (MSWD = 0.48; probability of fit = 62%). Fraction A1 plots slightly to the right of the cluster defined by these three analyses likely owing to the presence of a minor component of older inherited material. Baddeleyite occurs as tan to brown, euhedral blades, several of which are broken (Fig. 32C). Three single-grain baddeleyite fractions were analyzed and yield discordant (0.4 to 0.9%) results with $^{207}Pb/^{206}Pb$ dates ranging between 2697.2 ± 1.5 and 2694.8 ± 1.5 Ma. A weighted average of their $^{207}Pb/^{206}Pb$ dates gives an age of 2696.0 ± 3.0 Ma but with a relatively high MSWD of 2.7 and low probability of fit of 0.08%, indicating some scatter in the results. Thus, the 2698.0 ± 0.8 Ma zircon age is considered a more robust estimate for the crystallization age of the Duprat gabbro (Table 1).

Sample 07-JG-9107 (Dufault gabbro; z9617) is from the Dufault gabbro, a large (~2.7 x 9 km) intrusion north of Rouyn-Noranda (Fig. 5) that varies in composition from gabbroic, dioritic, to anorthositic. The selected sample, which is from a small island in Lac Dufault (Fig. 33A), is described as a coarse-grained pegmatitic quartz-bearing gabbro (Fig. 34A, B) but comes from a portion of the intrusion that is equigranular (referred to Dufault phase I, equigranular facies, in Kuiper, 2010). The sample has 57.2 wt.% SiO_2 and 1.1 wt.% TiO_2, with 206 ppm Zr (Electronic Table 4). The Dufault gabbro is cut by the Lac Dufault felsic pluton, which was dated at 2690.2 ± 2.1 Ma (Mortensen, 1993b).

This sample yielded good quality zircon, dominantly colourless to pale brown and ranging in morphology from euhedral prismatic (aspect ratios of 2:1 to 5:1), equant grains to subhedral fragments, or tabular crystals (Fig. 34C). Six single zircon grains were analyzed, and all are slightly discordant (0.3–0.8%) with $^{207}Pb/^{206}Pb$ dates ranging from 2699.7 ± 2.1 Ma to 2696.5 ± 1.6 Ma (Electronic Table 2; Fig. 34C). The four youngest analyses (B1, B2, B3, and D1) yield a statistically robust weighted average $^{207}Pb/^{206}Pb$ age of 2697.3 ± 0.8 Ma (MSWD = 0.54, probability of fit = 65%), which is interpreted as the crystallization age of the Dufault gabbro (Table 1). Fractions A1 and C1 have slightly older $^{207}Pb/^{206}Pb$ dates of 2699.7 ± 2.1 Ma and 2699.6 ± 3.2 Ma, respectively, and likely reflect minor inheritance.

This age indicates that the Dufault gabbro is the same age as the Dufresnoy and Duprat gabbro, confirming a major phase of synvolcanic mafic (±intermediate) magmatism in the central Blake River Group. The younger phase of the Dufault gabbro (Dufault II in Kuiper, 2010) is perhaps

only slightly younger than phase I as indicated by the presence of rhyolite xenoliths that are associated with the Fish-roe rhyolite dated at 2696.5 ± 2.4 Ma (David et al., 2007).

Sample 08-DK-8286 (Horseshoe gabbro; z9878) is from the Horseshoe gabbro, a strongly elongated, locally layered intrusive body oriented southwest-northeast a few kilometres west of Rouyn-Noranda (Fig. 5) that appears to cut previously folded volcanic units. The sample comes from a small hill south of the gravel road, close to the northwestern contact with felsic to intermediate volcanic rocks of the Duprat-Montbray Formation (Fig. 33B). As indicated above for the R.M. Nickel gabbro, the Horseshoe gabbro was previously considered to be the continuity of the R.M. Nickel gabbro to the northeast and of the Dasserat gabbro to the north, but contrasting textures and compositions, and different U-Pb ages (see below), indicate that the three intrusive bodies consist of distinct magmatic elements that cannot be correlated (Kuiper, 2010). The sample selected for geochronology is from a flat outcropping area (Fig. 35A) and has a dark colouration on a fresh surface (Fig. 35B) and an intermediate to felsic composition with 66.3 wt.% SiO_2, 0.52 wt.% TiO_2, and 311 ppm Zr (Electronic Table 4), and is therefore considered to represent a more felsic (tonalitic) pod.

Zircon recovered from this gabbro sample display anhedral and lesser prismatic habits (Fig. 35C). Five single-grain and five multigrain fractions were analyzed, all of which were chemically abraded. The data are concordant to strongly discordant (up to 17.7%) with $^{207}Pb/^{206}Pb$ dates varying between 2702.8 ± 3.2 Ma and 2677.7 ± 2.5 Ma (Electronic Table 2; Fig. 35C). Eight of the ten analyses define a regression line with an upper intercept age of 2700.2 ± 0.9 Ma and a lower intercept of 58 ± 20 Ma (MSWD = 1.2; probability of fit = 30%). Fraction D1-8 plots slightly to the left of the discordia line indicating an additional component of Pb loss. The multigrain fraction CD16-1, which yields a distinctly younger, concordant $^{207}Pb/^{206}Pb$ date of 2677.7 ± 2.5 Ma, indicates a second episode of zircon growth.

The 2700.2 ± 0.9 Ma zircon age could potentially represent the crystallization age of the Horseshoe gabbro. However, considering the ca. 2700 Ma age of the surrounding rocks, the discordant nature of the gabbro, and the fact that it seems to cut previously folded volcanic stratigraphy, this could also represent local inheritance, as suggested by Kuiper (2010). Alternatively, the 2677.7 ± 2.5 Ma date obtained in sample 08-DK-8286 may potentially represent the age of the unit. More work would be necessary to validate the age of the Horseshoe gabbro.

Samples 06-PBA-385B and C (Stadacona Member, Rouyn-Pelletier Formation, rhyolite; z9312) are from an E-W-trending narrow band of rhyolite that is present on top (north of), or in the uppermost part of the Stadacona mafic volcaniclastic unit (Stadacona Member, Rouyn-Pelletier-Formation: Ross et al., 2007, 2008, 2011a, b) south of the town of Rouyn-Noranda (Figs. 2, 5). The dated samples come from a large outcropping area that has since been partly excavated as part of ongoing quarrying activity (Fig. 36A). The rhyolite appears to be massive to locally volcaniclastic, is moderately foliated, and is characterized by 5-10 vol.% quartz and feldspar (plagioclase) microphenocrysts (≤3 mm) in a very fine-grained matrix (Fig. 37A, B). A geochemical analysis of this rhyolite indicates a very felsic signature with 75.6 wt.% SiO_2, 11.5 wt.% Al_2O_3, and 0.26 wt.% TiO_2, with 228 ppm Zr (Electronic Table 4).

Rhyolite sample PBA06-385C (z9312) contained only sparse zircon with variable morphologies and colours (Fig. 37C). Together with rounded forms or edges/terminations, these characteristics suggest that many of the grains may be xenocrystic or inherited. Despite these features, ID-TIMS analysis of five single-grain and physically abraded fractions yielded fairly coherent data. Three of the five analyses yield $^{207}Pb/^{206}Pb$ dates between 2701.7 ± 2.1 and 2701.4 ± 3.0 Ma and all five analyses are colinear giving an upper intercept age of 2702.3 ± 2.8 Ma and lower intercept age of 1003 ± 120 Ma (MSWD = 1.6, probability of fit = 19%) (Electronic Table 2; Fig. 37C). Given the evidence for potential inheritance in this sample, the 2702.3 ± 2.8 Ma age is conservatively regarded as a maximum age of crystallization for the Stadacona member rhyolite.

Rhyolite sample PBA06-385B (z9114) yielded only a sparse recovery of zircon with diverse morphologies and colours (Fig. 38A), suggesting the potential presence of xenocrysts or inherited grains from country rocks. Initial attempts to date this rock by ID-TIMS yielded disparate results and no crystallization age could be determined from the data set (McNicoll et al., 2014). The remaining zircon grains in the sample were mounted and analyzed by SHRIMP. A total of 29 analyses from 29 individual grains yield concordant to near-concordant $^{207}Pb/^{206}Pb$ dates between 2754 ± 48 and 2602 ± 28 Ma, and a single older, discordant (5.8%) analysis at 2814 ± 24 (Electronic Table 3; Fig. 38B). On a probability density plot, the data define a dominant peak at ca. 2696 Ma, with a small shoulder at ca. 2710 Ma, and a subordinate peak at ca. 2604 Ma. The 20 analyses that comprise the dominant peak yield a weighted average $^{207}Pb/^{206}Pb$ age of 2697.5 ± 6.9 Ma (MSWD = 1.4, probability of fit = 14%). This weighted mean age of 2697.5 ± 6.9 Ma is in agreement with the TIMS age obtained from sample PBA06-385C. If this interpretation is correct, then the combined data suggest that the zircon grains were derived from a single source or alternatively from various sources of very similar age.

A ≤2702. 3 ± 2.8 Ma zircon for this dated rhyolite in the Stadacona member is in agreement with similar ages in the area (e.g. 2700.6 ± 0.9 Ma for the Evain rhyolite: McNicoll et al., 2014, and 2700.6 ± 1.6 Ma for a rhyolite part of the Fish-roe Member (Rouyn-Pelletier Formation) south of the Stadacona Member: Lafrance et al., 2005).

Bousquet-Cadillac area

The Bousquet-Cadillac area comprises the Doyon-Bousquet-LaRonde and the Cadillac mining camps, about 50 kilometres east of Noranda. This area has produced, and still produces, significant amounts of base and precious metals, and remains a prime exploration region.

The Doyon-Bousquet-LaRonde mining camp is one of Canada's largest VMS districts (Galley et al., 2007; Dubé et al., 2007a). It also ranks among the largest Canadian gold districts (Mercier-Langevin et al., 2017a, 2020). The camp hosts different styles of mineralization, including gold-rich VMS deposits, disseminated and stockwork-style gold deposits, and intrusion-associated gold deposits (Dubé et al., 2007a; Yergeau et al., 2022a, b; Galley and Mercier-Langevin, 2025). The deposits of the camp yielded a cumulative production of 107.5 Mt of ore at an average grade of 4.85 g/t Au by the end of 2019 (521 t of Au: Mercier-Langevin et al., 2021a, b). The total past production, current reserves, and estimated resources for the camp amount to approximately 894 t Au (Mercier-Langevin et al., 2021a, b). The deposits of the Doyon-Bousquet-LaRonde mining

camp are hosted by the volcanic rocks of the 2704–2695 Ma Blake River Group. The Blake River Group is structurally bounded to the north by the SE-trending Lac Parfouru fault zone, which separates the Blake River Group from the sedimentary rocks of the <2687 Ma (Davis, 2002) Kewagama Group, which belongs to the Porcupine assemblage (Lafrance et al., 2003). To the south, the Blake River Group is overlain by sedimentary rocks of the Cadillac Group that is also part of the Porcupine assemblage (<2689 Ma in the LaRonde Penna deposit area: Mercier-Langevin et al., 2007). Farther to the south, the sedimentary rocks of the Cadillac Group are truncated by the E-W–striking Larder Lake-Cadillac fault zone (Poulsen, 2017 and references therein).

The Cadillac mining camp hosts numerous, but relatively small, orogenic gold deposits that were mined in the past (Dubé and Gosselin, 2007; Mercier-Langevin et al., 2017b). These gold deposits are spatially associated with the Larder Lake-Cadillac fault zone (Trudel et al., 1992; Simard et al., 2013), an E-W–striking crustal structure that separates the Abitibi greenstone belt to the north from the Pontiac Subprovince to the south (Card, 1990; Daigneault and Archambault, 1990; Daigneault et al., 2002; Percival, 2007). The Larder Lake-Cadillac fault zone is characterized by various deformation styles along strike that result from a protracted history of extension, compression, and transpressive deformation (Robert, 1989; Bleeker, 2012; Bedeaux et al. 2017: Poulsen, 2017), involving north-south shortening and local strike-slip deformation (Daigneault et al., 2002; Robert et al., 2005). Numerous major gold districts and deposits are spatially associated to second and third-order faults related to the Larder Lake-Cadillac fault zone (e.g., Sigma-Lamaque in Val-d'Or and Kerr-Addison in Larder Lake; Robert and Poulsen, 1997; Dubé and Gosselin, 2007; Dubé and Mercier-Langevin, 2020).

Sample LAPL-2008-011 (Cadillac/Timiskaming Group conglomerate; z9903) is from a polygenic conglomerate unit exposed a few hundred metres west of road 395, between Highway 117 and the LaRonde metallurgic complex (Figs. 2, 4, and 36B). A hill under the powerline has numerous outcrops where the conglomerate unit outcrops. The conglomerate defines an east-trending, elongated lens up to a couple hundred metres thick between bands of finer-grained sedimentary units (sandstone) that are part of the Cadillac Group turbiditic succession north of the Piché Group and the Cadillac fault (Lafrance et al., 2003). The Cadillac Group rocks have been dated at <2687 ± 3 Ma (sandstone unit just north of the sampled conglomerate; Davis, 2002), at <2687.4 ± 1.2 Ma Ma in the nearby Doyon mine area to the west (Lafrance et al., 2005), and at <2689 ± 2 Ma at the LaRonde Penna mine (Mercier-Langevin et al., 2007) just a few hundred metres north of this location. The conglomerate is highly strained and contains a steeply south-dipping foliation (Fig. 39A), although strain is heterogeneously distributed and some beds are relatively well preserved, showing polygenic clasts that are generally well rounded (Fig. 39B). The conglomerate contains clasts of porphyritic rocks, clasts of quartz veins, and locally abundant, small green mica-altered (fuchsite) clasts, reminiscent of Timiskaming conglomerate elsewhere in the Abitibi belt. A bed with generally finer clasts and more matrix (sandstone) was selected for sampling. Although visibly not altered, a whole-rock geochemical analysis of the sample suggests significant chlorite and ankerite alteration with 11.91 wt.% CaO and 9.07 wt.% CO_2 (Electronic Table 4). Interestingly, this band of sedimentary rocks hosts numerous Au prospects and parts of the mineralized zones in the Cadillac camp a few kilometres to the east (Trudel et al., 1992; Mercier-Langevin et al., 2017b). The conglomerate, despite being considered part of the Cadillac Group,

was sampled to test the idea of a possible younger age and association with the Timiskaming Group as lenses of Timiskaming rocks were recently identified in the Cadillac Group further to the east (Pilote et al., 2014; David et al., 2018).

Zircon retrieved from this conglomerate occur as brown to colourless, mostly euhedral to subhedral, prismatic crystals (2:1–4:1) (Figs. 39C and 40A), many exhibiting prominent oscillatory growth zoning under the microscope. A few rounded grains are also present. Out of a total of thirteen single-grain fractions analyzed by ID-TIMS, five are from chemically abraded zircon (A2-1, A4-1, A6-1, A8-1, and A8-2) and the remaining ones are from physically abraded grains but there is no significant difference in discordance between the results. Except for a single strongly discordant (10.7%) analysis (A2-1), the analyses provide a range of near-concordant to concordant $^{207}Pb/^{206}Pb$ dates from 2729.4 ± 1.4 Ma to 2671.7 ± 1.5 Ma (Electronic Table 2; Fig. 39C). Fraction A4-1 yields a slightly reversely discordant (-0.3%) result but given its relatively high radiogenic Pb content and low proportion of common Pb, its $^{207}Pb/^{206}Pb$ date of 2672 ± 2 Ma is considered a reliable estimate of the maximum age of deposition of the conglomerate (Table 1). If correct, this result would suggest that conglomerate sample LAPL-2008-011 belongs to the Timiskaming Group instead of the Cadillac Group. This conglomerate occurrence therefore most likely represents a previously unrecognized Timiskaming age unit south of the LaRonde Penna mine complex and north of the Piché Group and the Larder Lake-Cadillac fault zone. Detailed mapping should be done in this area to assess the overall extent of the unit and its contact relationships with the Cadillac Group turbidites.

SHRIMP analyses for 44 zircon grains from this sample yield $^{207}Pb/^{206}Pb$ dates ranging from 3117 ± 14 to 2651 ± 58 Ma (Fig. 40B, inset; Electronic Table 3). On the probability density distribution plot, the data define a prominent peak at ca. 2696 Ma (representing 86% of the analyses) with a small flanking shoulder at ca. 2745 Ma. Two older concordant grains define minor peaks at 3117 and 2915 Ma. The 2696 Ma peak age may reflect dominant sourcing from the youngest, ca. 2696 (±5 Ma) Ma volcanic rocks of the Blake River Group and broadly contemporaneous synvolcanic tonalitic plutons (e.g., McNicoll et al., 2014), whereas the older Mesoarchean detritus may indicate derivation from hinterland to the north or northeast as suggested by Frieman et al. (2017) as no local source of Mesoarchean material exists (except perhaps reworked sedimentary rocks such as the Caste Formation for example: Feng and Kerrich, 1991; Davis, 2002)

Samples that could not be dated

Five samples collected between 2006 and 2010 as part of the TGI-3 and Plan Cuivre projects yielded only xenocrystic zircon or no minerals suitable for analysis and thus no dates. Despite unsuccessful U-Pb dating, information about these samples is reported in Electronic Table 5 so that future researchers studying any of the units know they might present some challenges for geochronology.

CONCLUDING REMARKS

This report releases twenty (20) high-precision TIMS zircon and titanite ages from volcanic, sedimentary, and intrusive units of the Abitibi greenstone belt (Chibougamau, Val-d'Or, and

Rouyn-Noranda mining districts). Most of these ages, generated through past joint research and mapping programs by the Geological Survey of Canada and the Ministère des Ressources naturelles et des Forêts, have been previously mentioned in conference abstracts, reports, and theses, but were never formally published with all the analytical data and information. Among the ages released here are some important anchor points in constraining the geological and metallogenic evolution of the Abitibi greenstone belt, including the potential for major structural discontinuities that were previously unknown. It also includes a newly recognized potential occurrence of Timiskaming Group conglomerate formerly attributed to the older Cadillac Group turbidite south of the Doyon-Bousquet-LaRonde mining camp.

The U-Pb ages reported herein add to a growing wealth of geochronological constraints in the Abitibi belt making it one of the best documented greenstone belts of the world and contributing to strong foundations on which to further advance our understanding of the geology and metallogeny during the Archean.

ACKNOWLEDGMENTS

This study was, for the most part, initiated during phase 3 of GSC-MRNF-OGS Targeted Geoscience Initiative (2005-2010) joint *Abitibi* and *Plan Cuivre* projects. Numerous colleagues and students were involved in these projects, many having been directly involved in the selection and sampling of the samples documented in this report, including: J. Ayer (OGS), C. Dion (MRNF), T. Hart (OGS), R. Kirkham (GSC), D. Kuiper (Laurentian University), M. Legault (MRNF), R. Marquis (MRNF), R. Parrish (GSC), J. Percival (GSC), F. Robert (GSC), P.-S. Ross (INRS), P. Roy (MRNF), A. Simard (MRNF), D. Sinclair (GSC), P. Thurston (Laurentian University), and O. van Bremen (GSC). The authors are most grateful to numerous industry and academic partners for access to samples and data, and for scientific support. The staff of the Geochronology Laboratories at the Geological Survey of Canada in Ottawa are thanked for their assistance in generating the ID-TIMS and SHRIMP U-Pb data. M. Boutin contributed to drafting some of the figures. Thanks to D. Hnatyshin and J. Moorhead for their constructive review of the manuscript.

REFERENCES

Allard, G.O., 2002, Roof rock assimilation in the Doré Lake Complex and its influence on vanadium concentration, in Taner, M.F., Riveros, P.A., Dutrizac, J.E., Gattrell, M., and Perron, L., eds., Vanadium—geology, processing and applications: Metallurgy and Materials Society, 41st Annual Conference of Metallurgists of Canadian Institute of Mining and Metallurgy, Montreal, Québec, Proceedings, p. 29−35.

Allard, G.O., Daigneault, R., and Gobeil, A., 1990, Part 2: Stratigraphic setting of the Chibougamau region; *In* Litho-tectonic framework and associated mineralization of the eastern extremity of the Abitibi Greenstone Belt, Quebec (IAGOD International geological 1990 meeting, Field Trip 3), *Edited by* J. Guha, E.H. Chown and R. Daigneault, Geological Survey of Canada, Open File 2158, p. 50–62.

Allard, G.O., Caty, J.L, Chown, E.H., Cimon, J., Gobeil, A., and Baker, D., 1979, Stratigraphie et métallogénie de la région de Chibougamau; Association minéralogique du Canada, Congrès de Québec (Université Laval), Livret guide excursion B1, 94 p.

Barnes, S.-J., Couture, J.-F., Poitras, A., and Tremblay, C., 1993, Les éléments du groupe du platine dans la partie Québécoise de la ceinture de roches vertes de l'Abitibi: Ministère de l'Énergie et des Ressources du Québec, ET 91-04, 100 p.

Bedeaux, P., Pilote, P., Daigneault, R., and Rafini, S., 2017, Synthesis of the structural evolution and associated gold mineralization of the Cadillac Fault, Abitibi, Canada: Ore Geology Reviews, v. 42, p. 49–69.

Bélanger, J., 1979, Étude de la zone de transition entre la Formation de Waconichi et la Formation de Gilman, Groupe de Roy, Chibougamau, Québec: Unpublished MSc thesis, Université du Québec à Chicoutimi, Saguenay, Canada, 83 p.

Berthelot, P., 2008, Rapport de la campagne de forage 2007 sur la propriété Kinojévis, Secteur St-Mathieu, Ressources Cartier: Ministère des Ressources naturelles, GM63531, 138 p.

Bleeker, W., 2012, Lode gold deposits in ancient deformed and metamorphosed terranes: The role of extension in the formation of Timiskaming basins and large gold deposits, Abitibi greenstone belt—a discussion: Ontario Geological Survey Open File Report 6280, p. 47-1–47-12.

Bleeker, W., and Parrish, R.R., 1996, Stratigraphy and U – Pb zircon geochronology of Kidd Creek: implications for the formation of giant volcanogenic massive sulphide deposits and the tectonic history of the Abitibi greenstone belt: Canadian Journal of Earth Sciences, v. 33, p. 1213–1231.

Bleeker, W., Parrish, R.R., and Sager-Kinsman, A., 1999, High-precision U-Pb geochronology of the late Archean Kidd Creek deposit and Kidd volcanic complex: Economic Geology Monograph 10, p. 43−70.

Boily, M., Pilote, P., and Raillon, H., 1989, La métallogénie des métaux de haute technologie en Abitibi-Témiscamingue: Ministère de l'Énergie et des Ressources naturelles, MB 89-29, 108 p., 1 map.

Boily-Auclair, E., Mercier-Langevin, P., Ross, P.-S., and Pitre, D., 2020, Stratigraphic setting of the LZ5 and Ellison mineralized zones, LaRonde Zone 5 Project, Doyon-Bousquet-LaRonde mining camp, Abitibi, Quebec: Geological Survey of Canada, Open File 8712, p. 57−73.

Boily-Auclair, E., Mercier-Langevin, P., Ross, P.-S., and Pitre, D., 2022, Alteration and ore assemblages of the LaRonde Zone 5 (LZ5) deposit and Ellison mineralized zones, Doyon-Bousquet-LaRonde mining camp, Abitibi, Quebec: Geological Survey of Canada, Open File 8867, 48 p.

Card, K.D., 1990, A review of the Superior Province of the Canadian Shield, a product of Archean accretion: Precambrian Research, v. 48, p. 99–156.

Card, K.D., and Poulsen, K.H., 1998, Geology and mineral deposits of the Superior Province of the Canadian Shield: Geological Survey of Canada, Geology of Canada No. 7, p. 13−194.

Carrier, A., Jébrak, M., Angelier, J., and Holyland, P., 2000, The Silidor deposit, Rouyn-Noranda district, Abitibi belt: Geology, structural evolution and paleostress modeling of an Au quartz vein-type deposit in an Archean trondhjemite: Economic Geology, v. 95, p. 1049−1065.

Cattalani, S., Barrett, T.J., MacLean, W.H., Hoy, L., Hubert, C., and Fox, J.S., 1993, Métallogenèse des gisements Horne et Quemont (région de Rouyn-Noranda): Ministère des Ressources naturelles, ET 90-07, 121 p., 4 maps.

Chown, E.H., Daigneault, R., Mueller, W., and Mortensen, J.K., 1992, Tectonic evolution of the Northern Volcanic Zone, Abitibi belt, Quebec; Canadian Journal of Earth Sciences, v. 29, p. 2211–2225.

Cimon, J., and Gobeil, A., 1976, The Stella Formation, its implication for the genesis and the relative age of the mineralization in the Chibougamau mining camp; Ministère des Ressources naturelles, GM 69596, 25 p.

Corfu, F., 1993, The evolution of the southern Abitibi greenstone belt in light of precise U-Pb geochronology: Economic Geology, v. 88, p. 1323−1340.

Côté-Mantha, O., Daigneault, R., Gaboury, D., Chartrand, F., and Pilote, P., 2012, Geology, alteration, and origin of Archean Au-Ag-Cu mineralization associated with the synvolcanic Chibougamau pluton: The Brosman prospect, Abitibi greenstone belt, Canada: Economic Geology, v. 107, p. 909–934.

Couture, J.-F., and Goutier, J., 1996, Métallogénie et évolution tectonique de la région de Rouyn-Noranda: Ministère des Ressources naturelles, MB 96-06, 102 p.

Couture, J.F., and Pilote, P., 1993, The geology and alteration patterns of a disseminated, shear zone-hosted mesothermal gold deposit; the Francoeur 3 deposit, Rouyn-Noranda, Quebec: Economic Geology, v. 88, p. 1664−1684.

Cumming, G.L., and Richards, J.R., 1975, Ore lead isotope ratios in a continuously changing Earth: Earth and Planetary Science Letters, v. 28, p. 155–171.

Daigneault, R., and Allard, G.O., 1990, Le Complexe du Lac Doré et son environnement géologique (région de Chibougamau–sous-province de l'Abitibi); Ministère de l'Énergie, des Mines et des Ressources du Québec, MM 89-03, 275 p.

Daigneault, R., and Archambault, G., 1990, Les grands couloirs de déformation de la sous-

province de l'Abitibi: The Canadian Institute of Mining and Metallurgy, Special Volume 43, p. 43–64.

Daigneault, R., St-Julien, P., and Allard, G.O., 1990, Tectonic evolution of the northeast portion of the Archean Abitibi greenstone belt, Chibougamau area, Quebec: Canadian Journal of Earth Sciences, v. 27, p. 1714–1736.

Daigneault, R., Mueller, W.U., Chown, E.H., 2002, Oblique Archean subduction: accretion and exhumation of an oceanic arc during dextral transpression, Southern Volcanic Zone, Abitibi Subprovince Canada: Precambrian Research, v. 115, p. 261-290.

Daigneault, R., Mueller, W.U., and Chown, E.H., 2004, Abitibi greenstone belt plate tectonics: The diachronous history of arc development, accretion and collision: The Precambrian Earth: Tempos and Events, Elsevier, p. 88−103.

David, J., 2020, Datations U-Pb dans les provinces du Supérieur et de Churchill effectuées au GEOTOP en 2017-2018: Ministère des Ressources naturelles et de la Faune, MB 2020-05, 29 p.

David, J., Davis, D.W., Dion, C., Goutier, J., Legault, M., and Roy, P., 2007, Datations U-Pb effectuées dans la Sous-province de l'Abitibi en 2006-2006: Ministère des Ressources naturelles et de la Faune, RP 2007-01, 17 p.

David, J., Vaillancourt, D., Bandyayera, D., Simard, M., Goutier, J., Pilote, P., Dion, C., and Barbe, P., 2011, Datations U-Pb effectuées dans les sous-provinces d'Ashuanipi, de La Grande, d'Opinaca et d'Abitibi en 2008-2009: Ministère des Ressources naturelles et de la Faune, RP 2010-11, 37 p.

David, J., Simard, M., Bandyayera, D., Goutier, J., Hammouche, H., Pilote, P., Leclerc, F., and Dion, C., 2012, Datations U-Pb effectuées dans les provinces du Supérieur et de Churchill en 2010-2011: Ministère des Ressources naturelles et de la Faune, RP 2012-01, 33 p.

David, J., Pilote, P., Hammouche, H., Leclerc, F., and Talla Takam, F., 2018, Datations U-Pb dans la Province du Supérieur effectuées au GEOTOP en 2013-14: Ministère des Ressources naturelles, RP 2017-03, 43 p.

Davis, D.W., 2002, U-Pb geochronology of Archean metasedimentary rocks in the Pontiac and Abitibi subprovinces, Quebec, constraints on timing, provenance and regional tectonics: Precambrian Research, v. 115, p. 97-117.

Davis, D., David, J., Dion, C., Goutier, J., Bandyayera, D., Rhéaume, P., and Roy, P., 2005, Datations U-Pb effectuées en support aux travaux de cartographie géologique et de compilation géoscientifique du SGNO (2003-2004): Ministère des Ressources naturelles et de la Faune, RP 2005-02, 20 p.

Davis, D.W., Simard, M., Hammouche, H., Bandyayera, D., Goutier, J., Pilote, P., Leclerc, F., and

Dion, C., 2014, Datations U-Pb effectuées dans les provinces du Supérieur et de Churchill en 2011-2012: Ministère de l'Énergie et des Ressources naturelles, RP 2014-05, 62 p.

Davis, W.J., McNicoll, V.J., Bellerive, D.R., Santowski, K., and Scott, D.J., 1997, Modified chemical procedures for the extraction and purification of uranium from titanite, allanite and rutile in the Geochronology Laboratory, Geological Survey of Canada: Radiogenic Age and Isotopic Studies, Report 10: Geological Survey of Canada, Current Research 97-F, p. 33–35.

Davis, W.J., Pestaj, T., Rayner, N., and McNicoll, V.M., 2019, Long-term reproducibility of $^{207}Pb/^{206}Pb$ age at the GSC SHRIMP lab based on the GSC Archean reference zircon z1242: Geological Survey of Canada, Scientific Presentation 111, 1 poster.

Dimroth, E., Imreh, L., Rocheleau, M., and Goulet, N., 1982, Evolution of the south-central part of the Archean Abitibi belt, Quebec. Part I: Stratigraphy and paleogeographic model: Canadian Journal of Earth Sciences, v. 19, p. 1729–1758.

Dimroth, E., Imreh, L., Goulet, N., and Rocheleau, M., 1983, Evolution of the south-central segment of the Archean Abitibi belt, Quebec. Part II: Tectonic evolution and geomechanical model: Canadian Journal of Earth Sciences, v. 20, p. 1355–1373.

Dion, C., and Maltais, G., 1998, La mine d'or Joe Mann: Ministère des Ressources naturelles du Québec, DV 98-03, p. 125−131.

Dubé, B., and Gosselin, P, 2007, Greenstone-hosted quartz-carbonate vein deposits, in Goodfellow, W.D., ed., Mineral deposits of Canada: A synthesis of major deposit-types, district metallogeny, the evolution of geological provinces, and exploration methods: Mineral Deposits Division, Geological Association of Canada, Special Publication no. 5, p. 49–73.

Dubé, B., and Guha, J., 1992, Relationship between northeast-trending regional faults and Archean mesothermal gold-copper mineralization: Cooke mine, Abitibi greenstone belt, Quebec, Canada: Economic Geology, v. 87, p. 1525−1540.

Dubé, B., and Mercier-Langevin, P., 2020. Gold deposits of the Archean Abitibi greenstone belt, Canada: Society of Economic Geologists Special Publication 23, p. 669–708.

Dubé, B., Poulsen K.H., and Guha, J., 1989, The effects of layer anisotropy on auriferous shear zones: The Norbeau mine, Quebec: Economic Geology, v. 84, p. 871–878.

Dubé, B., Gosselin, P., Mercier-Langevin, P., Hannington, M., and Galley, A., 2007a, Gold-rich volcanogenic massive sulphide deposits: Geological Association of Canada, Mineral Deposits Division Special Publication 5, p. 75–94.

Dubé, B., Mercier-Langevin, P., Hannington, M., Lafrance, B., Gosselin, G., and Gosselin, P., 2007b, The LaRonde Penna world-class Au-rich volcanogenic massive sulphide deposit, Abitibi, Quebec: Mineralogy and geochemistry of alteration and implications for genesis and exploration:

Economic Geology, v. 102, p. 633−666.

Dubé, B., Mercier-Langevin, P., Kjarsgaard, I., Hannington, M., Bécu, V., Côté, J., Moorhead, J., Legault, M., and Bédard, N., 2014, The Bousquet 2-Dumagami world-class Archean Au-rich volcanogenic massive sulfide deposit, Abitibi, Quebec: Metamorphosed submarine advanced argillic alteration footprint and genesis: Economic Geology, v. 109, p. 121−166.

Ducharme, Y., Stevenson, R.K., and Machado, N., 1997, Sm-Nd geochemistry and U-Pb geochronology of the Preissac and La Mothe leucogranites, Abitibi subprovince: Canadian Journal of Earth Sciences, v. 34, p. 1059−1071.

Feng, R., and Kerrich, R., 1991, Single zircon age constraints on the tectonic juxtaposition of the Archean Abitibi greenstone belt and Pontiac subprovince, Quebec, Canada: Geochimica et Cosmochimica Acta, v. 55, p. 3437–3441.

Ford, G.M., 1974, Campbell Chibougamau Mines Ltd - Mainland property, assessment report; Ministère de l'Énergie et des Ressources, Québec, GM-30763.

Frieman, B.M., Kuiper, Y.D., Kelly, N.M., Monecke, T., and Kylander-Clark, A., 2017, Constraints on the geodynamic evolution of the southern Superior Province: U-Pb LA-ICP-MS analysis of detrital zircon in successor basins of the Archean Abitibi and Pontiac subprovinces of Ontario and Quebec, Canada: Precambrian Research, v. 292, p. 398−416.

Galley, A.G., Watkinson, D.H., Jonasson, I.R., and Riverin, G., 1995, The subseafloor formation of volcanogenic massive sulphide: Evidence from the Ansil deposit, Rouyn-Noranda, Canada: Economic Geology, v. 90, p. 2006−2017.

Galley, A.G., Hannington, M.D., and Jonasson, I.R., 2007, Volcanogenic massive sulphide deposits, in Goodfellow, W.D., ed., Mineral deposits of Canada: A synthesis of major deposit-types, district metallogeny, the evolution of geological provinces, and exploration methods: Mineral Deposits Division, Geological Association of Canada, Special Publication no. 5, p. 141–161.

Galley, A.G., and Mercier-Langevin, P., 2025, Mineralization and alteration at the Doyon deposit, Doyon-Bousquet-LaRonde mining camp, Québec, Canada: Example of an Archean subsea-floor Au(-Cu) porphyry-epithermal-style system: Geological Survey of Canada, Open File 9238, 141 p.

Gauthier, N., Rocheleau, M., Kelly, D., and Gagnon, Y., 1990, Controls on the location of gold mineralization within the Cadillac tectonic zone, Rouyn-Beauchastel segment, Abitibi belt, Quebec: CIM Special Volume 43, p. 185−198.

Gibson, H.L., and Galley, A.G., 2007, Volcanogenic massive sulphide deposits of the Archean, Noranda district, Quebec: Geological Association of Canada, Mineral Deposits Division, Special Publication 5, p. 533-552.

Gibson, H.L., and Watkinson, D.H., 1990, Volcanogenic massive sulphide deposits of the Noranda cauldron and shield volcano, Quebec: CIM Special Volume 43, p. 119−132.

Goldie, R., Kotila, B., and Seward, D., 1979, The Don Rouyn mine: an Archean porphyry copper deposit near Noranda, Quebec: Economic Geology, v. 74, p. 1680–1684.

Goutier, J., 1997, Géologie de la région de Destor (SNRC 32D/07-200-0201): Ministère de l'Énergie et des Ressources naturelles, RG 96-13, 37 p., 1 map.

Goutier, J., 2017, Chapitre 5: (Day 3 – Part I) Geology of the Blake River Group: Geological Survey of Canada, Open File 8317, p. 31−39.

Goutier, J., Dion, C., Legault, M., Ross, P.-S., McNicoll, V.J., de Kemp, E., Percival, J.A., Monecke, T., Bellefleur, G., Mercier-Langevin, P., Lauzière, K., Thurston, P., and Ayer, J., 2007, Units in the Blake River Group: Correlations, geometry and mineral potential: Résumés des conférences et des photoprésentations, Québec Exploration 2007, p. 99.

Goutier, J., McNicoll, V., Dion, C., Lafrance, B., Legault, M., Ross, P.-S., Mercier-Langevin, P., Cheng, L.-Z., de Kemp, E., and Ayer, J., 2009, L'impact du Plan cuivre et de l'IGC-3 sur la géologie de l'Abitibi et du Groupe de Blake River: Ministère des Ressources naturelles et de la Faune, GM 64195, p. 9−13.

Goutier, J., Mercier-Langevin, P., McNicoll, V., and Ayer, J., 2010, The Abitibi Subprovince: Its evolution and its VMS deposits – an overview: Geological Survey of Western Australia, Record 2010/20, p. 37−41.

Goutier, J., Ross, P.-S., McNicoll, V., Dion, C., Mercier-Langevin, P., Thurston, P., Dubé, B., and Gibson, H., 2011, Day 1: Geology, stratigraphy and geochronology of the Blake River Group and relationships with VMS deposits: Geological Survey of Canada, Open File 6869, p. 10−21.

Guay, F., 2018, Minéralisation aurifères et déformation de l'indice aurifère « rive du lac Malartic », sous-province de l'Abitibi; unpublished M.Sc. thesis, Université du Québec à Chicoutimi, Chicoutimi, Canada, 136 p.

Guay, F., Pilote, P., Daigneault, R., and V. MicNicoll, 2018, Early gold-bearing quartz veins within the Rivière-Héva fault zone, Abitibi subprovince, Quebec, Canada: Canadian Journal of Earth Sciences, v. 55, p. 1139–1157.

Guha, J., Dubé, B., Pilote, P., Chown, E.H., Archambault, G., and Bouchard, G., 1988, Gold mineralization patterns in relation to the lithologic and tectonic evolution of the Chibougamau mining district, Quebec, Canada: Mineralium Deposita, v. 23, p. 293−298.

Guha, J., Chown, E.H., Archambault, G., Barnes, S.-J., Brisson, H., Daigneault, R., Dion, C., Dube, B., Mueller, W., and Pilote, P., 1990, Metallogeny in relation to magmatic and structural evolution of an Archaean greenstone belt; Chibougamau mining district: University of Western

Australia 24: p. 121–166.

Hannington, M.D., Barrie, C.T., and Bleeker, W., 1999, The giant Kidd Creek volcanogenic massive sulfide deposit, western Abitibi subprovince, Canada: Economic Geology Monograph 10, p. 1−30.

Houlé, M., Lesher, C.M., and Préfontaine, S., 2017, Physical volcanology of komatiites and Ni-Cu-(PGE) deposits of the southern Abitibi greenstone belt: Reviews in Economic Geology, v. 19, p. 103−132.

Jaffey, A.H., Flynn, K.F., Glendenin, L.E., Bentley, W.C., and Essling, A.M., 1971, Precision measurement of half-lives and specific activities of 235U and 238U: Physical Review C, v. 4, p. 1889–1906.

Joanisse, A., 1998, Géochronologie des minéralisations filoniennes à Cu-Au retrouvées dans le Complexe du Lac Doré: Unpublished M.Sc. thesis, Université du Québec à Montréal, Montréal, Canada, 51 p.

Kirkham, R.V., 1972, Geology of copper and molybdenum deposits; Survey of Canada, Paper 72-1, p. 82–87.

Knuckey, M.J., Comba, C.D.A., and Riverin, G., 1982, Structure, metal zoning and alteration at the Millenbach deposit, Noranda, Quebec: Geological Association of Canada, Special Paper 25, p. 255−295.

Krogh, T.E., 1982. Improved accuracy of U-Pb zircon ages by the creation of more concordant systems using an air abrasion technique: Geochimica et Cosmochimica Acta, v. 46, p. 637−649.

Krushnisky, A., Mercier-Langevin, P., Ross, P.-S., Goutier, J., McNicoll, Moore, L., Monecke, T., Jackson, S.E., Yang, Z., Petts, D.C., and Pilote, C., 2023, Geology and controls on gold enrichment at the Horne 5 deposit and implications for the architecture of the gold-rich Horne volcanogenic massive sulfide complex, Abitibi greenstone belt, Canada: Economic Geology, v. 118, p. 285−318.

Kuiper, D., 2010, Geology, geochemistry, and geochronology of the Dufault, Séguin and Horseshoe gabbroic-dioritic intrusions, Blake River Group (2704-2695 Ma), Abitibi Subprovince, Québec: Unpublished M.Sc. thesis, Laurentian University, Sudbury, Canada, 130 p.

Lafrance, B., Moorhead, J., and Davis, D., 2003, Cadre géologique du camp minier de Doyon-Bousquet-LaRonde: Ministère des Ressources naturelles, de la Faune et des Parcs du Québec, ET 2002-07, 43 p., 1 map.

Lafrance, B., Davis, D.W., Goutier, J., Moorhead, J., Pilote, P., Mercier-Langevin, P., Dubé, B., Galley, A.G., and Mueller, W.U., 2005, Nouvelles datations isotopiques dans la portion québécoise du Groupe de Blake River et des unités adjacentes: Ministère des Ressources naturelles et de la Faune, RP 2005-01(A), 15 p.

Lafrance, V., 2015, Caractérisation de l'environnement géologique de la mine Marbridge, Abitibi, Québec: Unpublished M.Sc. thesis, Université du Québec à Chicoutimi, Saguenay, Canada, 140 p.

Leclerc, F., Roy, P., Fallara, F., McNicoll, V., Keating, P., Houle, P., Cheng, L.Z., Rabeau, O., Harris, L.B., and Bédard, J.H., 2009, Application des nouvelles technologies en géologie régionale: Impacts dans le secteur de Chibougamau: Ministère des Ressources naturelles et de la Faune, MB 2009-09, p. 37−40.

Leclerc, F., Harris, L.B., Bédard, J.H., van Breemen, O., and Goulet, N., 2012, Structural and stratigraphic controls on magmatic, volcanogenic, and shear zone-hosted mineralization in the Chapais-Chibougamau mining camp, northeastern Abitibi, Canada: Economic Geology, v. 107, p. 963–989.

Ludwig, K.R., 2009, SQUID 2: A User's Manual, rev. 12 Apr, 2009: Berkeley Geochronology Center, Special Publication No. 5, 110 p.

Ludwig, K.R., 2012, Isoplot 3.75–4.15, A geochronological toolkit for Microsoft Excel: Berkeley Geochronology Center Special Publication No. 5, 75 p.

Magnan, M., Pilote, P., and Daigneault, R., 1998, Minéralisations et altérations à la mine Copper Rand, Chibougamau; Ministère des Ressources naturelles, ET 98-01, 34 p.

Mattinson, J., 2005, Zircon U-Pb chemical abrasion (CA-TIMS) method: Combined annealing and multi-step partial dissolution analysis for improved precision and accuracy of zircon ages: Chemical Geology, v. 220, p. 47–66.

McNicoll, V., Dubé, B., Goutier, J., Mercier-Langevin, P., Dion, C., Monecke, T., Ross, P.-S., Thurston, P., Pilote, P., Bédard, J., Leclerc, F., Bécu, V., Percival, J., Legault, M., Gibson, H., and Ayer, J., 2008, Nouvelles datations U-Pb dans le cadre du projet ICG-3 Abitibi/Plan cuivre : incidences pour l'interprétation géologique et l'exploration des métaux usuels: Ministère des Ressources naturelles et de la Faune, DV 2008-06, p. 40.

McNicoll, V., Goutier, J., Dubé, B., Mercier-Langevin, P., Ross, P.-S., Dion, C., Monecke, T., Legault, M., Percival, J., and Gibson, H., 2014, U-Pb geochronology of the Blake River Group, Abitibi greenstone belt, Quebec, and implications for base metal exploration: Economic Geology, v. 109, p. 27–59.

Mercier-Langevin, P., Dubé, B., Hannington, M., David, D.W., Lafrance, B., and Gosselin, G., 2007, The LaRonde Penna Au-rich volcanogenic massive sulfide deposit, Abitibi greenstone belt, Quebec: Part I. Geology and geochronology: Economic Geology, v. 102, p. 585–609.

Mercier-Langevin, P., Dubé, B., Hannington, M., Goutier, J., McNicoll, V., Dion, C., Monecke, T., Gibson, H., Bécu, V., and Galley, A., 2009, Les sulfures massifs volcanogènes de la Sous-

province de l'Abitibi; aspects principaux et implications pour l'exploration, avec accent sur le Groupe de Blake River et les sulfures massifs volcanogènes riches en or: Ministère des Ressources naturelles, MB 2009-09, p. 23-27.

Mercier-Langevin, P., Goutier, J., Ross, P.-S., McNicoll, V., Monecke, T., Dion, C., Dubé, B., Thurston, P., Bécu, V., Gibson, H., Hannington, M., and Galley, A., 2011a, The Blake River Group of the Abitibi greenstone belt and its unique VMS and gold-rich VMS endowment: Geological Survey of Canada, Open File 6869, 61 p.

Mercier-Langevin, P., Hannington, M.D., Dubé, B., Bécu, V., 2011b, The gold content of volcanogenic massive sulphide deposits: Mineralium Deposita, v. 46, p. 509-539.

Mercier-Langevin, P., Gibson, H.L., Hannington, M.D., Goutier, J., Monecke, T., Dubé, B., and Houlé, M.G., 2014a, A special issue on Archean magmatism, volcanism and ore deposits: Part 2. Volcanogenic massive sulfide deposits – Preface: Economic Geology, v. 109, p. 1−9.

Mercier-Langevin, P., Lafrance, B., Bécu, V., Dubé, B., Kjarsgaard, I., and Guha, J., 2014b, The Lemoine auriferous volcanogenic massive sulfide deposit, Chibougamau camp, Abitibi greenstone belt, Québec, Canada: geology and genesis: Economic Geology, v. 109, p. 231−269.

Mercier-Langevin, P., Goutier, J., and Dubé, B., 2017a, Precious and base metal deposits of the southern Abitibi greenstone belt, Superior Province, Canada: A field trip to the 14th Biennial Society for Geology Applied to Mineral Deposits meeting: Geological Survey of Canada, Open File 8317, 86 p.

Mercier-Langevin, P., Simard, M., Dubuc, R., Côté, J., Doucet, P., Daigneault, R., and Gaboury, D., 2017b, Geology of the Lapa orogenic gold deposit: Reviews in Economic Geology, v. 19, p. 247−262.

Mercier-Langevin, P., Lawley, C.J.M., Castonguay, S., Dubé, B., Bleeker, W., Pinet, N., Bécu, V., Pilote, J.-L., Jackson, S.E., Wodicka, N., Honsberger, I.W., Davis, W.J., Petts, D.C., Yang, Z., Jautzy, J., and Lauzière, K., 2020, Targeted Geoscience Initiative 5, Gold Project: A summary of contributions to the understanding of Canadian gold systems: Geological Survey of Canada, Open File 8712, p. 1-30.

Mercier-Langevin, P., Dubé, B., et Fortin, D., 2021a, Le camp minier Doyon-Bousquet-LaRonde : Apercu historique et géologique d'un camp exceptionnel : Ressources & Industrie – Mines, v. 7, No. 1, p. 46-63.

Mercier-Langevin P., Dubé, B., and Fortin, D., 2021b, The Doyon-Bousquet-LaRonde mining camp – Historical and geological overview of an exceptional camp: Resources & Industry – Mines, v. 2, p. 44−61.

Mercier-Langevin, P., Dubé, B., Houlé, M.G., Bécu, V., Sappin, A.-A., Pilote, J.-L., and Castonguay, S., 2022, Métallogénie de la ceinture de roches vertes de l'Abitibi, Canada: In S.

Decrée (ed.), Ressources Métalliques 2 Cadre Géodynamique et Exemples Remarquables dans le Monde, Série Sciences – Géosciences – Ressources Naturelles : la Recherche Fondamentale Appliquée, ISTE Éditions, Londres, p. 61−134.

Mercier-Langevin, P., Dubé, B., Houlé, M.G., Bécu, V., Sappin, A.-A., Pilote, J.-L., and Castonguay, S., 2023, Metallogeny of the Abitibi greenstone belt, Canada: In S. Decrée (ed.), Metallic Resources 2 Geodynamic Settings and Remarkable Examples of the World, Sciences – Geosciences – Natural Resources Series: Applied Fundamental Research, ISTE Editions, London, p. 63–142.

Mercier-Langevin, P., Creaser, R., Goutier, J., and Kjarsgaard, I., 2024, Rhenium-rich molybdenite and Re-Os age of the Archean porphyry-style Don Rouyn deposit, Abitibi greenstone belt, Rouyn-Noranda, Québec: Geological Survey of Canada, Open File 9161, 31 p.

Monecke, T., Gibson, H., and Goutier, J., 2017a, Volcanogenic massive sulphide deposits of the Noranda camp: Reviews in Economic Geology, v. 19, p. 169−223.

Monecke, T., Mercier-Langevin, P., Dubé, B., and Frieman, B., 2017b, Geology of the Abitibi greenstone belt: Reviews in Economic Geology, v. 19, p. 7−49.

Mortensen, J.K., 1993a, U-Pb geochronology of the eastern Abitibi subprovince. Part 1: Chibougamau-Matagami-Joutel region: Canadian Journal of Earth Sciences, v. 30, p. 11–28.

Mortensen, J.K., 1993b, U-Pb geochronology of the eastern Abitibi subprovince. Part 2: Noranda-Kirkland Lake area: Canadian Journal of Earth Sciences, v. 30, p. 29–41.

Mueller, W.U., Daigneault, R., Mortensen, J.K., and Chown, E.H., 1996, Archean terrane docking: upper crust collision tectonics, Abitibi greenstone belt, Quebec, Canada: Tectonophysics, v. 265, p. 127−150.

Mueller, W.U., Stix, J., Corcoran, P.L., and Daigneault, R., 2009, Subaqueous calderas in the Archean Abitibi greenstone belt: An overview and new ideas: Ore Geology Reviews, v. 35, p. 4-46.

Mueller, W.U., Friedman, R., Daigneault, R., Moore, L., and Mortensen, J., 2012, Timing and characteristics of the Archean subaqueous Blake River megacaldera complex, Abitibi greenstone belt, Canada: Precambrian Research, v. 214-215, p. 1−27.

Parrish, R.R., Roddick, J.C., Loveridge, W.D., and Sullivan, R.W., 1987, Uranium-lead analytical techniques at the Geochronology Laboratory, Geological Survey of Canada: Radiogenic age and isotopic studies, Report 1: Geological Survey of Canada Paper 87-2, p. 3–7.

Percival, J.A., 2007, Geology and metallogeny of the Superior Province, Canada, in Goodfellow, W.D., ed., Mineral deposits of Canada: A synthesis of major deposit-types, district metallogeny, the evolution of geological provinces, and exploration methods: Mineral Deposits Division,

Geological Association of Canada, Special Publication no. 5, p. 903–928.

Piette-Lauzière, N., Guilmette, C., Bouvier, A., Perrouty, S., Pilote, P., Gaillard, N., Lypaczewski, P., Linnen, R.L., and Olivo, G.R., 2019, The timing of prograde metamorphism in the Pontiac Subprovince, Superior craton; implications for Archean geodynamics and gold mineralization: Precambrian Research, v. 320, p. 111−136.

Pilote, P., 1987, Stratigraphie, structure et gîtologie de la région du lac Berrigan, canton de McKenzie: Ministère de l'Énergie et des Ressources, ET 86-02, 34 p., 1 map.

Pilote, P. (ed.), 1995, Metallogenic evolution and geology of the Chibougamau area – from porphyry Cu-Au-Mo to mesothermal lode gold deposits: Geological Survey of Canada, Open File 3143, 154 p.

Pilote, P., and Guha, J., 1995, Metallogeny of the Eastern extremity of the Abitibi belt; *in* Metallogenic evolution and geology of the Chibougamau area - from porphyry Cu-Au-Mo to mesothermal lode gold deposits, (ed.) P. Pilote: Geological Survey of Canada, Open File 3143, p. 31–43.

Pilote, P., Robert, F., Sinclair, W.D., Kirkham, R.V., and Daigneault, R., 1996, Thème 3: Minéralisations de type porphyrique et filoniennes dans le complexe du lac Doré – Les secteurs du Lac Clark et de l'île Merrill: Ministère des Ressources naturelles, MB 96-14, p. 69−92.

Pilote, P., Dion, C., Joanisse A., David, J., Machado, N., Kirkham, R.V., and Robert, F., 1997, Géochronologie des minéralisations d'affiliation magmatique de l'Abitibi, secteurs Chibougamau et de Troilus-Frotet : implications géotectoniques: Ministère des Ressources naturelles, DV 97-03, p. 47.

Pilote, P., Robert, F., Kirkham, R.V., Daigneault, R., and Sinclair, W.D., 2006, Minéralisations de type porphyrique et filoniennes dans le Complexe du Lac Doré – Les secteurs du Lac Clark et de l'Île Merrill: Geological Association of Canada, Field trip guidebook B1, p. 89–108.

Pilote, P., McNicoll, V., Daigneault, R., and Moorhead, J., 2009, Géologie et nouvelles corrélations dans la partie ouest du Groupe de Malartic et dans le Groupe de Kinojévis, Québec: Ministère de l'Énergie et des Ressources naturelles, MB 2009-09, p. 55−60.

Pilote, P., Daigneault, R., David, J., and McNicoll, V., 2014, L'architecture des groupes de Malartic, de Piché et de Cadillac et de la Faille Cadillac, Abitibi : révision géologique, nouvelles datations et interprétations: Ministère de l'Énergie et des Ressources naturelles, DV 2015-03, p. 37.

Pilote, P., Daigneault, R., and Moorhead, J., 2018, Géologie de la région de Barraute Ouest, Sous-province de l'Abitibi, région de l'Abitibi-Témiscamingue, Québec, Canada: Ministère des Ressources naturelles et de la Faune, sheet 32C05-200-0201, BG 2018-05, 2 maps.

Pilote, P., Marleau, J., David, J., and Daigneault, R., 2019, Géologie de la région de Barraute-Est, Sous-province de l'Abitibi, région de l'Abitibi-Témiscamingue, Québec, Canada: Ministère de l'Énergie et des Ressources naturelles, sheet 32C05-200-0202, BG 2019-06.

Poulsen, K.H., 2017, The Larder Lake-Cadillac break and its gold districts: Reviews in Economic Geology, v. 19, p. 133–167.

Powell, W.G., Carmichael, D.M., and Hodgson, C.J., 1995, Conditions and timing of metamorphism in the southern Abitibi greenstone belt, Quebec: Canadian Journal of Earth Sciences, v. 32, p. 787-805.

Riopel, J., Hubert, C., Cattalani, S., Barrett, T.J., and Hoy, L.D., 1995, Gîtologie, structure et géochimie du gisement de sulfures massifs Mobrun (district de Rouyn-Noranda): Ministère des Ressources naturelles, ET 92-02, 142 p.

Robert, F., 1989, Internal structure of the Cadillac tectonic zone southeast of Val d'Or, Abitibi greenstone belt, Quebec: Canadian Journal of Earth Sciences, v. 26, p. 2661–2675.

Robert, F., 1994, Timing relationships between Cu-Au mineralization, dykes and shear zones in the Chibougamau camp, northeastern Abitibi: Geological Survey of Canada, Current Research 1994-C, p. 287−294.

Robert, F., and Poulsen, K.H., 1997, World-class Archean gold deposits in Canada: An overview: Australian Journal of Earth Sciences, v. 44, p. 329–351.

Robert, F., Poulsen, K.H., Cassidy, K.F., and Hodgson, C.J., 2005, Gold metallogeny of the Superior and Yilgarn Cratons: Economic Geology 100th Anniversary Volume, p. 1001–1033.

Roddick, J.C., 1987, Generalized numerical error analysis with applications to geochronology and thermodynamics: Geochimica Cosmochimica et Acta, v. 51, p. 2129–2135.

Ross, P.-S., Percival, J.A., Mercier-Langevin, P., Goutier, J., McNicoll, V.J., and Dubé, B., 2007, Intermediate to mafic volcaniclastic units in the peripheral Blake River Group, Abitibi greenstone belt, Québec: origin and implications for volcanogenic massive sulphide exploration: Geological Survey of Canada, Current Research 2007-C3, 25 p.

Ross, P.-S., Goutier, J., Percival, J., Mercier-Langevin, P., and Dubé, B., 2008, New volcanological and geochemical observations from the Blake River Group, Abitibi greenstone belt, Quebec: the D'Alembert tuff, the Stadacona unit, and surrounding lavas: Geological Survey of Canada, Current Research 2008-17, 24 p.

Ross, P.-S., Goutier, J., Mercier-Langevin, P., and Dubé, B., 2011a, Basaltic to andesitic volcaniclastic rocks in the Blake River Group, Abitibi greenstone belt: 1. Mode of emplacement in three areas: Canadian Journal of Earth Sciences, v. 48, p. 728–756.

Ross, P.-S., McNicoll, V., Goutier, J., Mercier-Langevin, P., and Dubé, B., 2011b, Basaltic to andesitic volcaniclastic rocks in the Blake River Group, Abitibi greenstone belt: 2. Origin, geochemistry, and geochronology: Canadian Journal of Earth Sciences, v. 48, p. 757–777.

Savoie, A., Trudel, P., Sauvé., P., Hoy, L., and Lao, K., 1991, Géologie de la mine Doyon (région de Cadillac): Ministère des Ressources naturelles, ET 90-05, 80 p.

SIGÉOM, carte interactive: https://sigeom.mines.gouv.qc.ca/signet/classes/I1108_afchCarteIntr

Simard, M., Gaboury, D., Daigneault, R., and Mercier-Langevin, P., 2013, Multistage gold mineralization at the Lapa Mine, Abitibi Subprovince: Insights into auriferous hydrothermal and metasomatic processes in the Cadillac-Larder Lake fault zone: Mineralium Deposita, v. 48, p. 883–905.

Sinclair, W.D., Pilote, P., Kirkham, R.V., Robert, F., and Daigneault, R., 1994, A preliminary report of porphyry Cu-Mo-Au and shear zone-hosted Cu-Au deposits in the Chibougamau area, Quebec: Geological Survey of Canada, Current Research 1994-C, p. 303−309.

Sircombe, K.N., 2004, AGEDISPLAY: an EXCEL workbook to evaluate and display univariate geochronological data using binned frequency histograms and probability density distributions: Computers & Geosciences, v. 30, p. 21–31.

Steiger, R.H., and Jäger, E., 1977, Subcommission on geochronology: Convention on the use of decay constants in geo-and cosmochronology: Earth and Planetary Science Letters, v. 36, p. 359–362.

Sterckx, S., 2018, Géochimie des roches volcaniques archéennes du Groupe de Blake River, ceinture de roches vertes de l'Abitibi, Québec: Unpublished M.Sc. thesis, Institut national de la recherche scientifique, Québec, Canada, 227 p.

Stern, R.A., 1997, The GSC Sensitive High Resolution Ion Microprobe (SHRIMP): analytical techniques of zircon U-Th-Pb age determinations and performance evaluation: in Radiogenic Age and Isotopic Studies, Report 10: Geological Survey of Canada, Current Research 1997-F, p. 1–31.

Stern, R.A., and Amelin, Y., 2003, Assessment of errors in SIMS zircon U–Pb geochronology using a natural zircon standard and NIST SRM 610 glass: Chemical Geology, v. 197, p. 111–146.

Taner, H., Williams-Jones, A.E., and Wood, S.A., 1998, The nature, origin and physicochemical controls on hydrothermal Mo-Bi mineralization in the Cadillac deposit, Quebec, Canada: Mineralium Deposita, v. 33, p. p. 579−590.

Théberge, L., Daigneault, R., Labbé, J.-Y., and Brisson, T., 1999, Reconnaissance de l'héritage volcanogène d'une minéralisation de sulfures massifs en zone de forte déformation : le cas type du gisement de la mine Langlois, Lebel-sur-Quévillon, Abitibi: Ministère des Ressources naturelles, MB 99-38, 53 p.

Tourigny, G., Hubert, C., Brown, A.C., Crépeau, R., Trudel, P., Hoy, L., and Kheang, L., 1992, Géologie de la mine Bousquet: Ministère de l'Énergie et des Ressources, ET 89-09, 99 p.

Trudel, P., Sauvé, P., Tourigny, G., Hubert, C., and Hoy, L., 1992, Synthèse des caractéristiques géologiques des gisements d'or de la région de Cadillac (Abitibi): Ministère de l'Énergie et des Ressources du Québec, report MM 91-01, 106 p.

Vite-Sanchez, O., Ross, P.-S., and Mercier-Langevin, P., 2024, Mafic to intermediate volcanic rocks of the Blake River Group, Abitibi greenstone belt, Canada: Geochemistry, petrogenesis and relation with VMS deposits: Precambrian Research 404 (May 2024) 107331.

Yergeau, D., Mercier-Langevin, P., Dubé, B., Malo, M., and Savoie, A., 2022a, The Westwood deposit, southern Abitibi greenstone belt, Canada: An Archean Au-rich polymetallic magmatic-hydrothermal system - Part I. Volcanic architecture, deformation, and metamorphism: Economic Geology, v. 117, p. 545–575.

Yergeau, D., Mercier-Langevin, P., Dubé, B., McNicoll, V., Jackson, S., Malo, M., and Savoie, A., 2022b, The Westwood deposit, southern Abitibi greenstone belt, Canada: An Archean Au-rich polymetallic magmatic-hydrothermal system – Part II. Hydrothermal alteration, mineralization, and geological model: Economic Geology, v. 117, p. 577–608.

York, D., 1969, Least-squares fitting of a straight line with correlated errors: Earth and Planetary Science Letters, v. 5, p. 320–324.

Table 1. Summary of age interpretations.

Sample	Interpreted age[(1)]	Number of analyses used (rejects)	Interpretation	Comment on age interpretation	MSWD[(2)]	POF[(3)]
Chibougamau area						
Leucotonalite 06-PR-246-A (z9418)	2701.7 ± 0.7 Ma (Z)	7	Crystallization age	Upper intercept age; lower intercept at 450 ± 83 Ma	0.58	0.71
Blondeau Formation, sandstone OVB-1 (z9678)	<2721 ± 3 Ma (Z)	1 (5)	Max.depositional age	$^{207}Pb/^{206}Pb$ date of concordant analysis		
Stella Formation, conglomerate OVB-3 (z9679)	<2704 ± 2 Ma (Z)	1 (5)	Max. depositional age	$^{207}Pb/^{206}Pb$ date of concordant analysis		
Intermineral porphyry dyke KQ-91-7 (z3611)	2715.2 ± 0.7 Ma (Z)	3	Crystallization age	Upper intercept age; lower intercept at origin	0.54	0.58
Val-d'Or-Malartic-Amos area						
Dubuisson Formation, felsic tuff PP-06-89 (z9341)	2708.0 ± 1.5 Ma (Z)	5 (4)	Crystallization age	Upper intercept age; lower intercept at 1089 ± 94 Ma	0.87	0.46
Dubuisson Formation, felsic tuff PP-06-117A (z9084)	2705 ± 3 Ma (Z)	1 (6)	Crystallization age	$^{207}Pb/^{206}Pb$ date of concordant analysis		
Lanaudière Formation, rhyolite PP-06-118A (z9085)	2716.2 ± 0.8 Ma (Z)	4 (1)	Crystallization age	Weighted average $^{207}Pb/^{206}Pb$ age	0.26	0.85
Lanaudière Formation, rhyolite PP-07-144 (z9439)	2719.0 ± 1.0 Ma (Z)	6 (3)	Crystallization age	Upper intercept age; lower intercept at origin	1.30	0.27
Deguisier Formation, intermediate tuff P8-6-D (z9630)	2719.4 ± 1.0 Ma (Z)	4 (2)	Crystallization age	Weighted average $^{207}Pb/^{206}Pb$ age	0.53	0.66
Deguisier Formation, rhyolite P8-41-C2 (z9629)	2718.5 ± 1.1 Ma (Z)	5 (1)	Crystallization age	Upper intercept age; lower intercept at 408 ± 59 Ma	1.05	0.37
Tonalite dyke PP-07-143 (z9508)	2718.5 ± 0.8 Ma (Z)	5 (1)	Crystallization age	Weighted average $^{207}Pb/^{206}Pb$ age	0.43	0.79
La Pause pluton, tonalite-granodiorite PP-06-64A (z9086)	2709.8 ± 1.0 Ma (Z)	3 (3)	Crystallization age	Weighted average $^{207}Pb/^{206}Pb$ age	0.54	0.58
	2656.4 ± 9.3 Ma (T)	4	Late disturbance	Upper intercept age; lower intercept at origin	0.30	0.83
Caste Formation, conglomerate KI-07-09 (z9920)	<2697 ± 3 Ma (Z)	1 (13)	Max. depositional age	$^{207}Pb/^{206}Pb$ date of concordant analysis		
Rouyn-Noranda area						
R.M. Nickel gabbro 06-CD-3037 (z9026)	2695.0 ± 1.0 Ma (Z)	4 (2)	Crystallization age	Weighted average $^{207}Pb/^{206}Pb$ age	0.69	0.56
Dufresnoy gabbro 07-PCT-014 (z9314)	2697.9 ± 0.8 Ma (Z)	4 (1)	Crystallization age	Weighted average $^{207}Pb/^{206}Pb$ age	0.39	0.76
Duprat gabbro 07-CD-3554C (z9344)	2698.0 ± 0.8 Ma (Z)	3 (4)	Crystallization age	Weighted average $^{207}Pb/^{206}Pb$ age	0.48	0.62
Dufault gabbro 07-JG-9107 (z9617)	2697.3 ± 0.8 Ma (Z)	4 (2)	Crystallization age	Weighted average $^{207}Pb/^{206}Pb$ age	0.54	0.65
Horseshoe gabbro 08-DK-8286 (z9878)	2700.2 ± 0.9 Ma (Z)	8 (2)	Crystallization age? or inheritance?	Upper intercept age; lower intercept at 58 ± 20 Ma	1.20	0.30
	2677.7 ± 2.5 Ma (Z)		Crytallization age?	Concordant $^{207}Pb/^{206}Pb$ date		
Stadacona Member, rhyolite PBA06-385C (z9312)	2702.3 ± 2.8 Ma (Z)	5	Max. crystallization age	Upper intercept age; lower intercept at 1003 ± 120 Ma	1.60	0.19
Bousquet-Cadillac area						
Cadillac/Timikaming Group, conglomerate LAPL-2008-011 (z9903)	<2672 ± 2 Ma (Z)	1 (12)	Max. depositional age	$^{207}Pb/^{206}Pb$ date of near-concordant analysis		

[(1)]Z = zircon; T = Titanite

[(2)]MSWD = mean square of weighted deviates

[(3)]POF = probability of fit

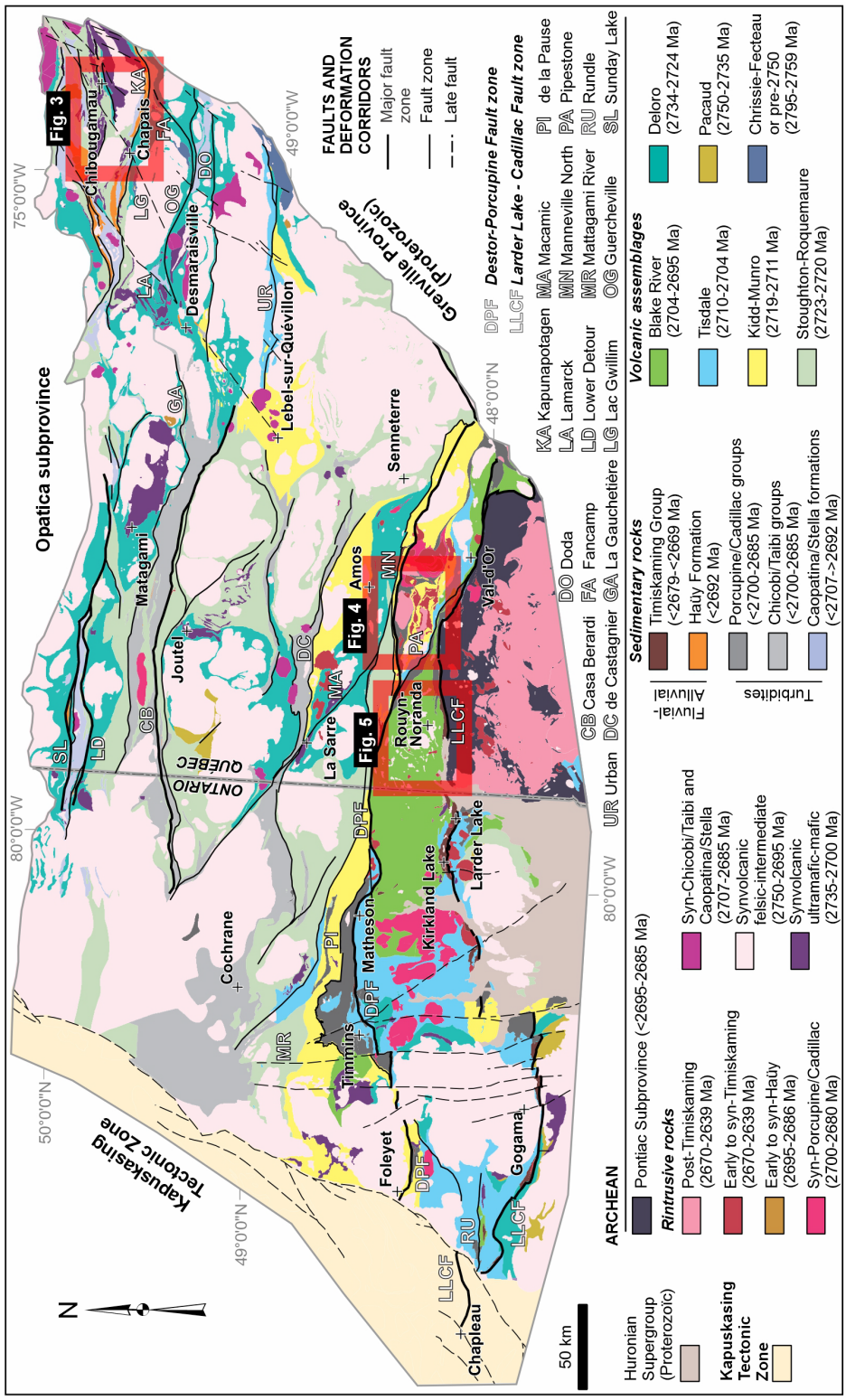


Figure 1. Geological map of the Abitibi greenstone belt showing the major volcanic and sedimentary assemblages and the different groups of intrusions (modified from Dubé and Mercier-Langevin, 2020, and Mercier-Langevin et al., 2023). Highlighted regions (thick red squares) indicate where dated samples were located, see figures 2–5 for details.

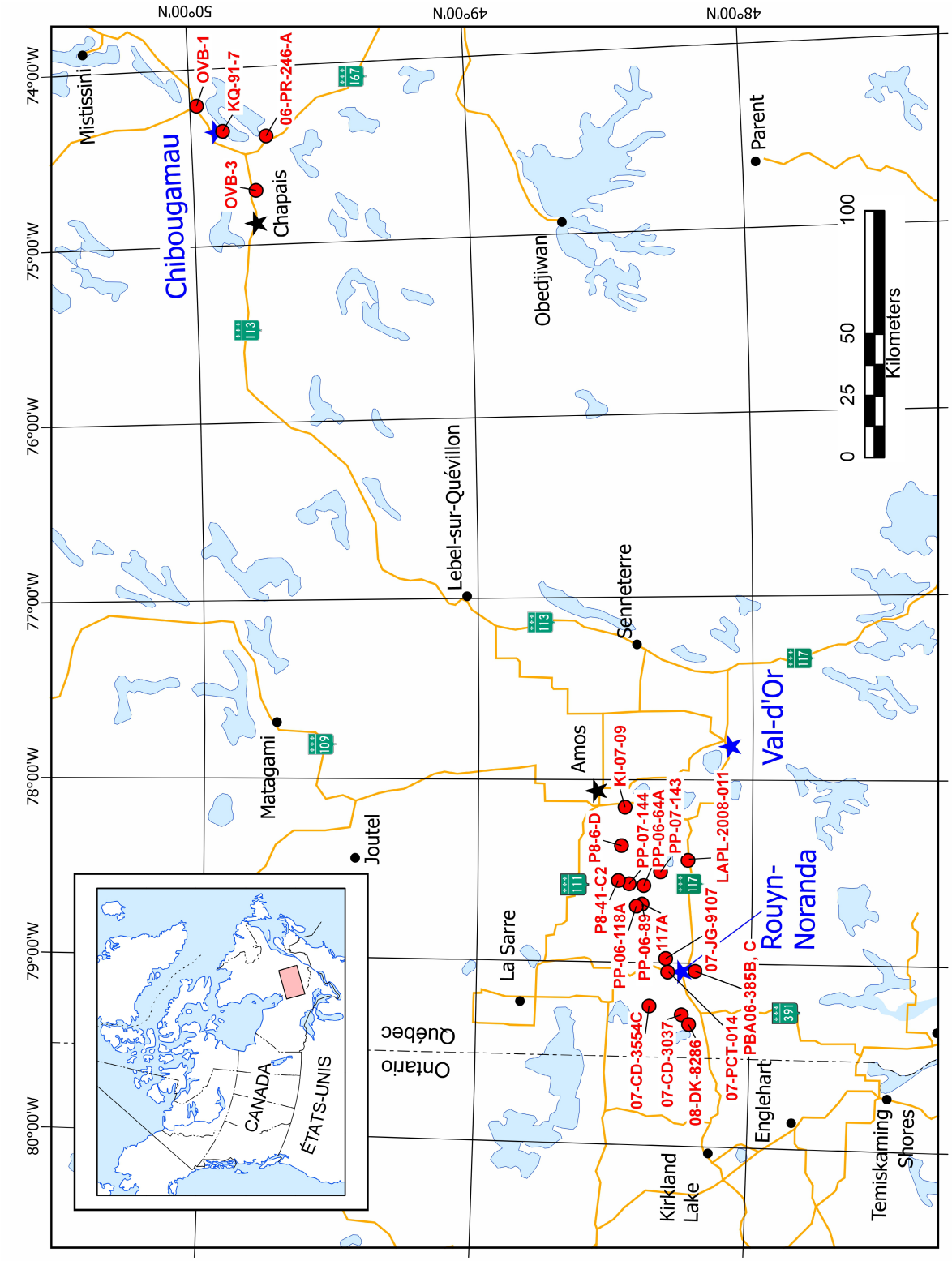


Figure 2. Location of samples (red circles) dated in this study.

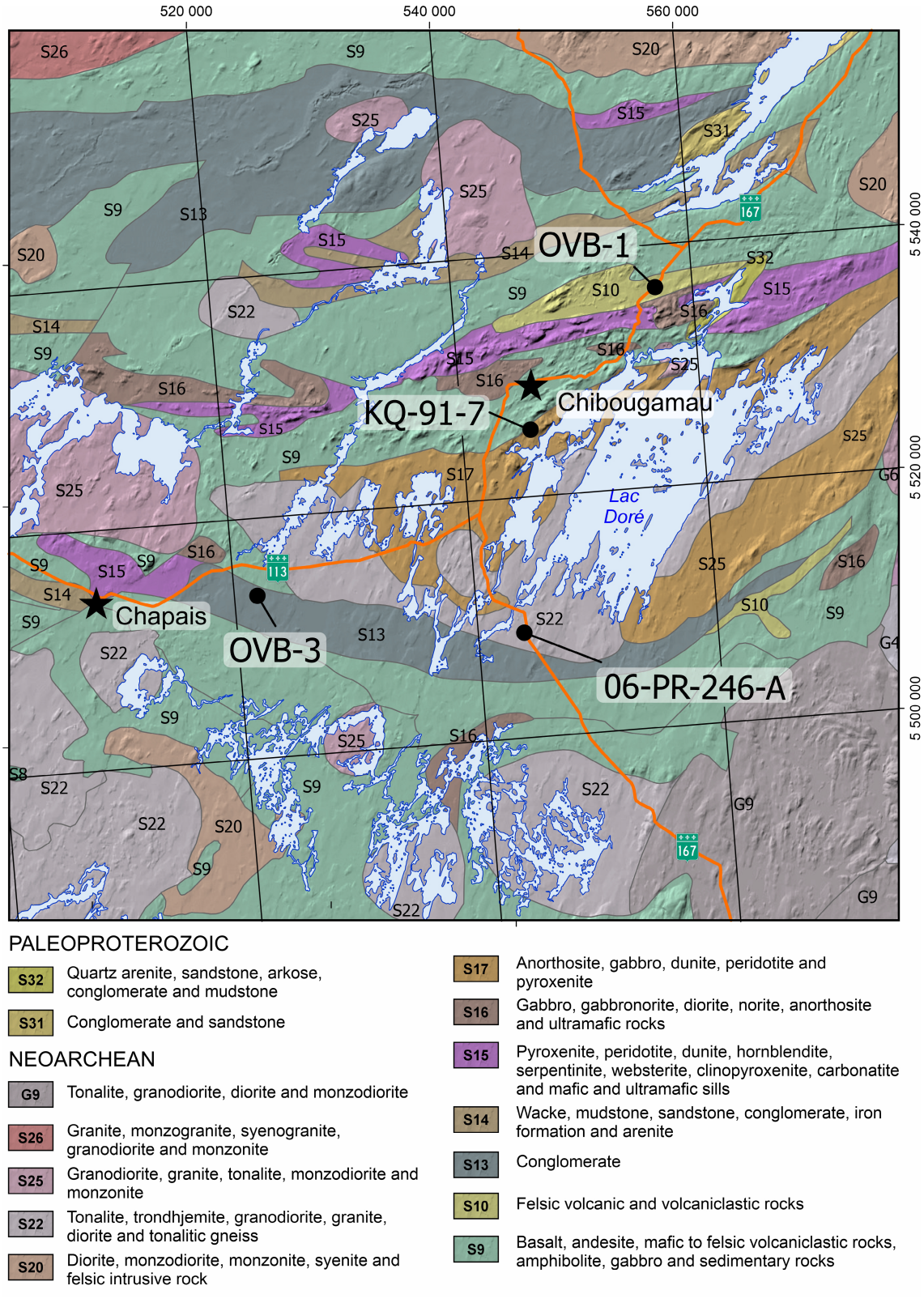


Figure 3. Location of samples in the Chibougamau area. UTM NAD83 Zone 18. Lithological map from SIGÉOM.

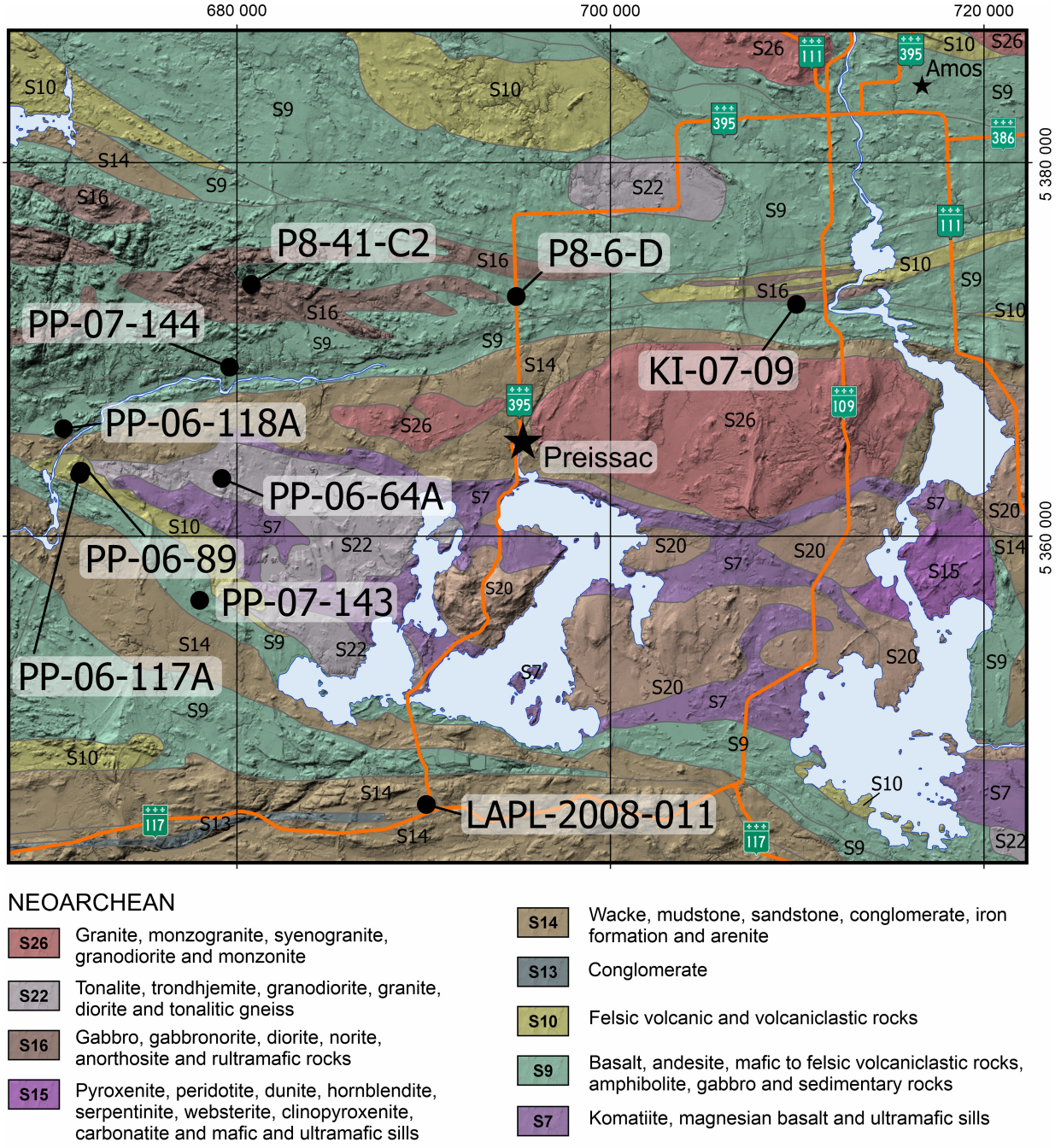


Figure 4. Location of samples in the Val-d'Or-Malartic-Amos, and Bousquet-Cadillac areas. UTM NAD83 Zone 17. Lithological map from SIGÉOM.

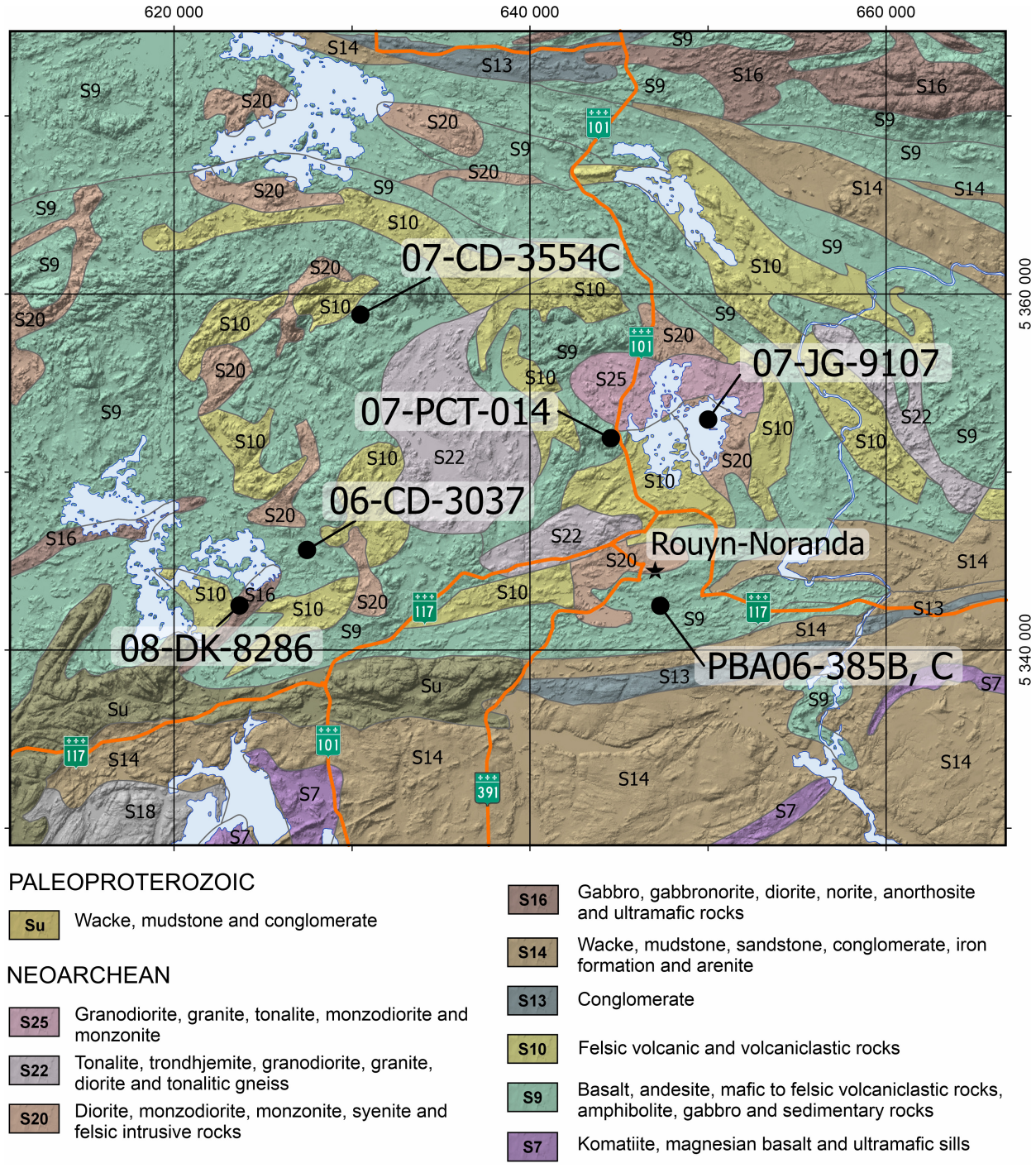


Figure 5. Location of the samples in the Rouyn-Noranda area. UTM NAD83 Zone 17. Lithological map from SIGÉOM.

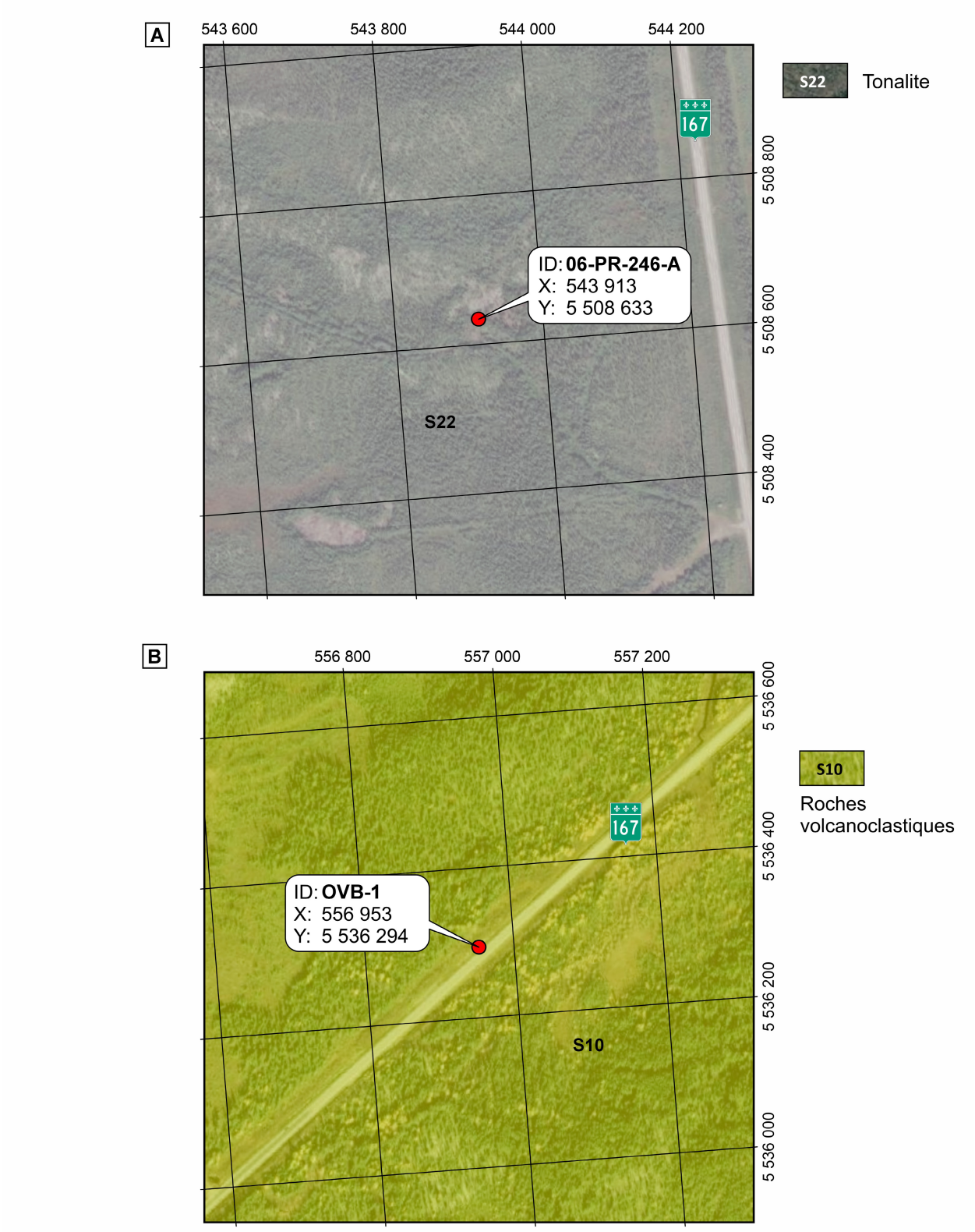


Figure 6. A. Location of sample 06-PR-246-A. UTM NAD83 Zone 18. Lithological map from SIGÉOM. **B.** Location of sample OVB-1. UTM NAD83 Zone 18. Lithological maps from SIGÉOM.

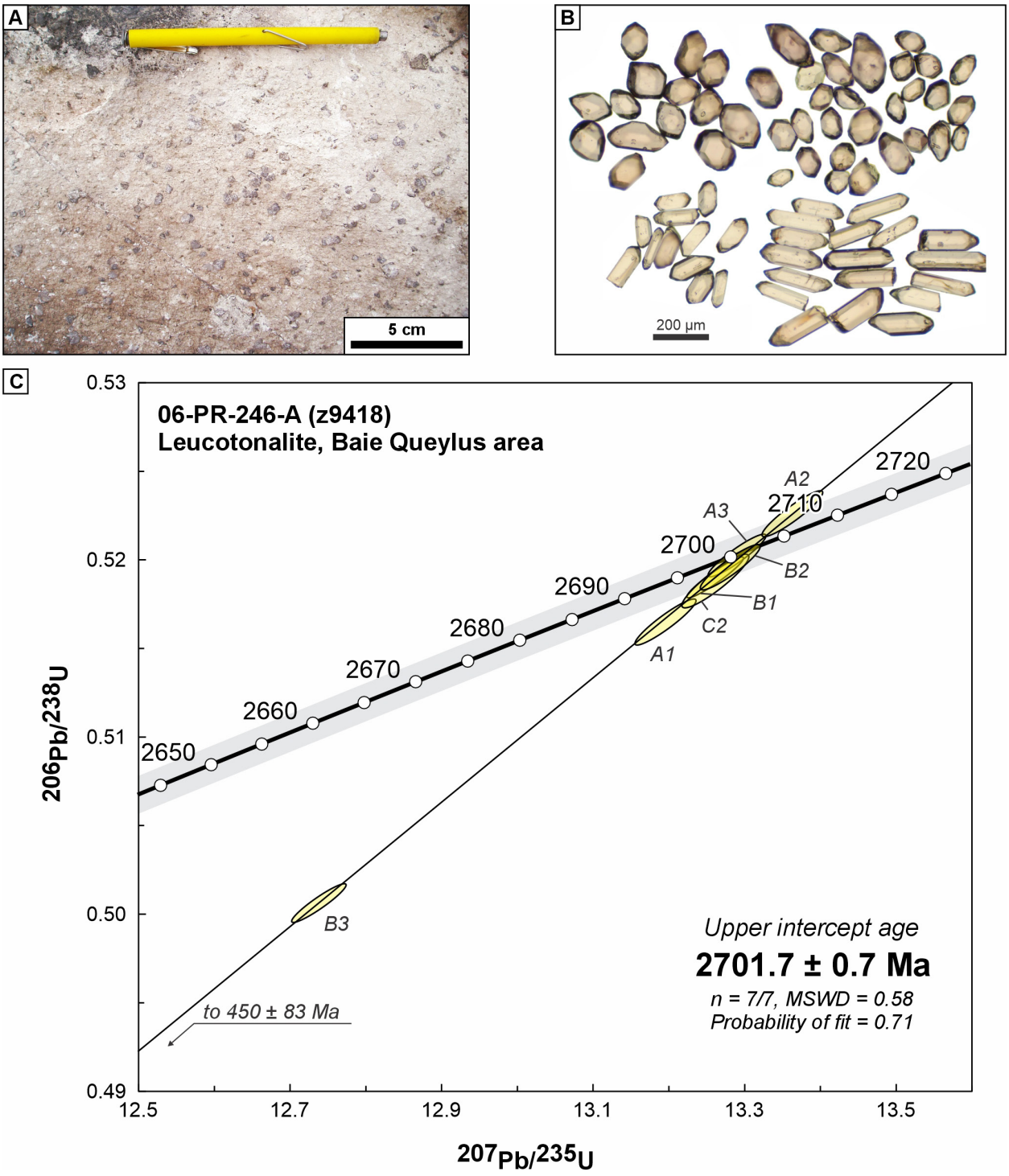


Figure 7. A. Field photograph of the leucotonalite sampling site in the Baie Queylus area south of the town of Chibougamau (sample 06-PR-246-A). The photograph shows a fine-grained quartzo-feldspathic matrix with quartz phenocrysts. NRCan photograph 2023-709, taken by F. Leclerc (MRNF). **B.** Transmitted light image of representative zircon from the sample. **C.** U-Pb concordia diagram for sample 06-PR-246-A. Uncertainties are plotted at the 95% confidence level. Coloured ellipses are included in age calculation.

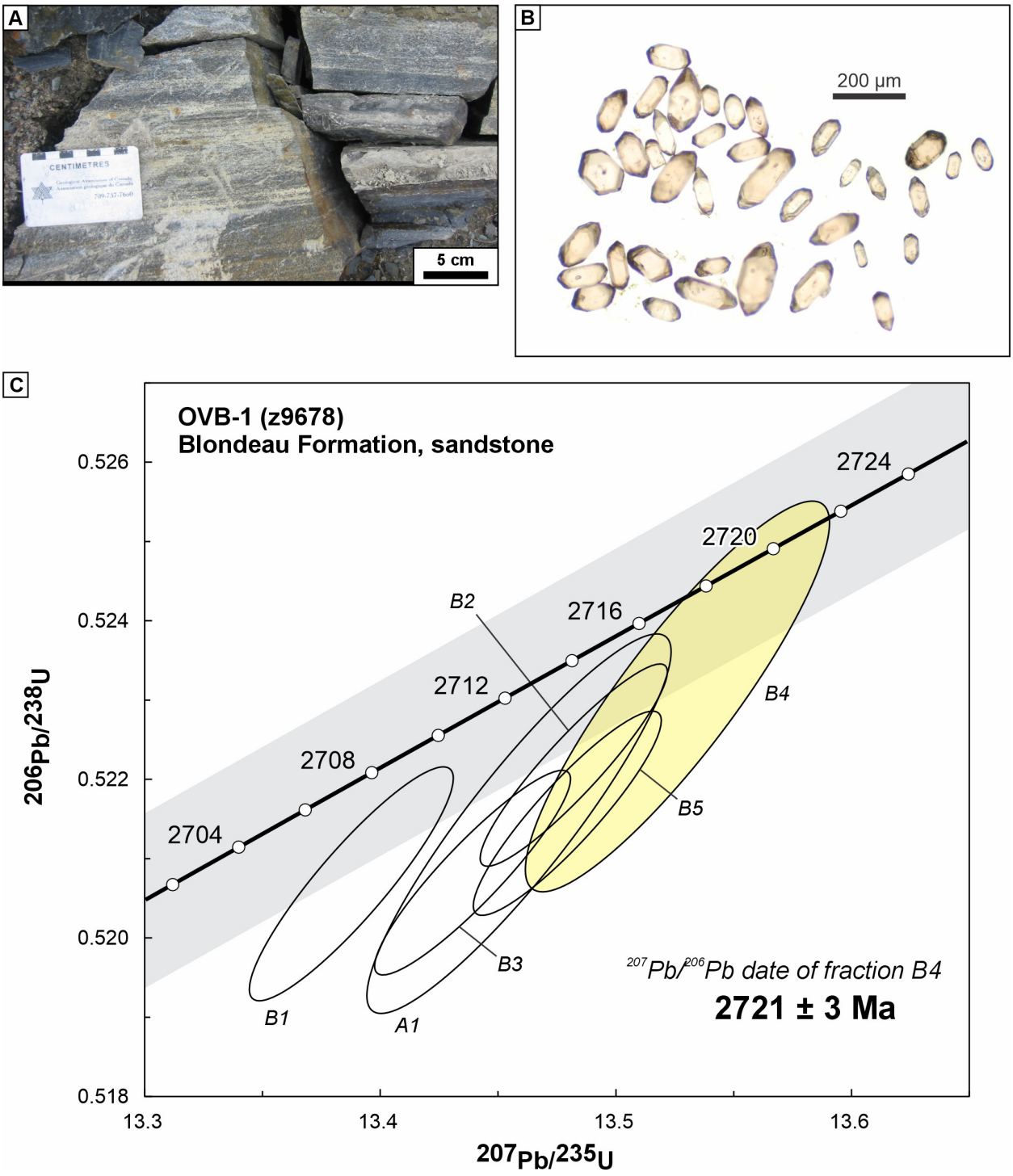


Figure 8. A. Field photograph of the Blondeau Formation finely laminated sandstone where sample OVB-1 was collected. Photograph NRCan 2023-710, taken by F. Leclerc (MRNF). **B.** Transmitted light image of representative zircon from the sample for ID-TIMS analysis. **C.** U-Pb concordia diagram for ID-TIMS results from sample OVB-1. Uncertainties are plotted at the 95% confidence level. Coloured ellipse was used for the age calculation.

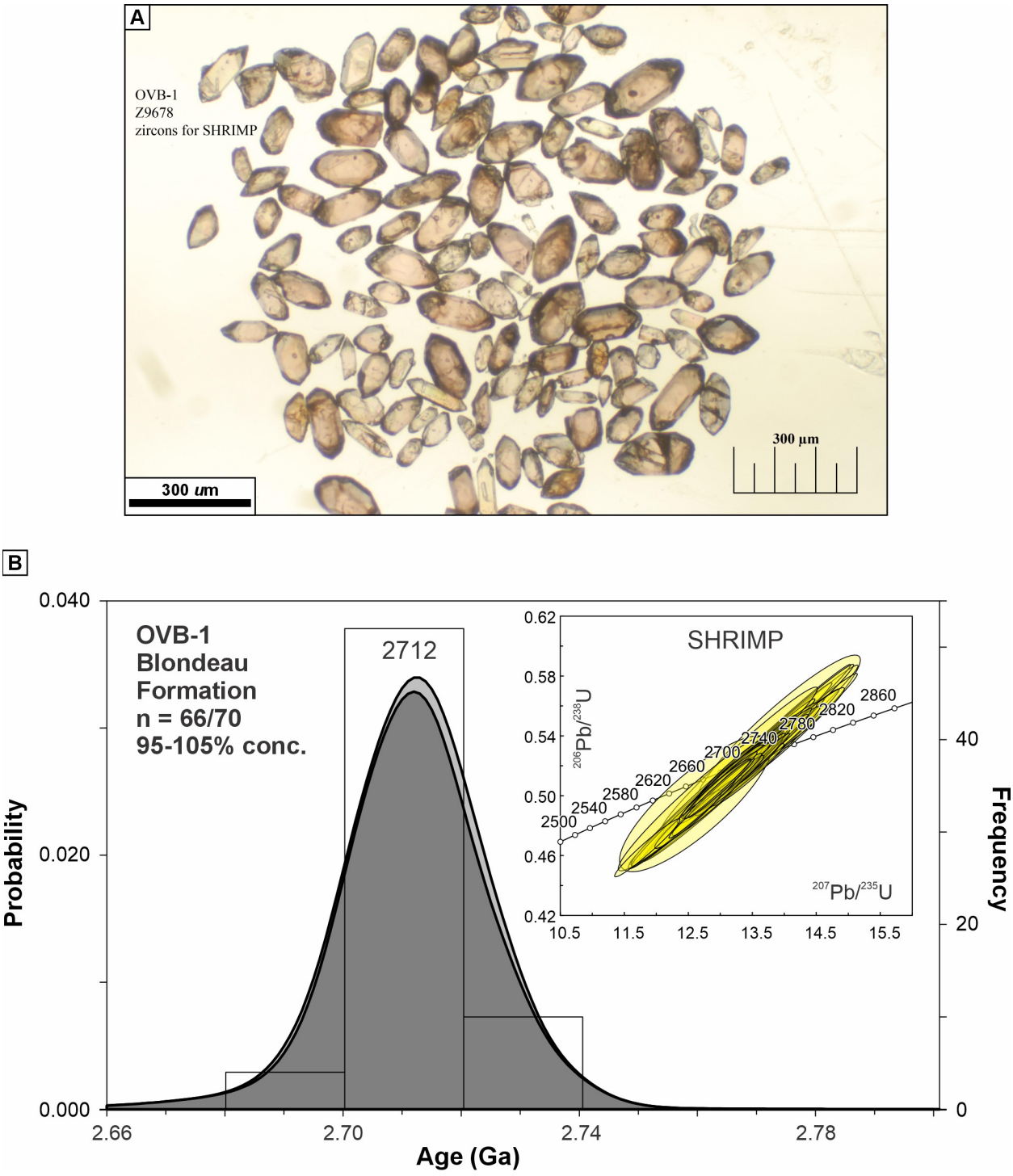


Figure 9. A. Transmitted light image of representative OVB-1 zircons used for SHRIMP analysis. **B.** Probability density distribution diagram and histogram (20 Ma bins) of $^{207}Pb/^{206}Pb$ dates for SHRIMP spot analyses of detrital zircon from sample OVB-1. Dark grey curve includes only data that fall within a ±5% concordance threshold, whereas the light grey curve incorporates all data. Inset shows the U-Pb concordia diagram with uncertainties plotted at the 95% confidence level.

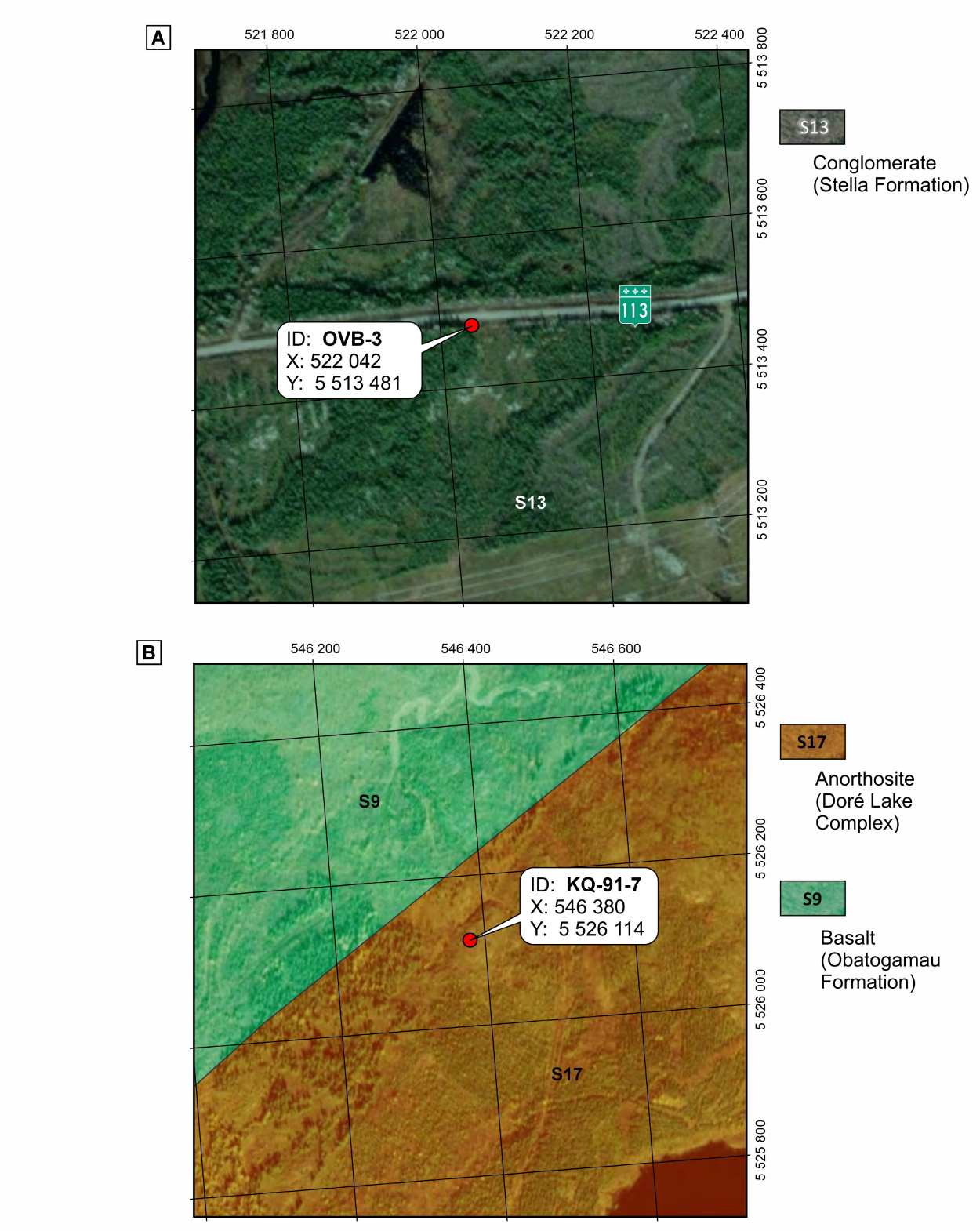


Figure 10. A. Location of sample OVB-3. UTM NAD83 Zone 18. Lithological map from SIGÉOM. **B.** Location of sample KQ-91-7. UTM NAD83 Zone 18. Lithological maps from SIGÉOM.

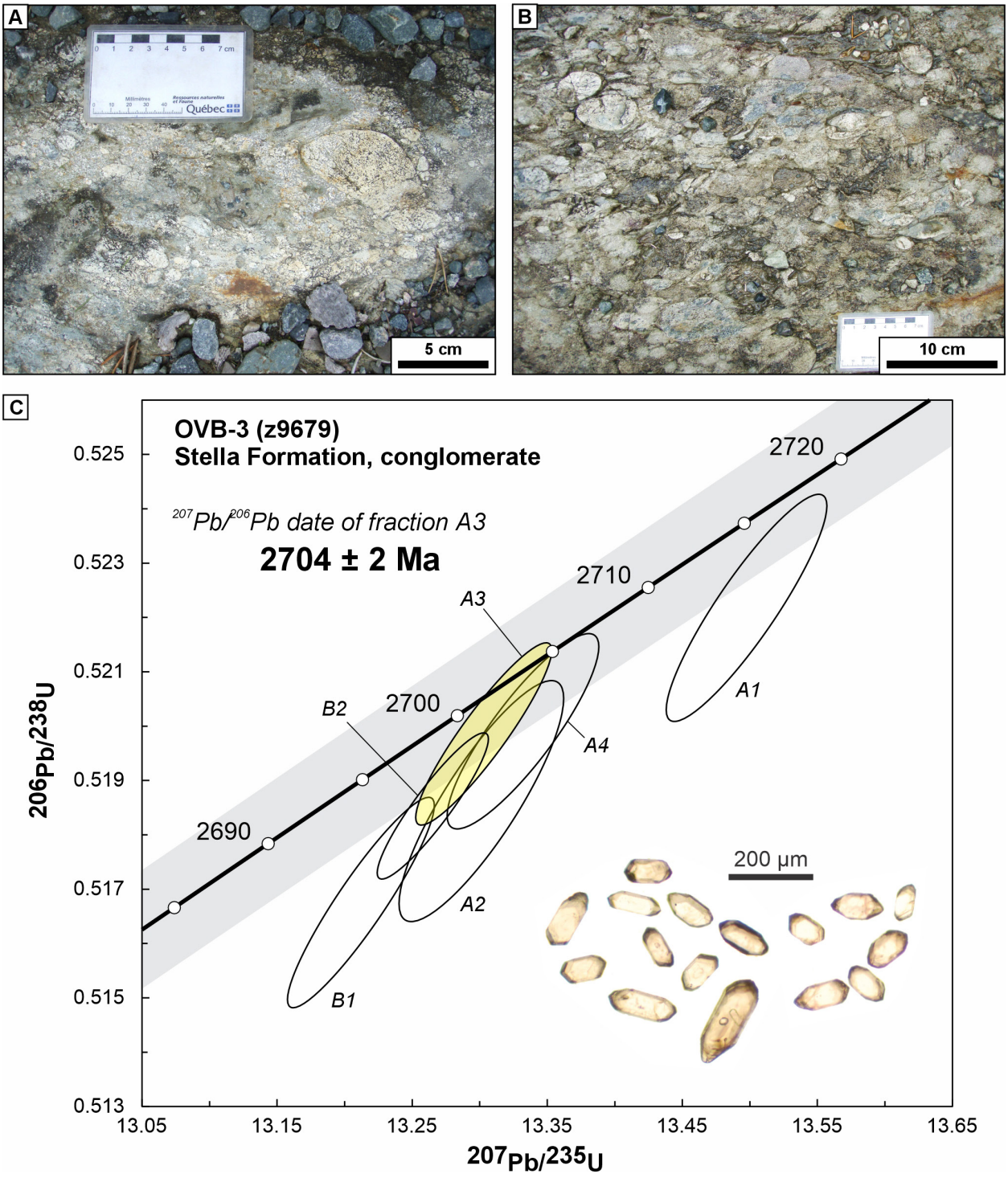


Figure 11. A. Field photograph of the Stella Formation conglomeratic unit where sample OVB-3 was collected. Photograph NRCan 2023-711, taken by F. Leclerc (MRNF). **B.** Field photograph of the Stella Formation conglomerate. Photograph NRCan 2023-712. **C.** U-Pb concordia diagram for ID-TIMS results from sample OVB-3. Uncertainties are plotted at the 95% confidence level. The coloured ellipse was used for the age calculation. Inset: Transmitted light image of representative zircon from the sample for ID-TIMS analysis.

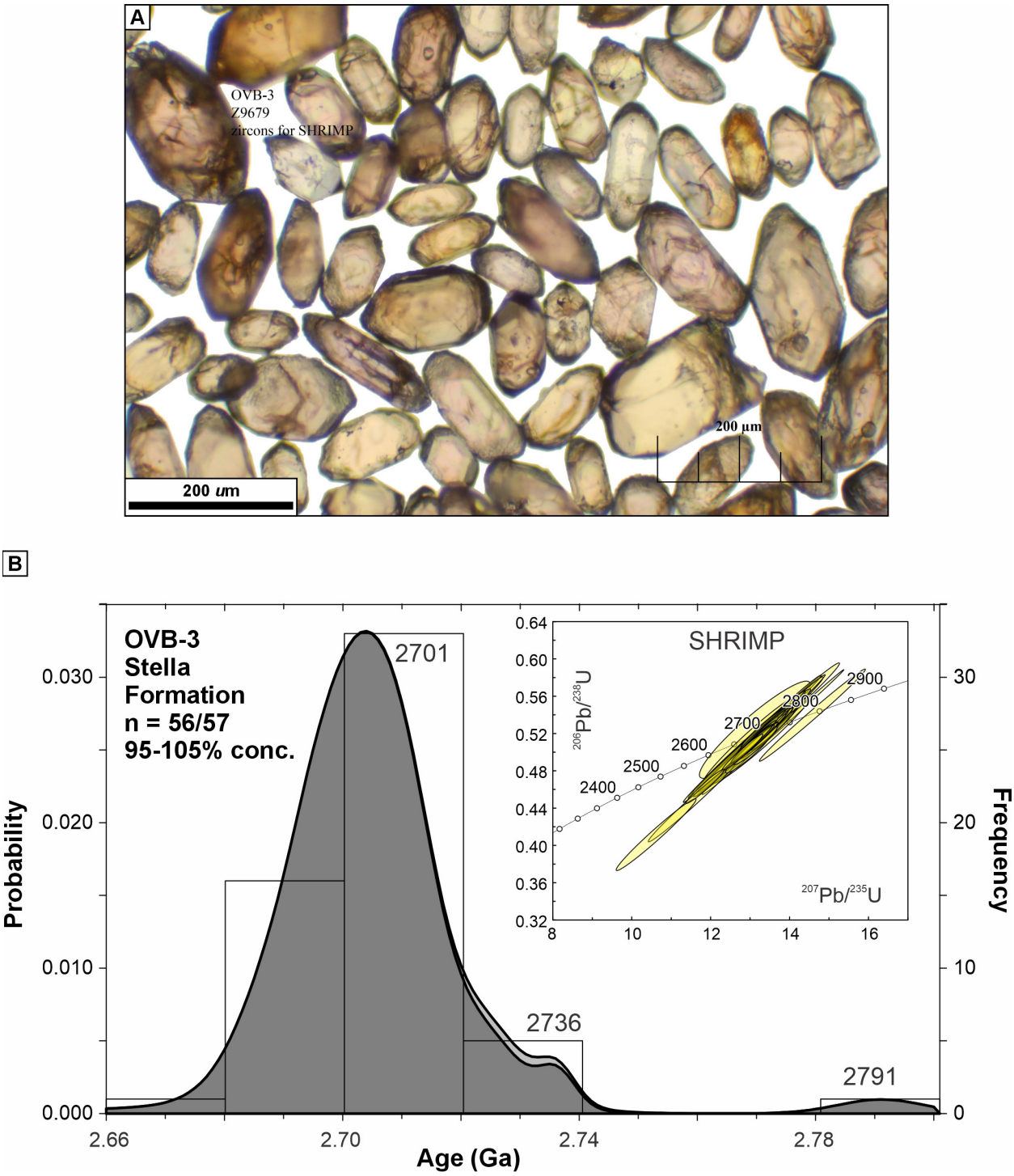


Figure 12. A. Transmitted light image of representative OVB-3 zircons used for SHRIMP analysis. **B.** Probability density distribution diagram and histogram (20 Ma bins) of $^{207}Pb/^{206}Pb$ dates for SHRIMP spot analyses of detrital zircon from sample OVB-3. Dark grey curve includes only data that fall within a ±5% concordance threshold, whereas the light grey curve incorporates all data. In the instance of multiple analyses on a single crystal, only the mean $^{207}Pb/^{206}Pb$ age was included in the combined plots. Inset shows the U-Pb concordia diagram with uncertainties plotted at the 95% confidence level.

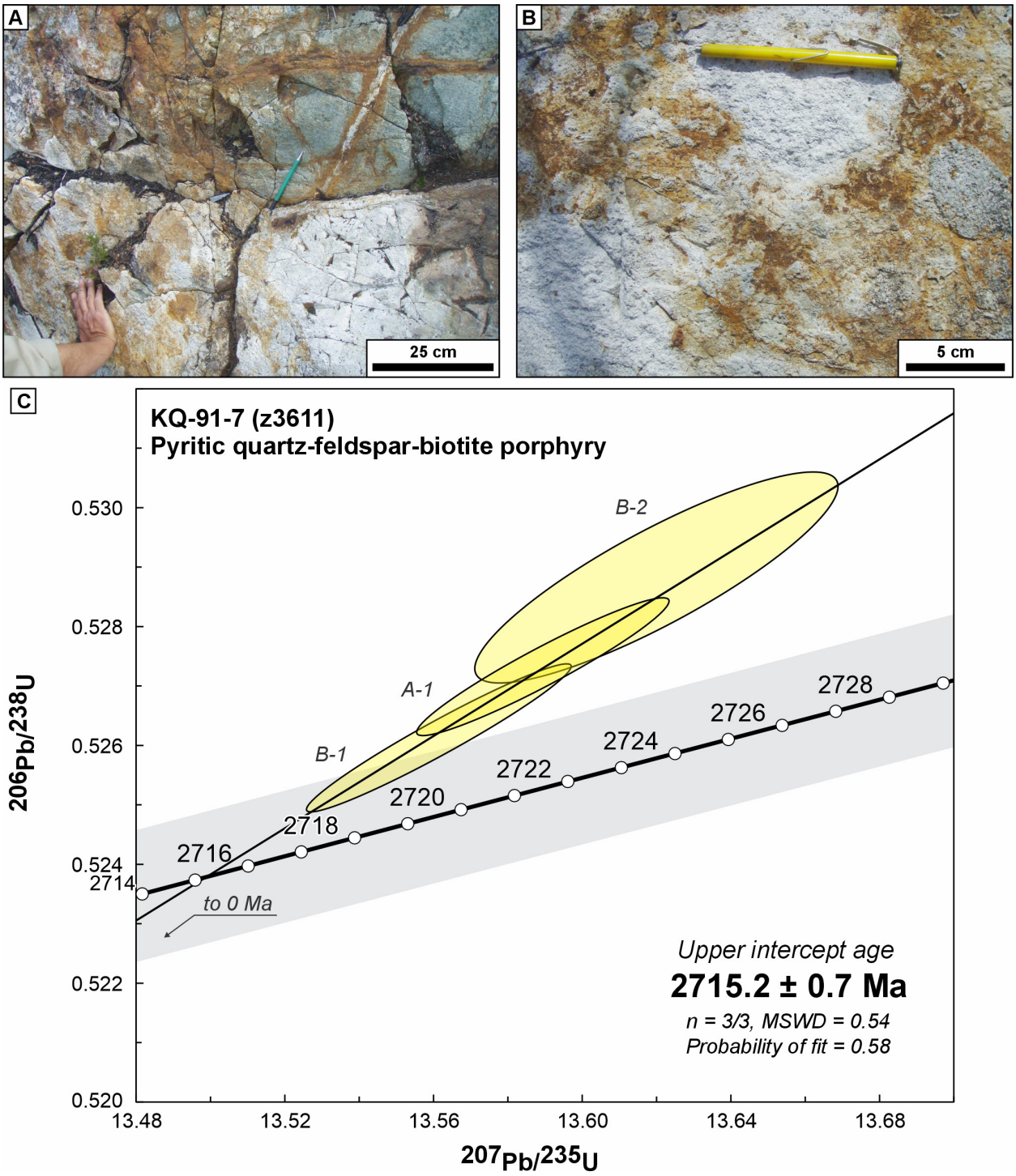


Figure 13. A. KQ-91-7 sampling area showing a felsic dyke cutting mineralized veins. Photograph by P. Roy (MRNF), NRCan photograph 2023-713. **B.** Close-up view of the sampled post-ore dyke. Photograph by P. Roy (MRNF), NRCan photograph 2023-714. **C.** U-Pb concordia diagram for sample KQ-91-7. Uncertainties are plotted at the 95% confidence level. Coloured ellipses are included in age calculation. Note that high-quality transmitted light images of zircon from this sample are not available.

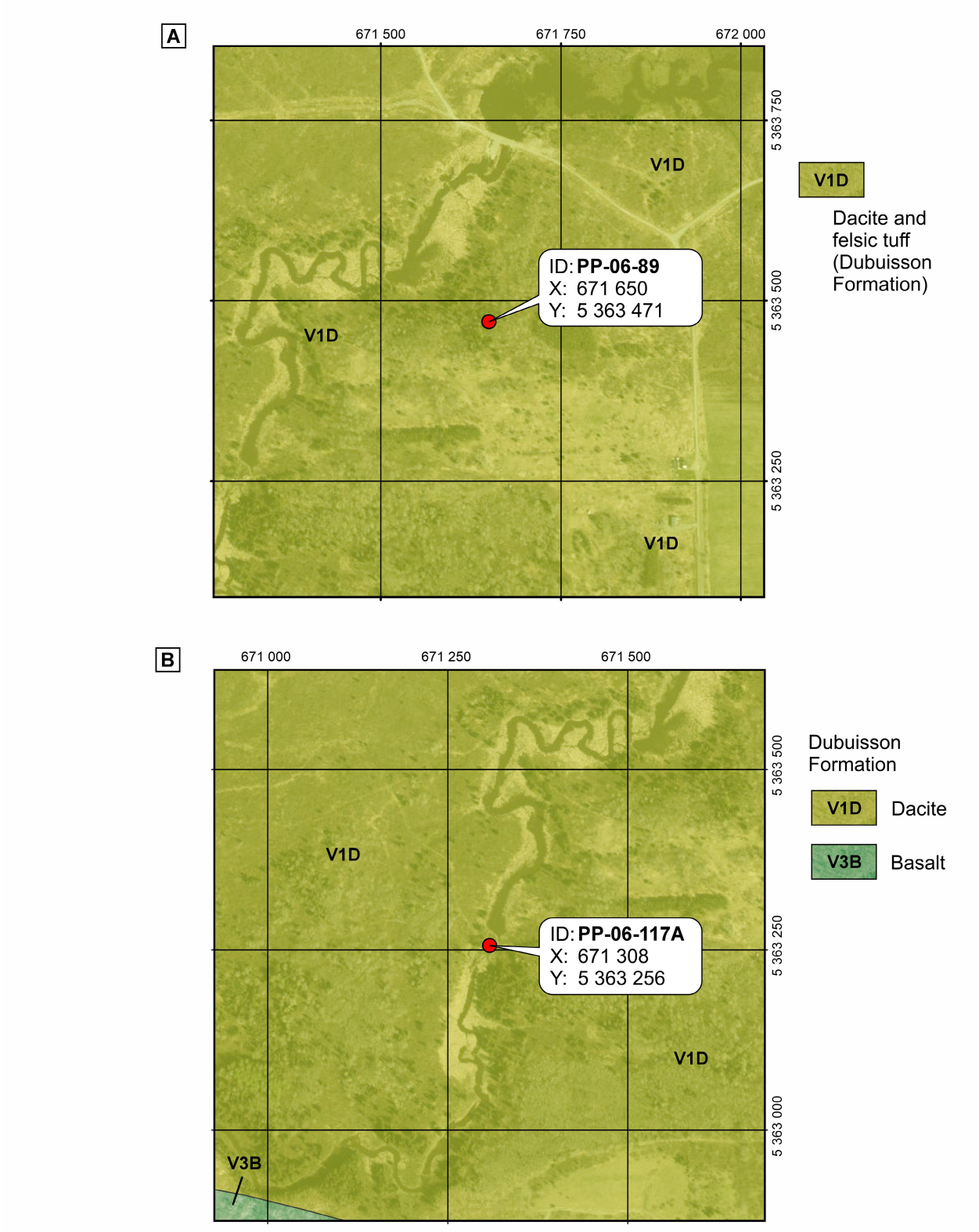


Figure 14. A. Location of sample PP-06-89. UTM NAD83 Zone 17. Lithological map from SIGÉOM. **B.** Location of sample PP-06-117A. UTM NAD83 Zone 17. Lithological map from SIGÉOM.

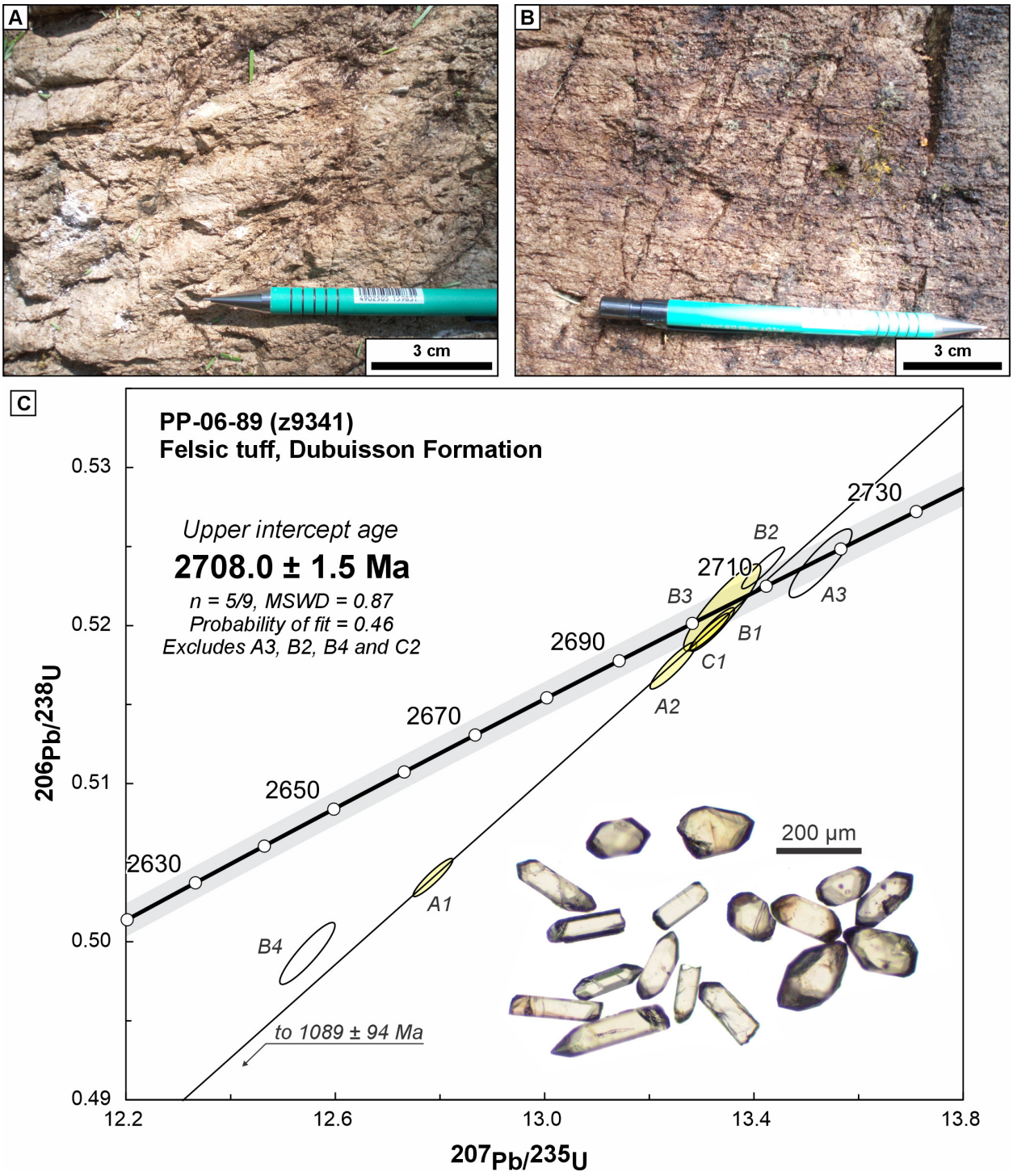


Figure 15. A. PP-06-89 sampling site showing a weakly foliated felsic tuff. Photograph by P. Pilote (MRNF), NRCan photograph 2023-715. **B.** PP-06-89 sampling site showing a foliated, homogenous felsic tuff unit, Dubuisson Formation. Photograph by P. Pilote (MRNF), NRCan photograph 2023-716. **C.** U-Pb concordia diagram for sample PP-06-89 (highly discordant analysis C2 not plotted; see text for further details). Uncertainties are plotted at the 95% confidence level. Coloured ellipses are included in age calculation. Inset: Transmitted light image of representative zircon from the sample.

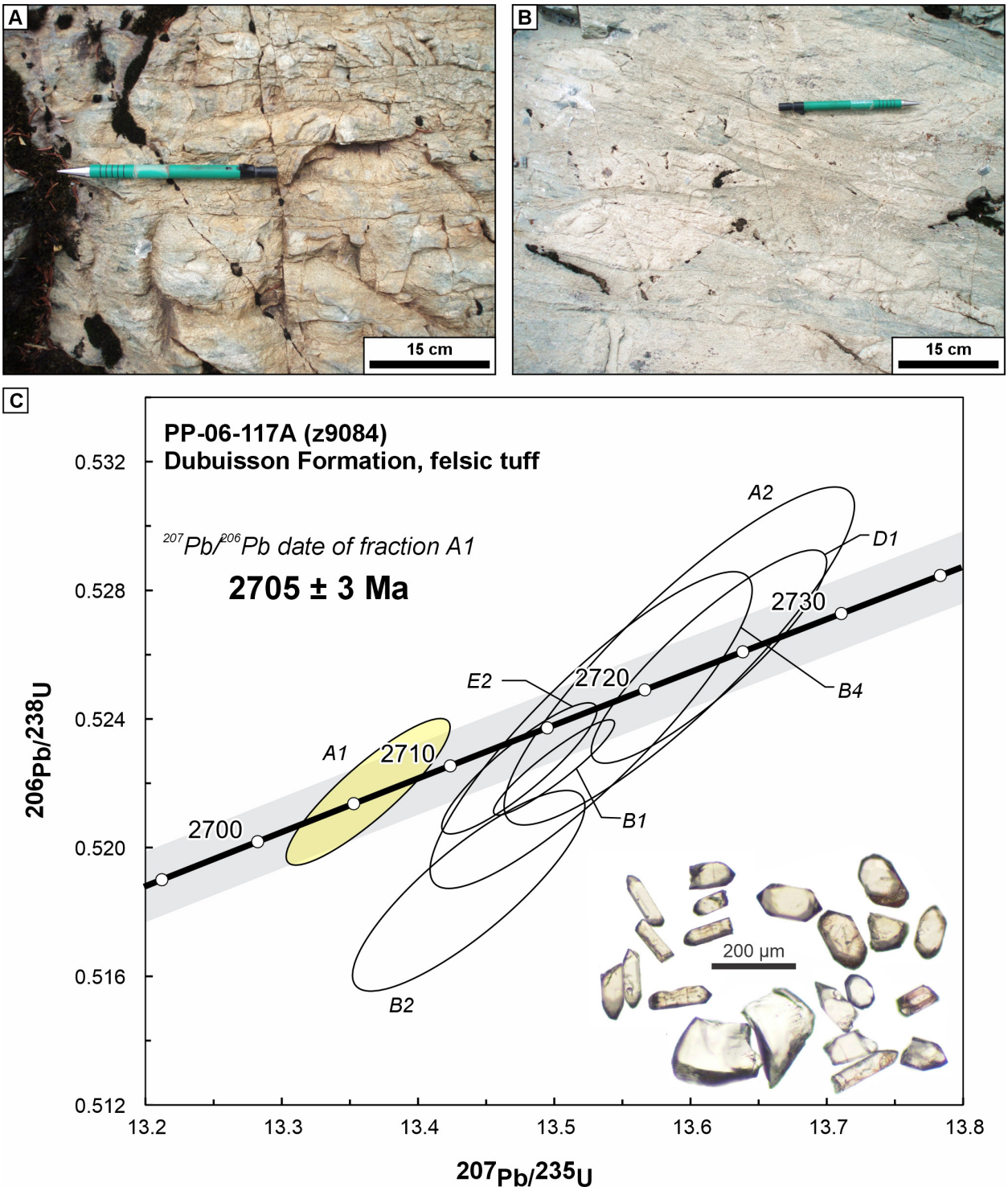


Figure 16. A. PP-06-117A sampling site showing a felsic volcaniclastic rock. Photograph by P. Pilote (MRNF). **B.** PP-06-117A sampling site showing a weakly foliated and weakly altered, monomictic felsic volcaniclastic unit, Dubuisson Formation. Photograph by P. Pilote (MRNF). **C.** U-Pb Concordia diagram for ID-TIMS results from sample PP-06-117A. Uncertainties are plotted at the 95% confidence level. Coloured ellipse is included in age calculation. Inset: Transmitted light image of representative zircon from the sample for ID-TIMS analysis.

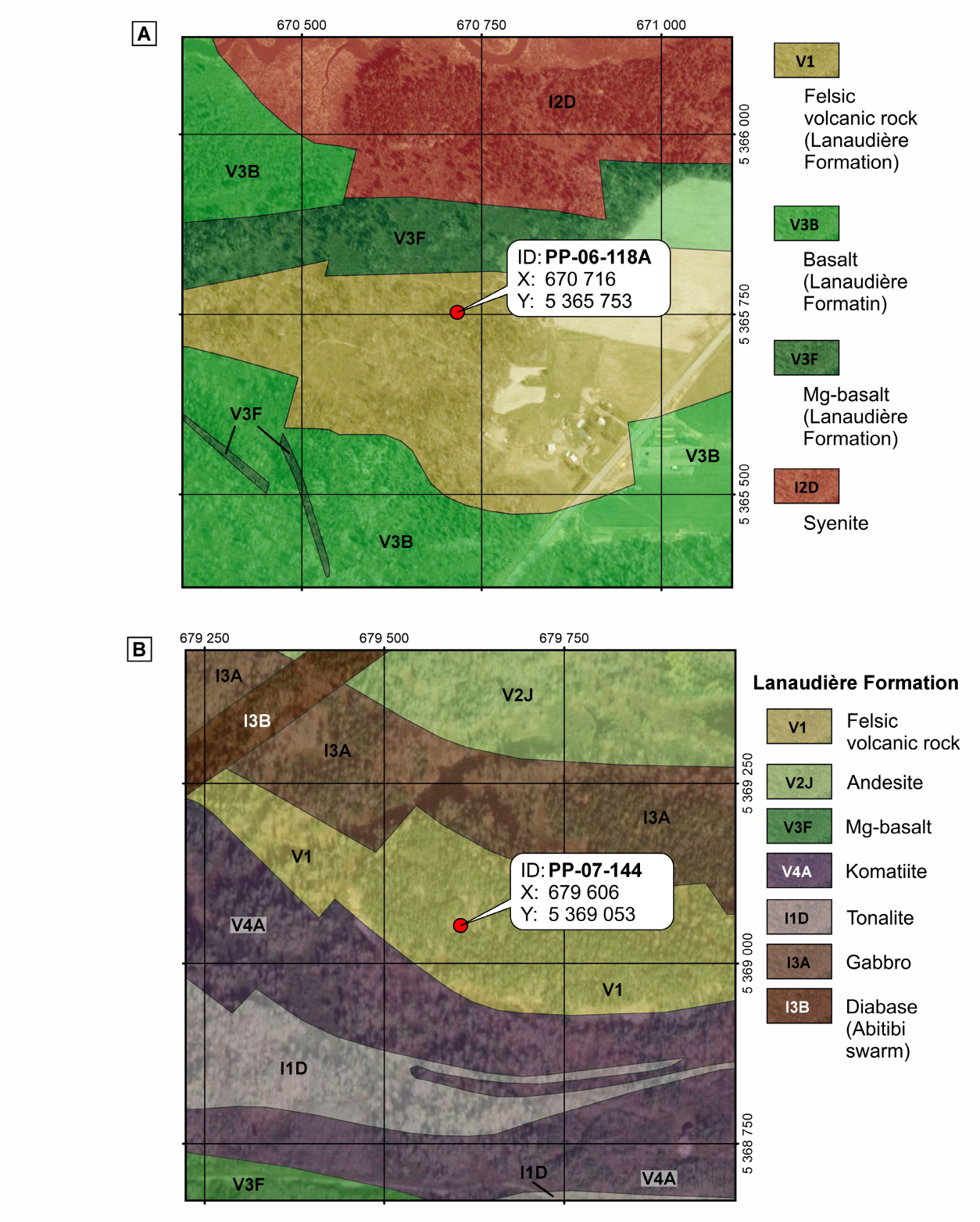


Figure 17. A. Location of sample PP-06-118A. UTM NAD83 Zone 17. Lithological map from SIGÉOM. **B.** Location of sample PP-07-144. UTM NAD83 Zone 17. Lithological map from SIGÉOM.

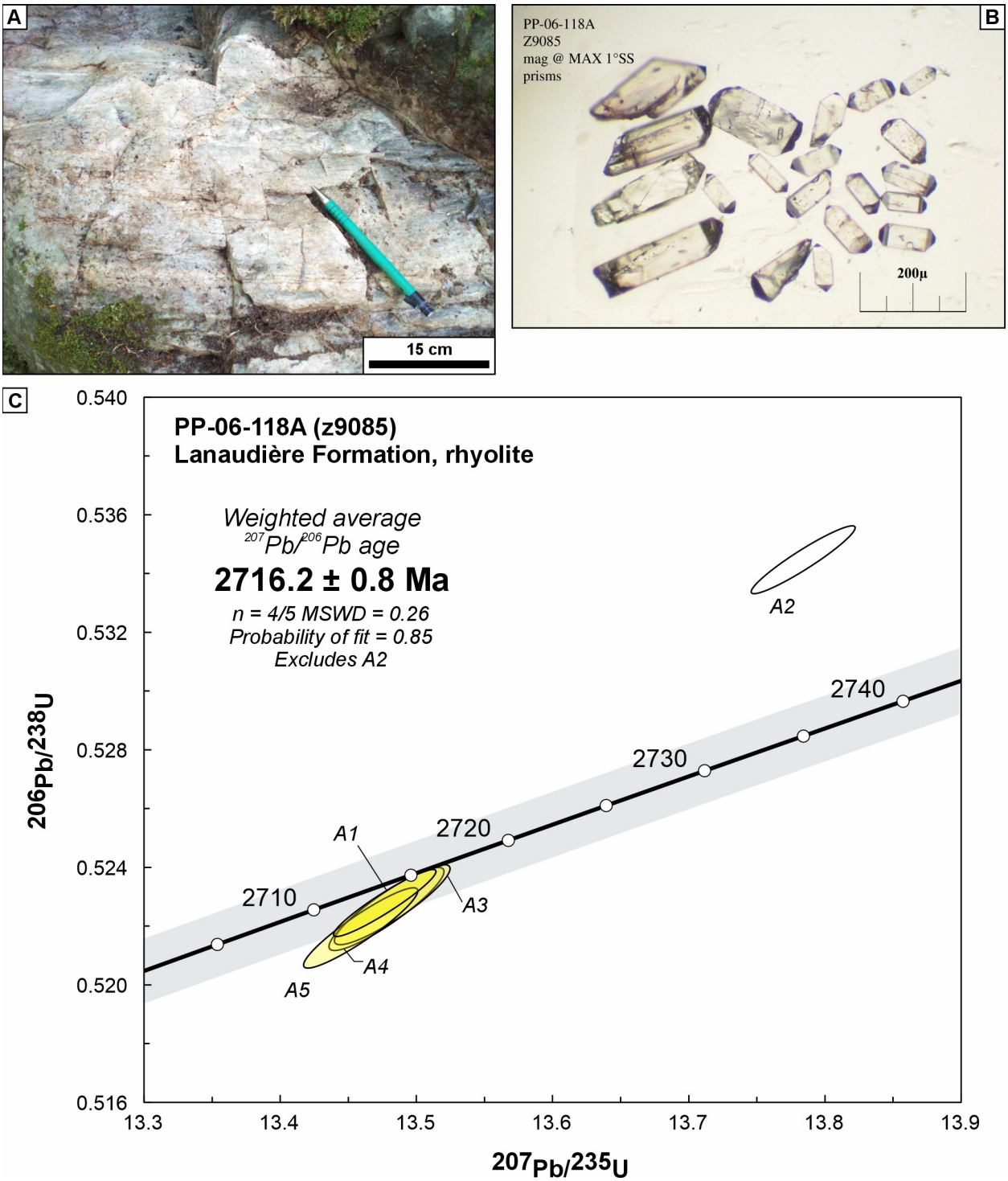


Figure 18. A. Flow-banded rhyolite, Lanaudière Formation, PP-06-118A sampling site. Photograph by P. Pilote (MRNF), NRCan photo 2023-717. **B.** Transmitted light image of representative zircon from the sample. **C.** U-Pb concordia diagram for sample PP-06-118A. Uncertainties are plotted at the 95% confidence level. Coloured ellipses are included in age calculation.

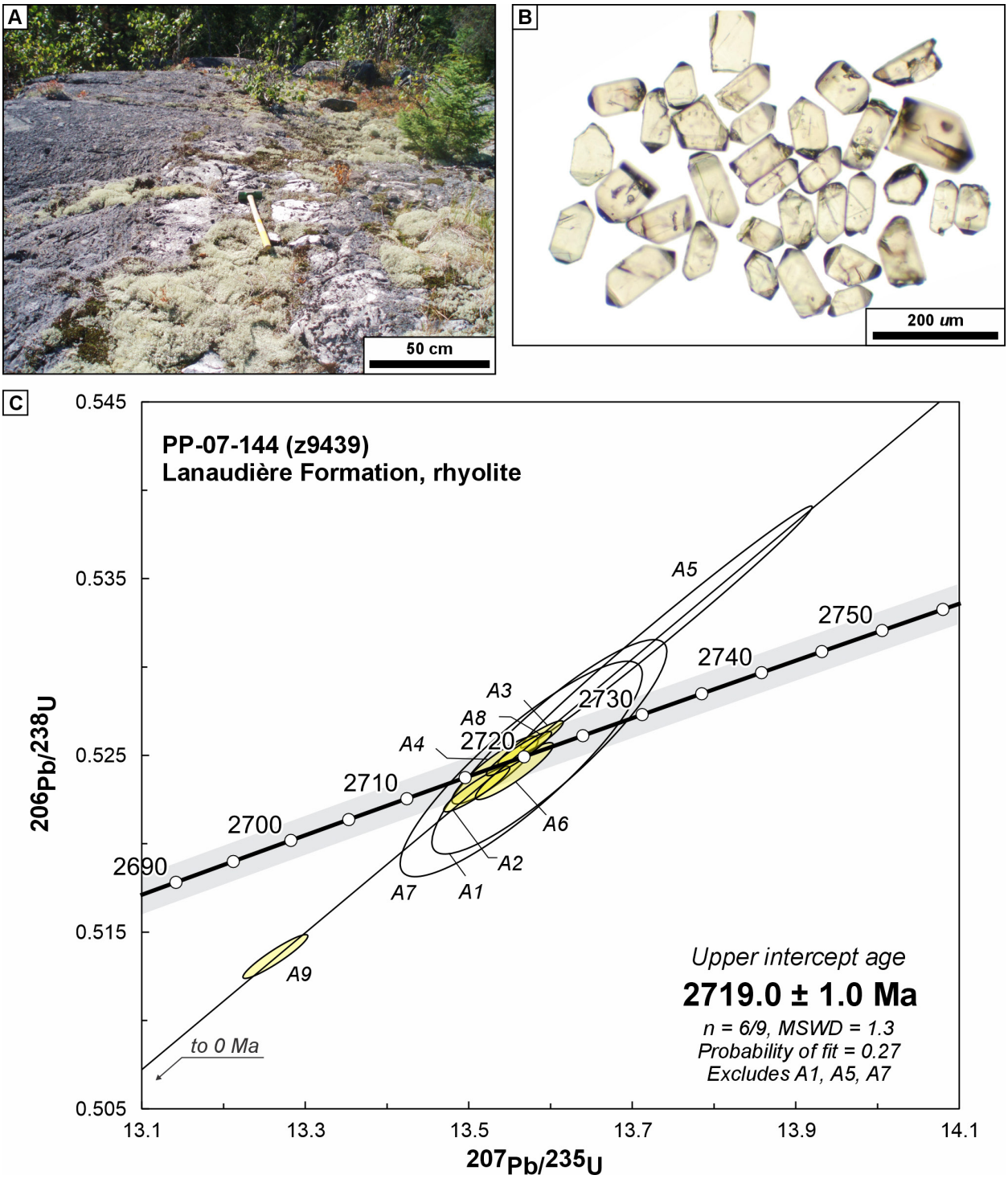


Figure 19. A. Rhyolite lobe emplaced in rhyolitic block and lapilli tuff of similar composition, Lanaudière Formation, PP-07-144 sampling site. Photograph by P. Pilote (MRNF), NRCan photo 2023-718. **B.** Transmitted light image of representative zircon from the sample. **C.** U-Pb concordia diagram for sample PP-07-144. Uncertainties are plotted at the 95% confidence level. Coloured ellipses are included in age calculation.

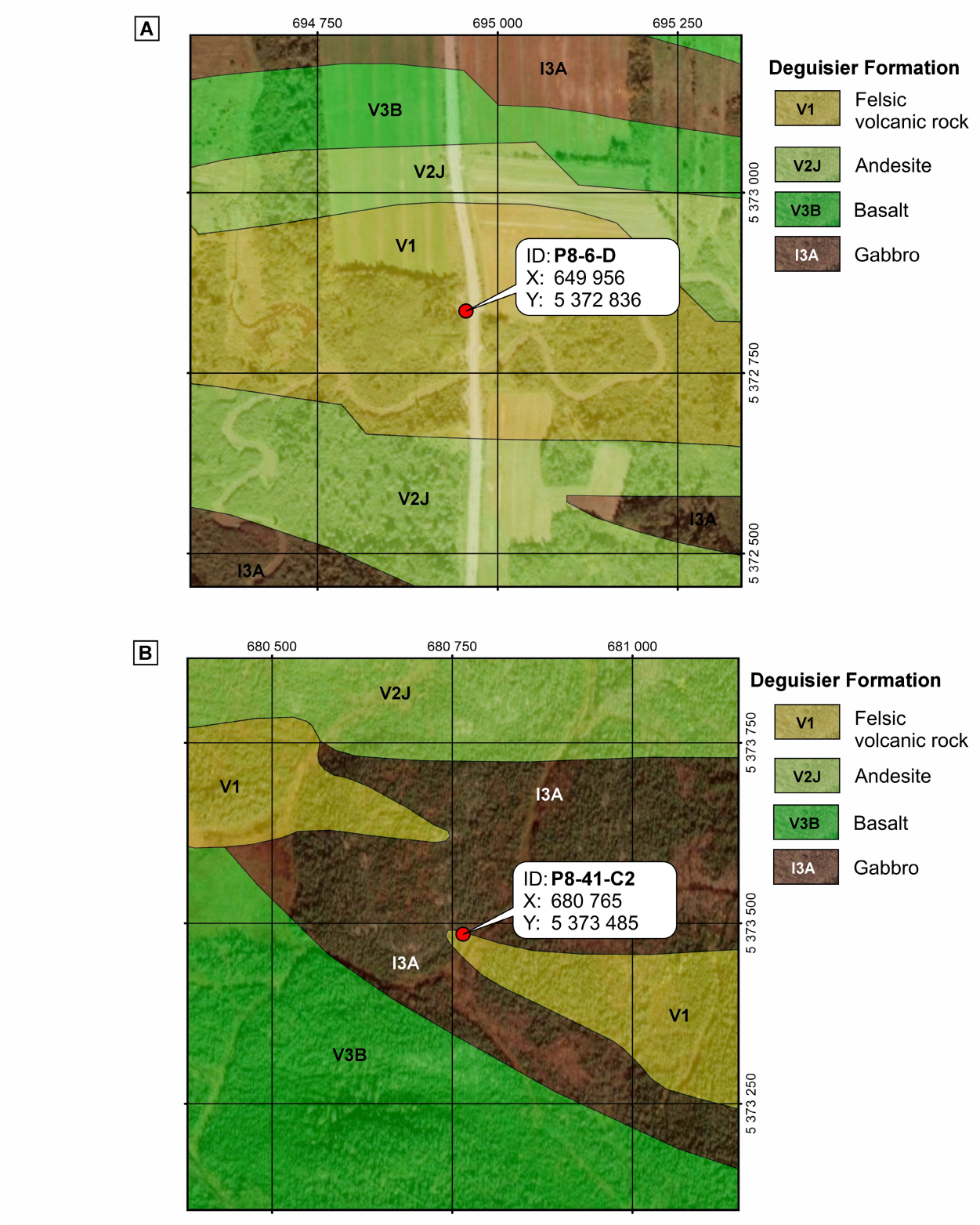


Figure 20. A. Location of sample P8-6-D. UTM NAD83 Zone 17. Lithological map from SIGÉOM. **B.** Location of sample P8-41-C2. UTM NAD83 Zone 17. Lithological map from SIGÉOM.

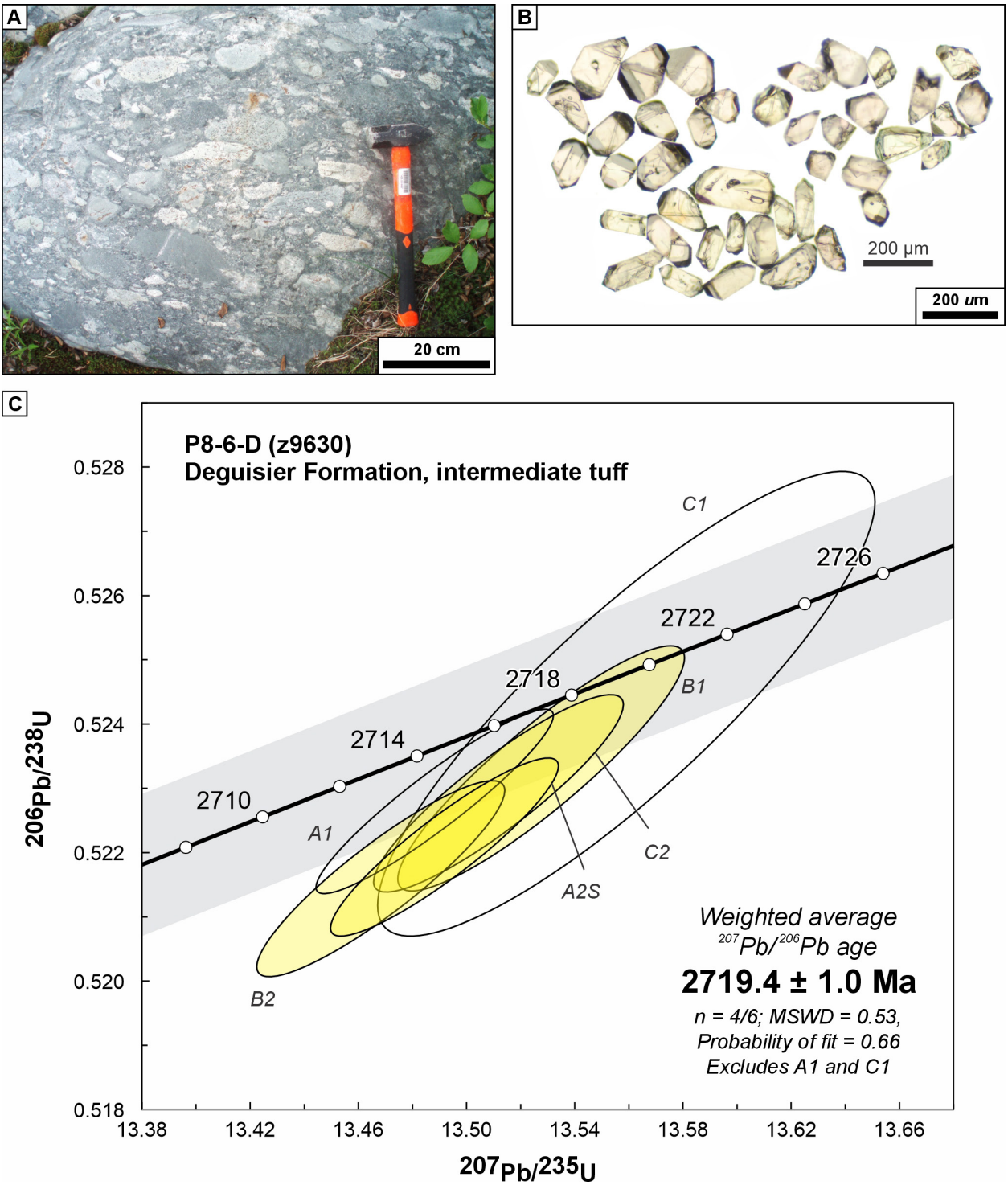


Figure 21. A. Intermediate polymictic block and lapilli tuff, Deguisier Formation, P8-6-D sampling site. Photography by P. Pilote (MRNF), NRCan photo 2023-719. **B.** Transmitted light image of representative zircon from the sample. **C.** U-Pb concordia diagram for sample P8-6-D. Uncertainties are plotted at the 95% confidence level. Coloured ellipses are included in age calculation.

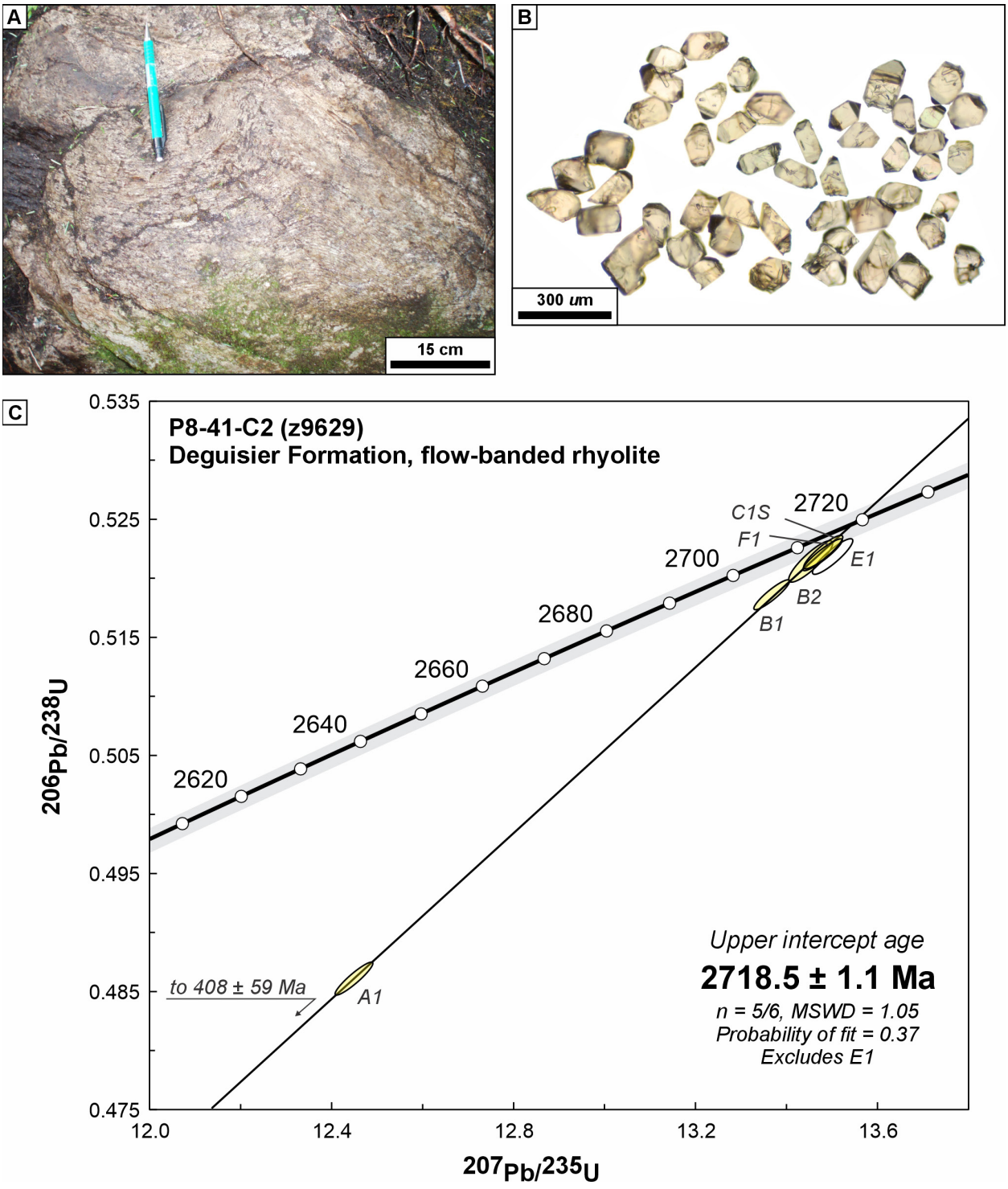


Figure 22. A. Flow-banded rhyolite lobe, Deguisier Formation, P8-41-C2 sampling site. Photograph by P. Pilote (MRNF), NRCan photo 2023-720. **B.** Transmitted light image of representative zircon from the sample. **C.** U-Pb concordia diagram for sample P8-41-C2. Uncertainties are plotted at the 95% confidence level. Coloured ellipses are included in age calculation.

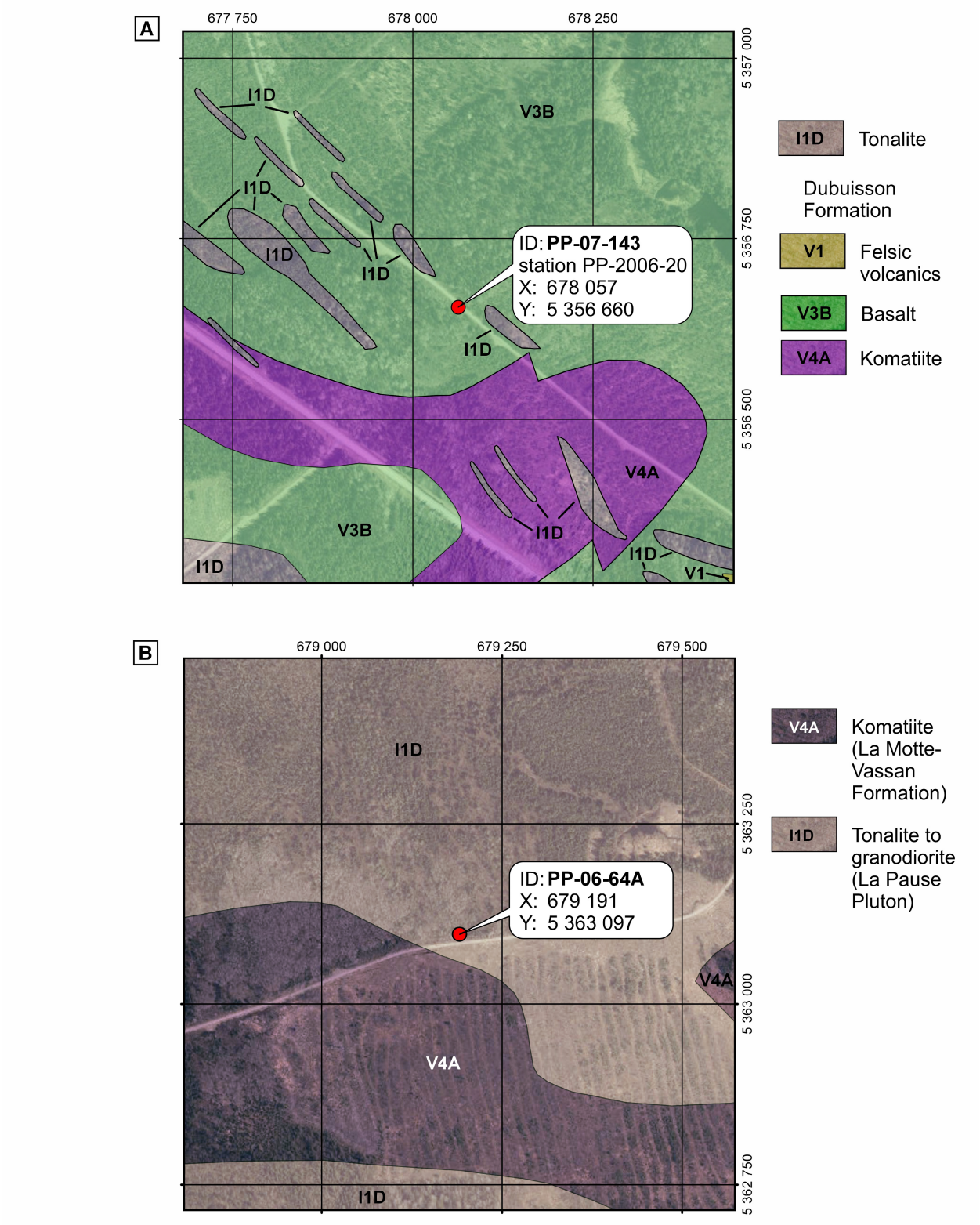


Figure 23. A. Location of sample PP-07-143. UTM NAD83 Zone 17. Lithological map from SIGÉOM. **B.** Location of sample PP-06-64A. UTM NAD83 Zone 17. Lithological map from SIGÉOM.

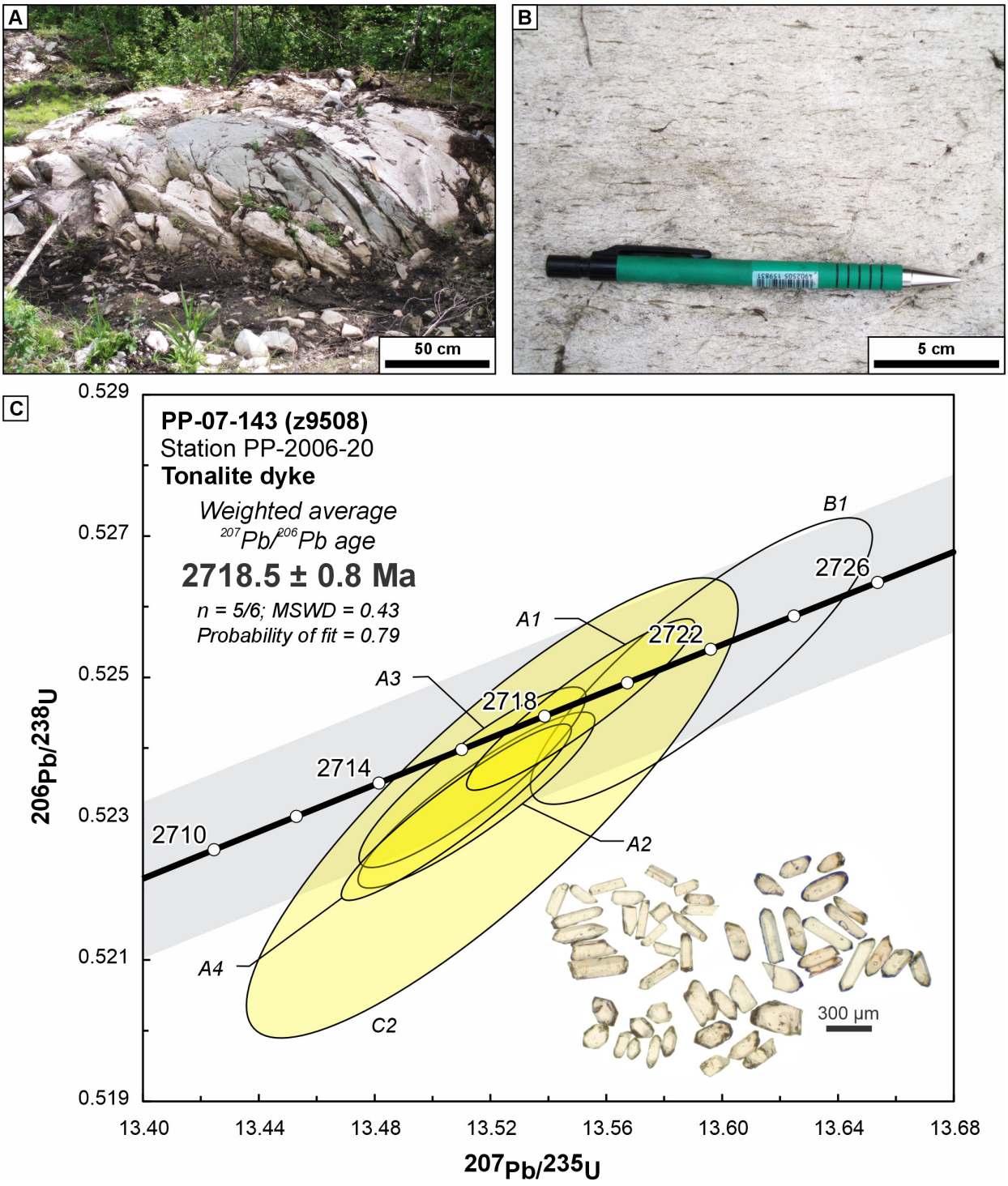


Figure 24. A. PP-07-143 sampling site (SIGEOM station PP-2006-20) showing a tonalitic dyke cutting mafic volcanic rocks. Photograph by P. Pilote (MRNF). **B.** Close-up photograph of sample PP-07-143 tonalitic dyke showing a leucocratic weathered surface and well developed foliation. **C.** U-Pb Concordia diagram for ID-TIMS results from sample PP-07-143. Uncertainties are plotted at the 95% confidence level. Coloured ellipses are included in age calculation. Inset: Transmitted light image of representative zircon from the sample for ID-TIMS analysis.

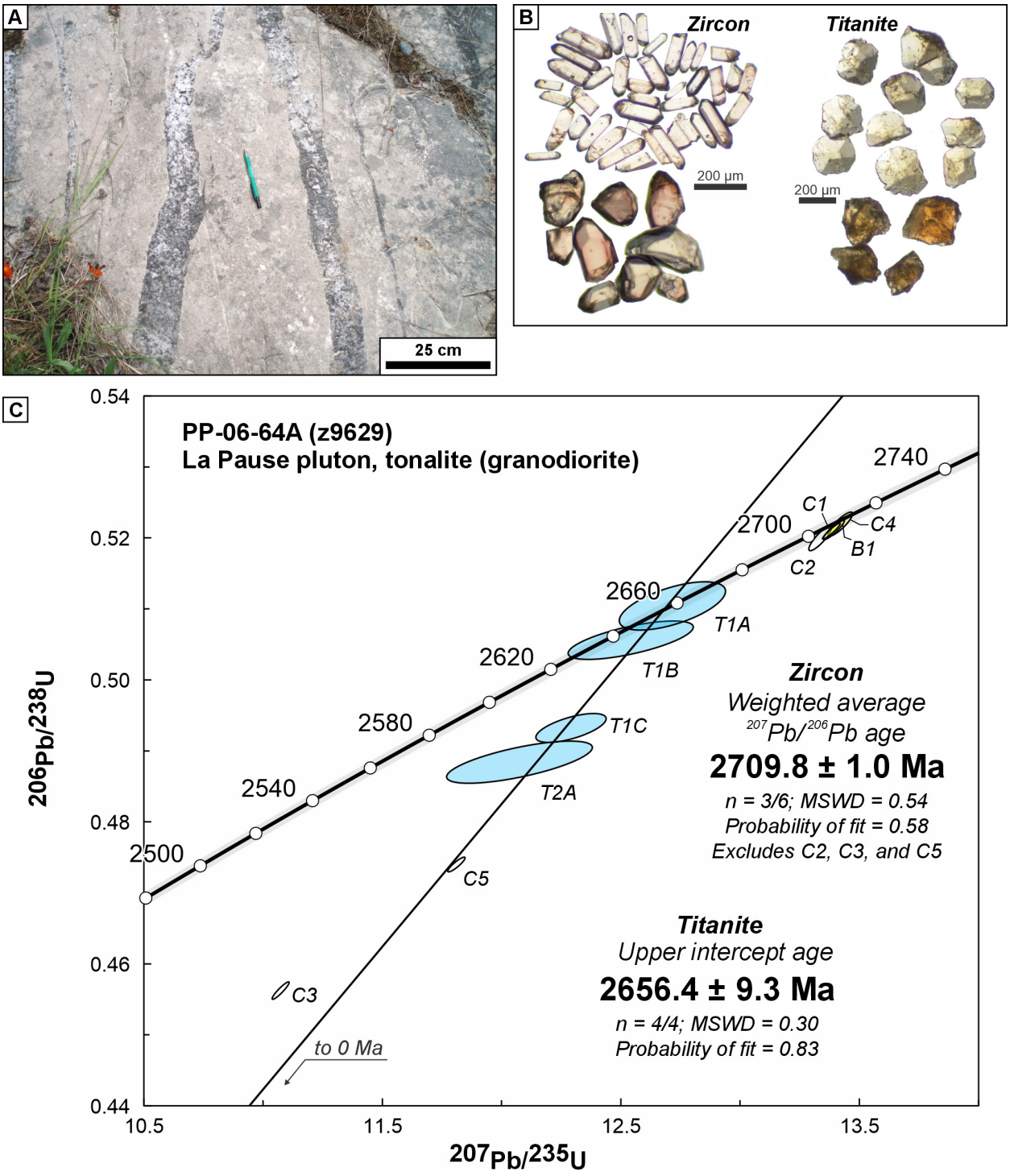


Figure 25. A. La Pause tonalite (granodiorite) cut by quartz veins, PP-06-64A sampling site. Photograph taken approximately 35 m SE of sampled outcrop by P. Pilote (MRNF), NRCan photo 2023-721. **B.** Transmitted light images of representative zircon and titanite from the sample. **C.** U-Pb concordia diagram for sample PP-06-64A. Uncertainties are plotted at the 95% confidence level. Coloured ellipses are included in age calculations.

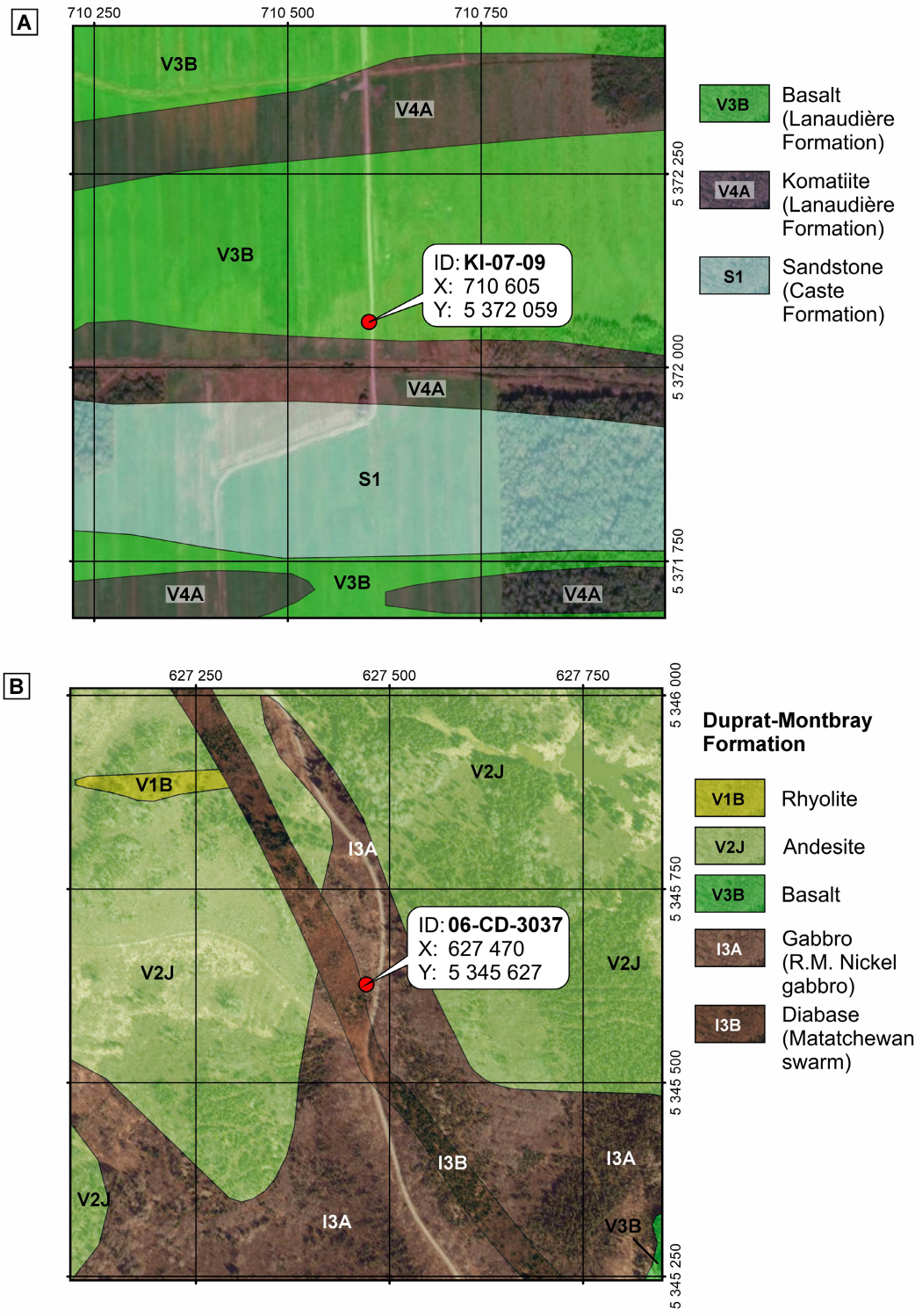


Figure 26. A. Location of Cartier Resources Inc. drill hole KI-07-09 collar. Sample KI-07-09 was taken at a depth of 140.5−186.5m along ddh KI-07-09 that is oriented to the South (N180°) dips -50° and intersects the dated S1 unit south of the volcanic rocks in which the drill hole is collared. UTM NAD83 Zone 17. Lithological map from SIGÉOM. **B.** Location of sample 06-CD-3037. UTM NAD83 Zone 17. Lithological map from SIGÉOM.

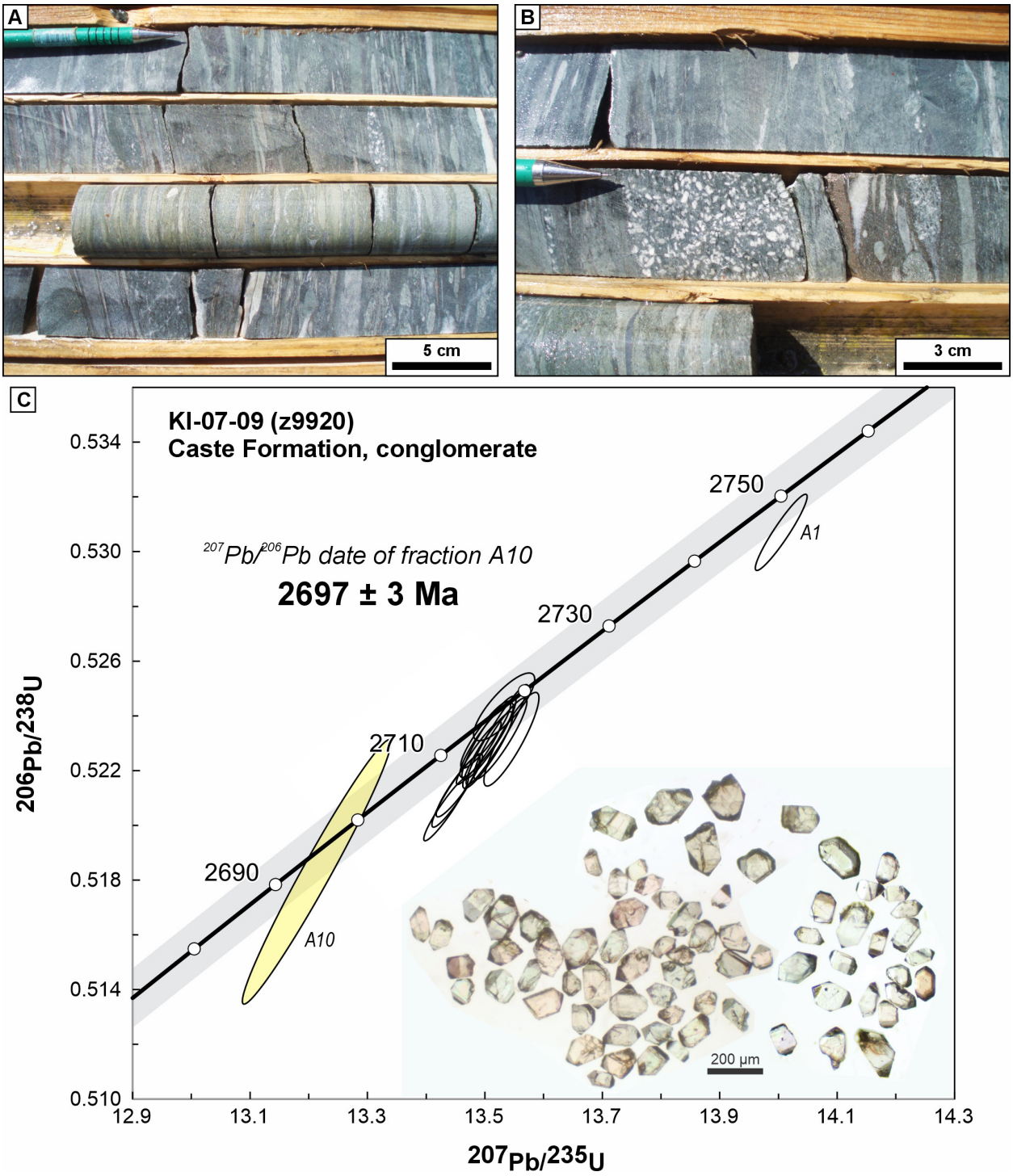


Figure 27. A. KI-07-09 sampling interval showing a moderately strained polygenic conglomerate. Photograph by P. Pilote (MRNF), NRCan photograph 2023-734. **B.** Close-up view of the sampled conglomerate with cm-scale clasts of intrusive and volcanic rocks, cut by a thin sulphide vein. Photograph by P. Pilote (MRNF), NRCan photograph 2023-735. **C.** U-Pb concordia diagram for sample KI-07-09. Uncertainties are plotted at the 95% confidence level. Coloured ellipse was used for the age calculation. Inset: transmitted light images of representative zircon from the sample for ID-TIMS analysis.

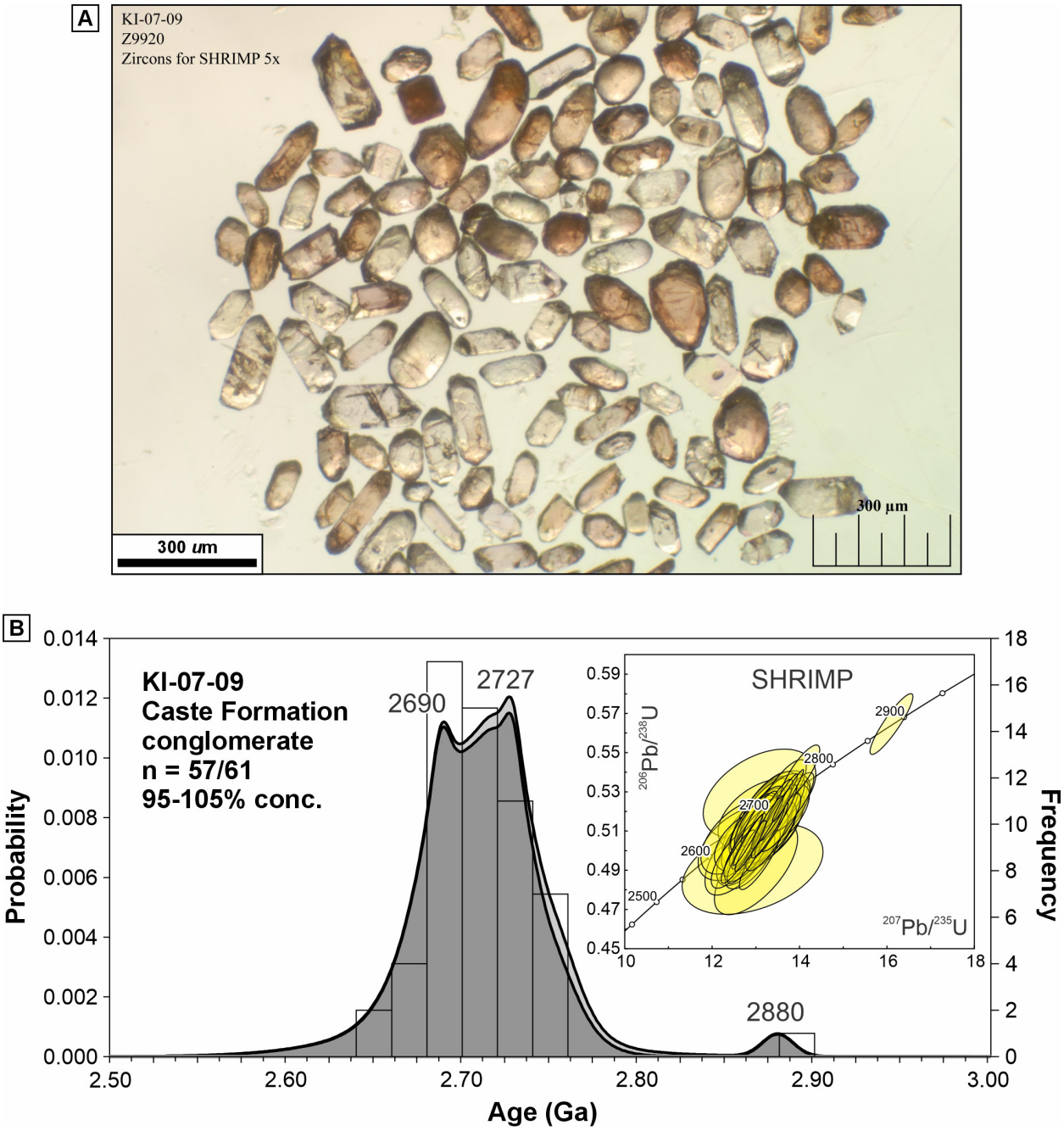


Figure 28. A. Transmitted light image of representative KI-07-09 zircons used for SHRIMP analysis. **B.** Probability density distribution diagram and histogram (20 Ma bins) of $^{207}Pb/^{206}Pb$ dates for SHRIMP spot analyses of detrital zircon from sample KI-07-09. Dark grey curve includes only data that fall within a ±5% concordance threshold, whereas the light grey curve incorporates all data. Inset shows the U-Pb concordia diagram with uncertainties plotted at the 95% confidence level.

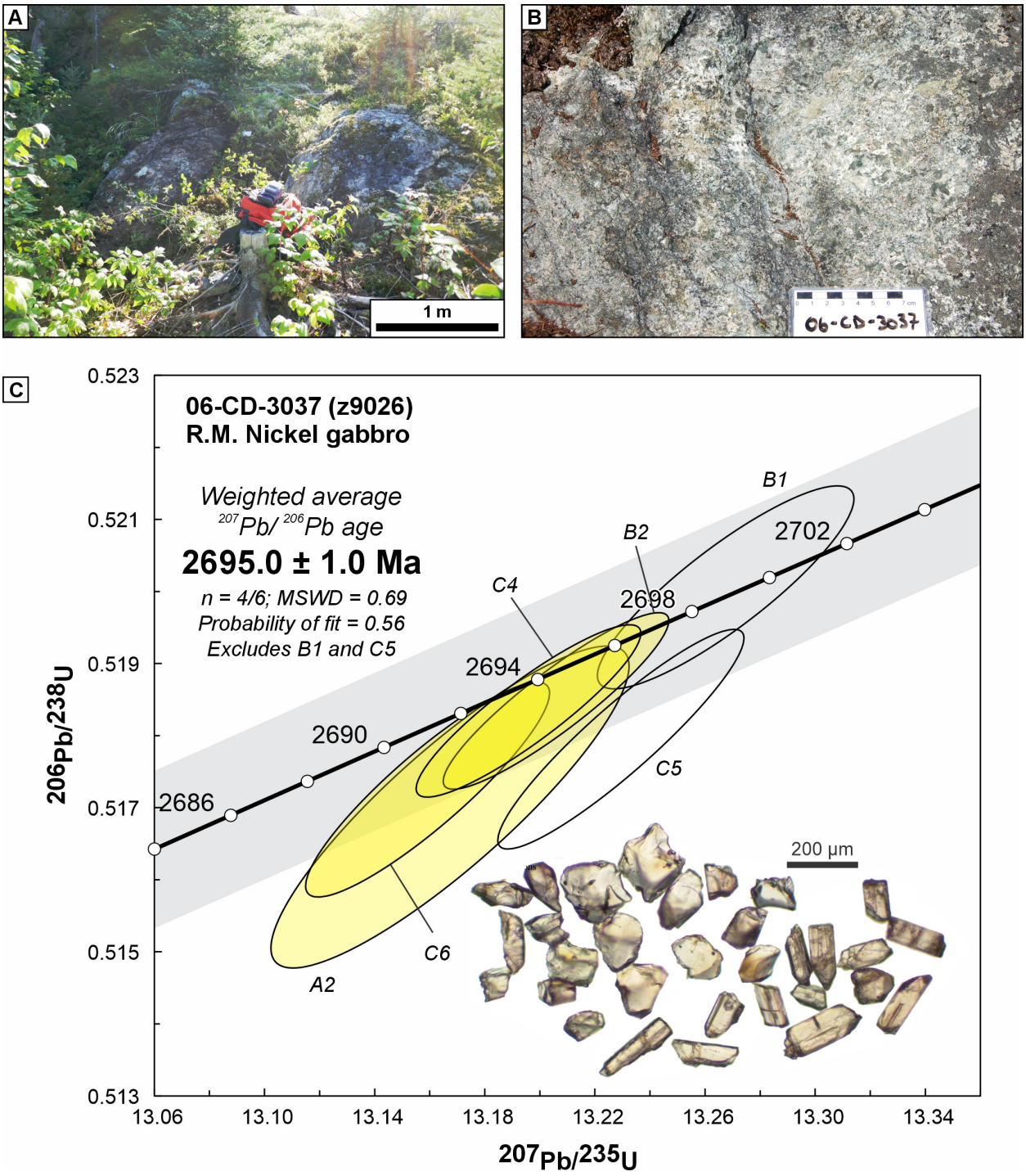


Figure 29. A. Sampling site for sample 06-CD-3037 (R.M. Nickel gabbro). Photograph by J. Goutier (MRNF), NRCan photo 2023-722. **B.** Close-up view of the R.M. Nickel gabbro on a slightly weathered surface. Photograph by J. Goutier (MRNF), NRCan photo 2023-723. **C.** U-Pb concordia diagram for sample 06-CD-3037. Uncertainties are plotted at the 95% confidence level. Coloured ellipses are included in age calculation. Inset: transmitted light image of representative zircon from the sample.

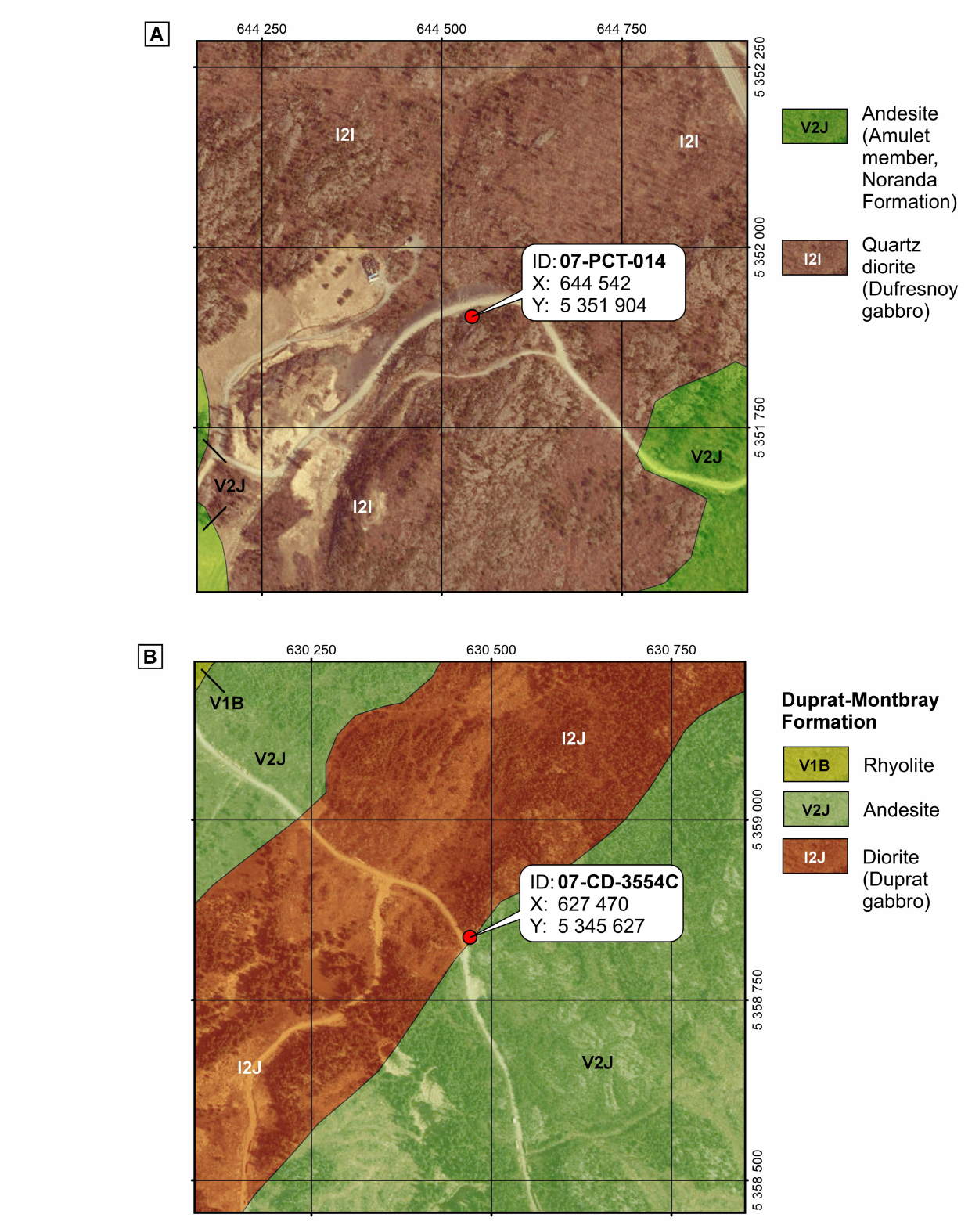


Figure 30. A. Location of sample 07-PCT-014. UTM NAD83 Zone 17. Lithological map from SIGÉOM. **B.** Location of sample 07-CD-3554C. UTM NAD83 Zone 17. Lithological maps from SIGÉOM.

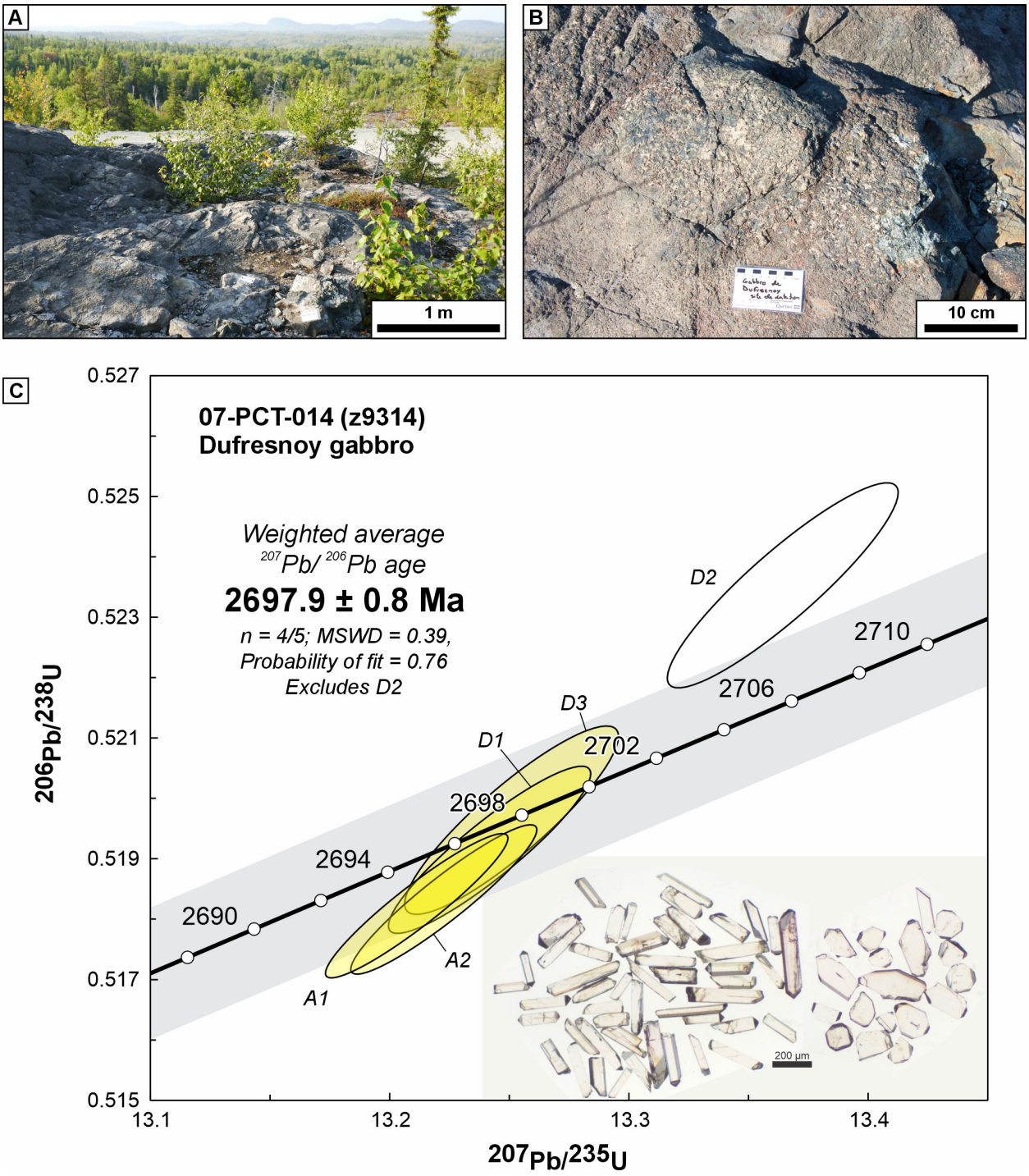


Figure 31. A. View of the sampling site for 07-PCT-014 (Dufresnoy gabbro). Photograph by J. Goutier (MRNF), NRCan photo 2023-724. **B.** Close-up view of the Dufresnoy gabbro on a slightly weathered surface. Photograph by J. Goutier (MRNF), NRCan photo 2023-725. **C.** U-Pb concordia diagram for sample 07-PCT-014. Uncertainties are plotted at the 95% confidence level. Coloured ellipses are included in age calculation. Inset: transmitted light image of representative zircon from the sample.

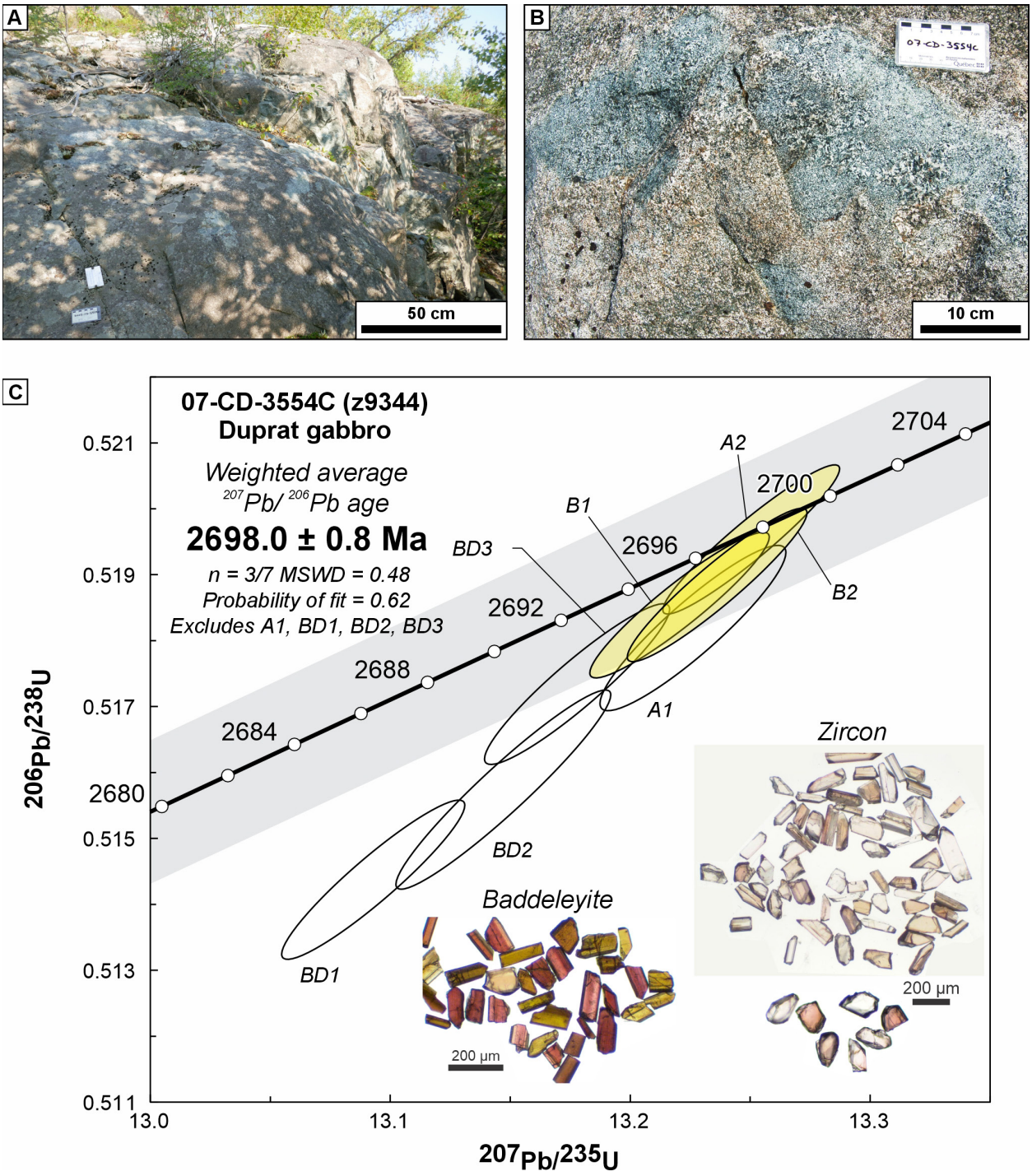


Figure 32. A. View of the sampling site for 07-CD-3554C (Duprat gabbro). Photograph by J. Goutier (MRNF), NRCan photo 2023-726. **B.** Close-up view of the Duprat gabbro on a slightly weathered surface. Photograph by J. Goutier (MRNF), NRCan photo 2023-727. **C.** U-Pb concordia diagram for sample 07-CD-3554C. Uncertainties are plotted at the 95% confidence level. Coloured ellipses are included in age calculation. Inset: transmitted light image of representative zircon and baddeleyite from the sample.

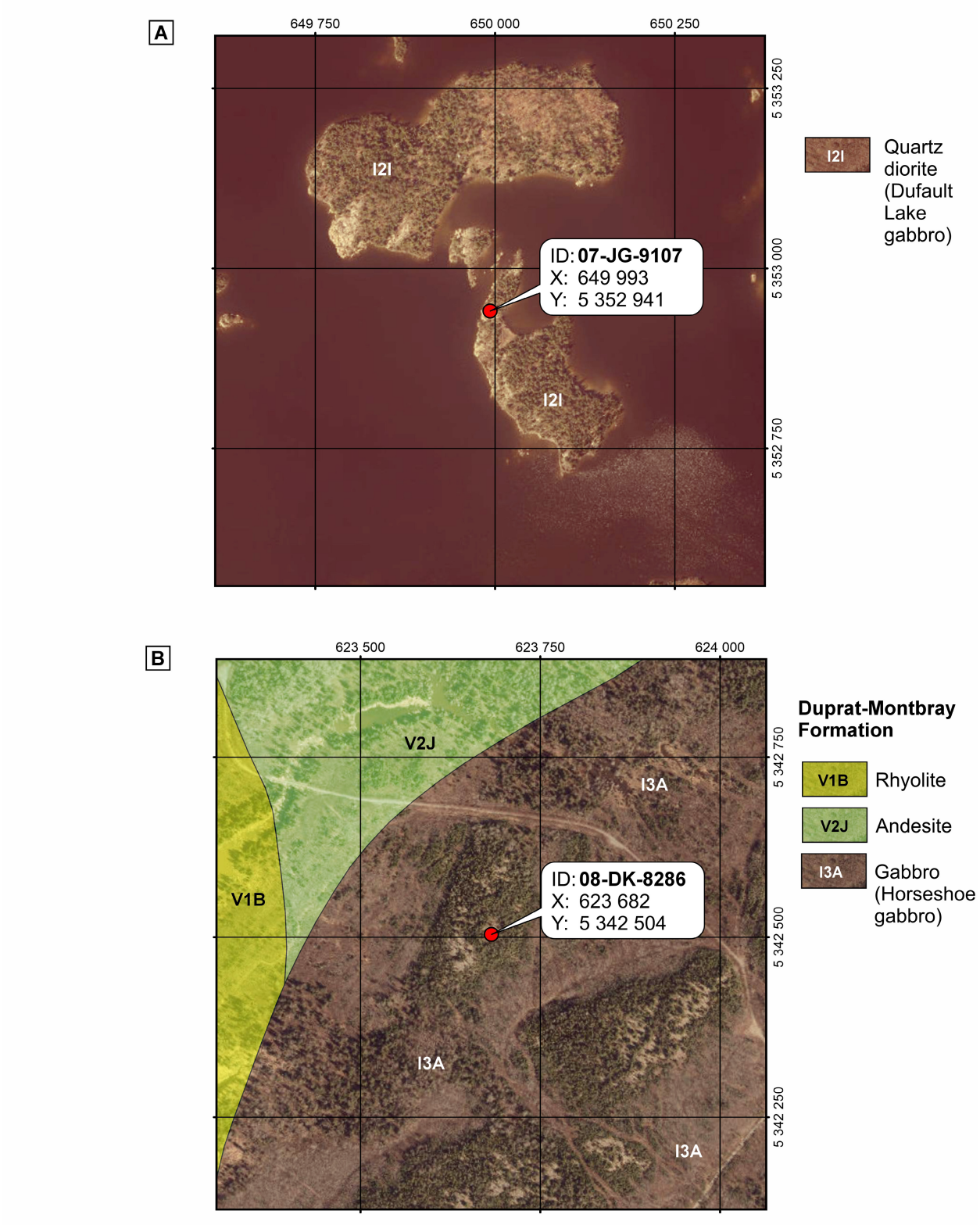


Figure 33. A. Location of sample 07-JG-9107. UTM NAD83 Zone 17. Lithological map from SIGÉOM. **B.** Location of sample 08-DK-8286. UTM NAD83 Zone 17. Lithological map from SIGÉOM.

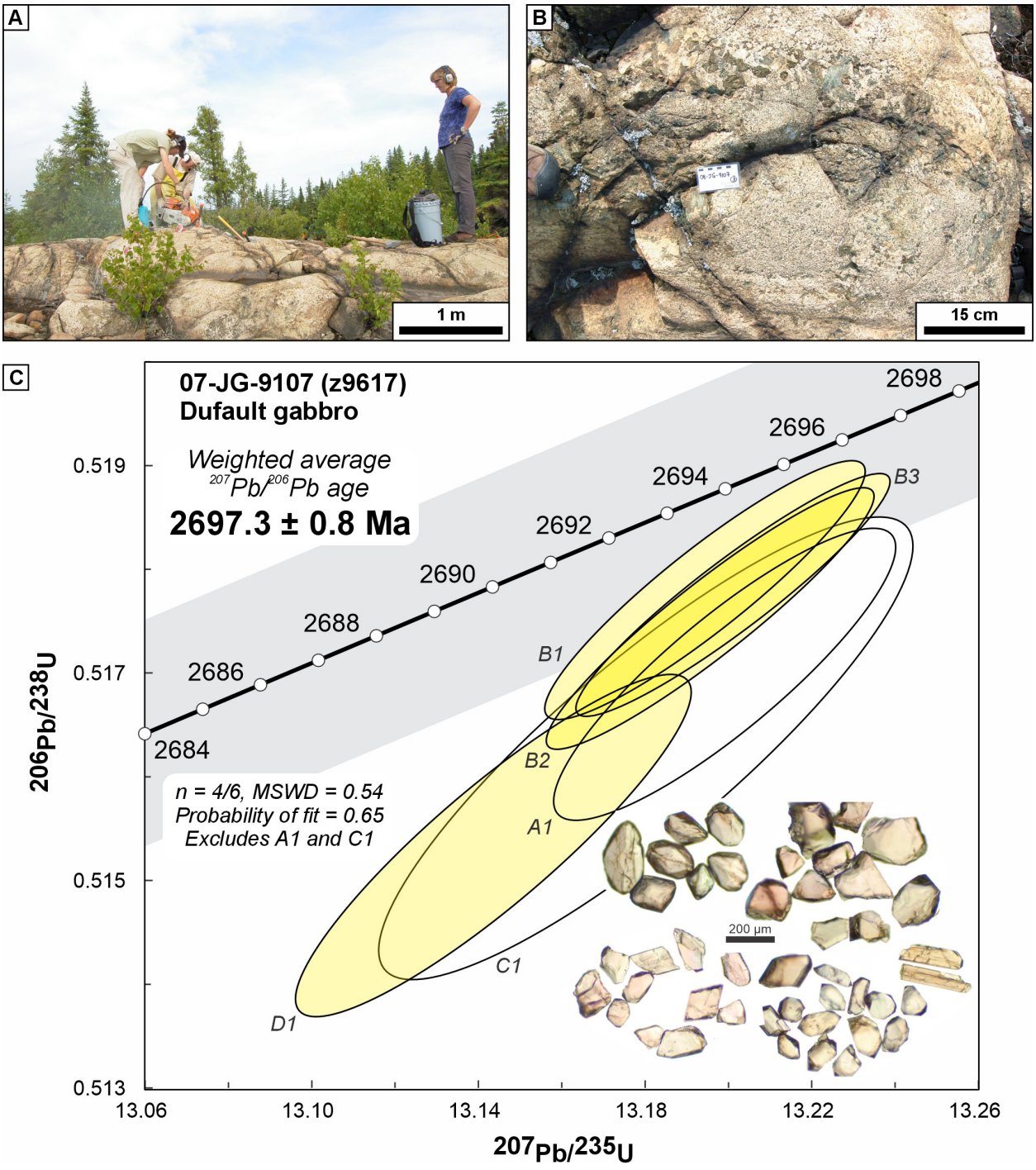


Figure 34. A. View of the sampling site for 07-JG-9107 (Dufault gabbro). Photograph by D. Kuiper, NRCan Photo 2023-728. **B.** Close-up view of the Dufault gabbro on a slightly weathered surface. Photograph by D. Kuiper, NRCan photo 2023-729. **C.** U-Pb concordia diagram for sample 07-JG-9107. Uncertainties are plotted at the 95% confidence level. Coloured ellipses are included in age calculation. Inset: transmitted light image of representative zircon from the sample.

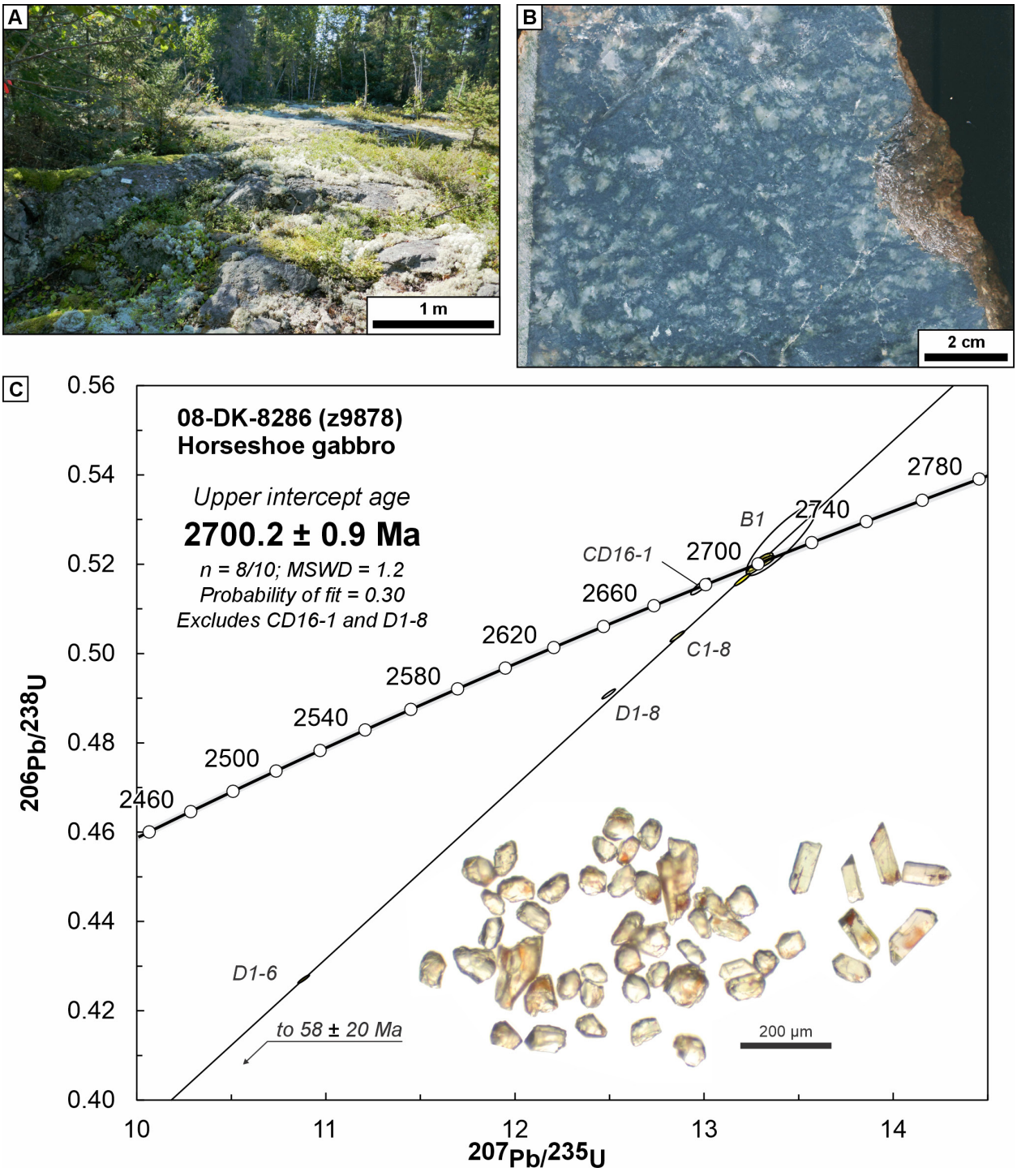


Figure 35. A. View of the sampling site for 08-DK-8286 (Horseshoe gabbro). Photograph by J. Goutier (MRNF), NRCan Photo 2023-730. **B.** Close-up view of a rock slab from the dated Horseshoe gabbro sample. Photograph by J. Goutier (MRNF) NRCan photo 2023-731. **C.** U-Pb concordia diagram for sample 08-DK-8286. Uncertainties are plotted at the 95% confidence level. Coloured ellipses are included in age calculation. Inset: transmitted light image of representative zircon from the sample.

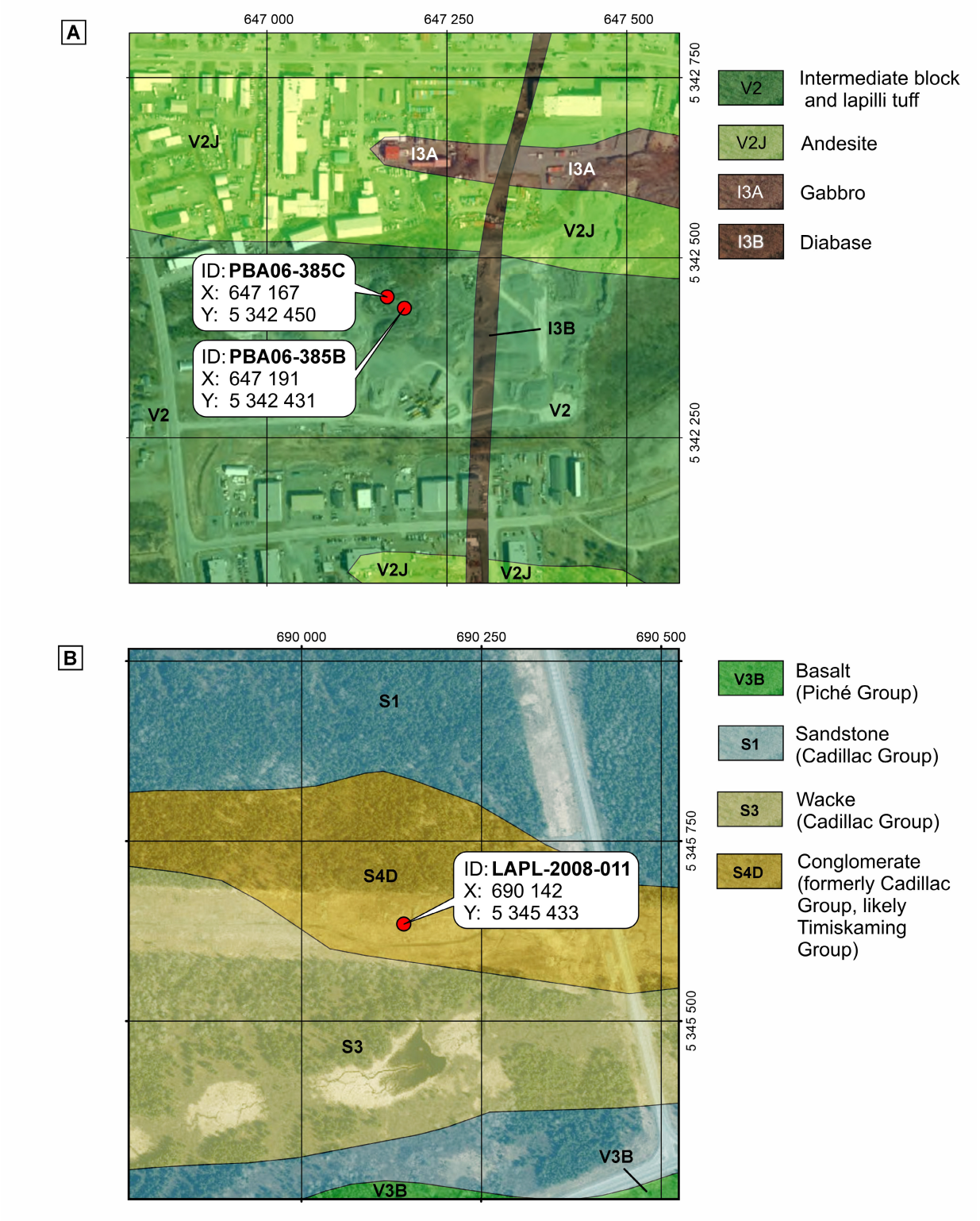


Figure 36. A. Location of sample PBA06-385B and -385C). UTM NAD83 Zone 17. Lithological map from SIGÉOM. **B.** Location of sample LAPL-2008-011. UTM NAD83 Zone 17. Lithological map from SIGÉOM.

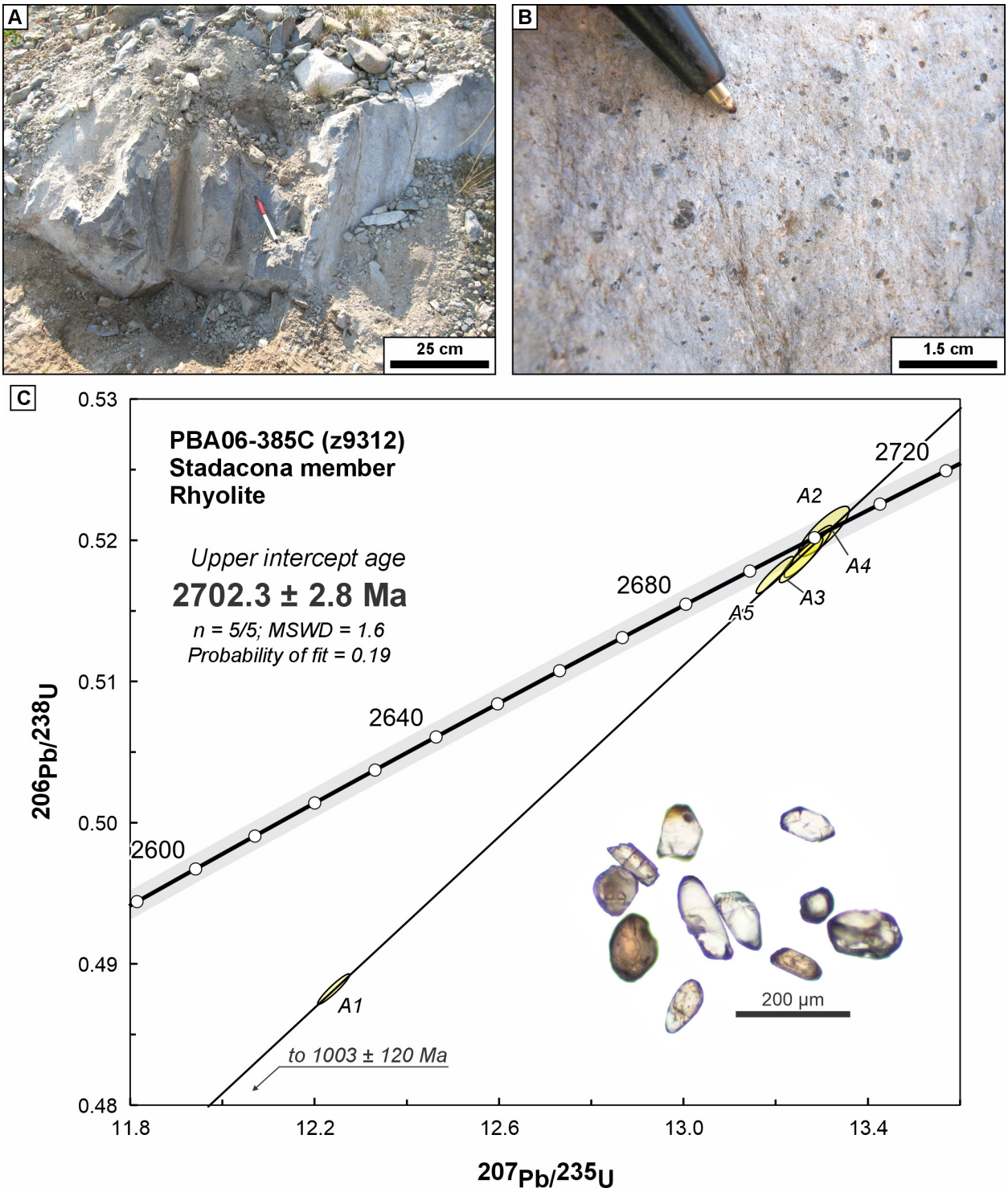


Figure 37. A. 06-PBA-385C rhyolite sampling site seen in section view perpendicular to the main foliation. Photograph NRCan 2025-002, taken by J. Percival. **B.** Close-up view of the rhyolite showing quartz and feldspar (plagioclase) microphenocrysts in a pale, fine-grained matrix. Photograph NRCan 2025-003, taken by J. Percival. **C.** U-Pb Concordia diagram for ID-TIMS results from sample PBA06-385C. Uncertainties are plotted at the 95% confidence level. Coloured ellipses are included in age calculation. Inset: Transmitted light image of representative zircon from the sample for ID-TIMS analysis.

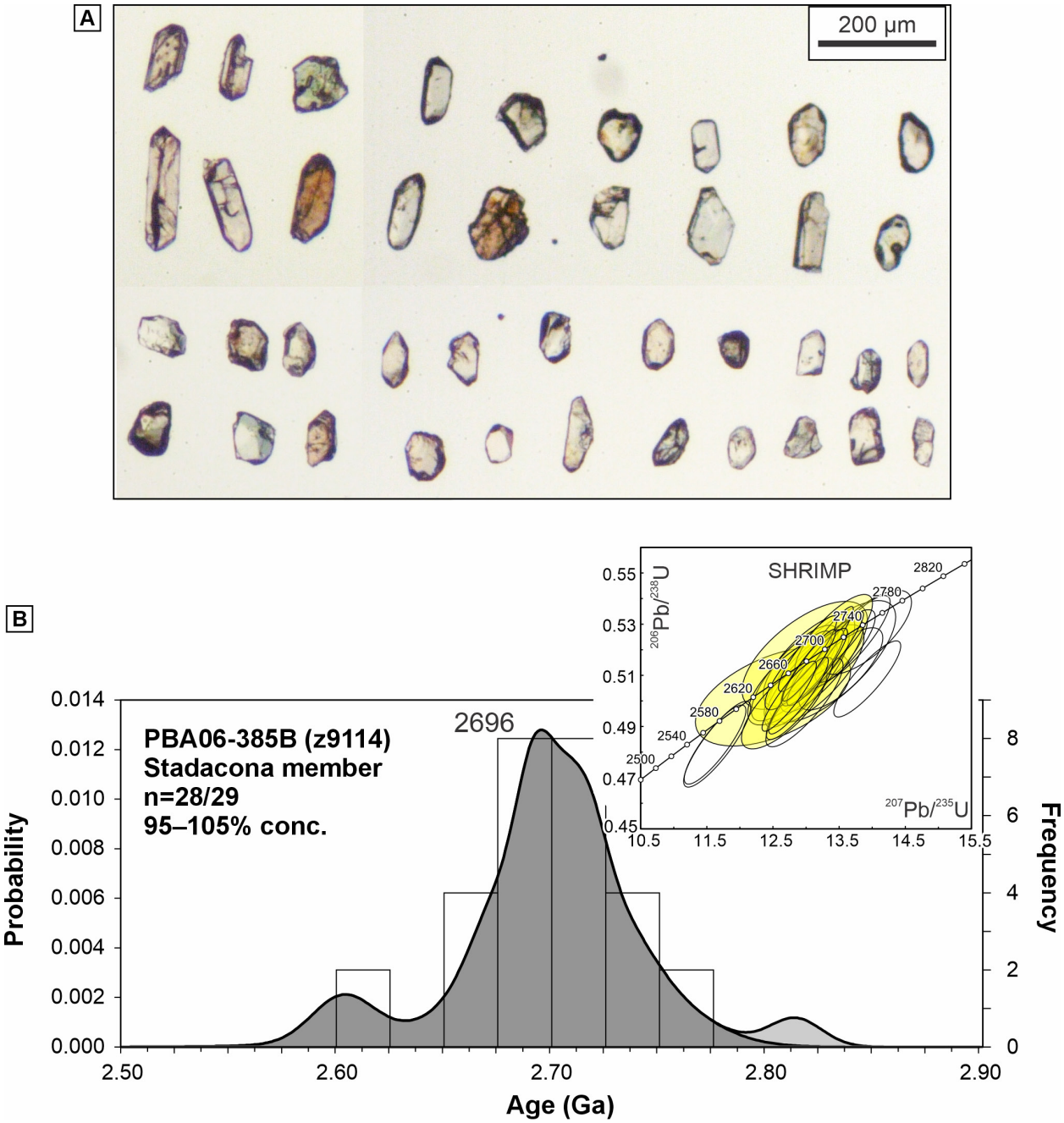


Figure 38. A. Transmitted light image of representative zircon from sample 06-PBA-385B used for SHRIMP analysis. **B.** Probability density distribution diagram and histogram (25 Ma bins) of $^{207}Pb/^{206}Pb$ dates for SHRIMP spot analyses of zircon from sample PBA06-385B. Dark grey curve includes only data that fall within a ±5% concordance threshold, whereas the light grey curve incorporates all data. Inset shows the U-Pb concordia diagram with uncertainties plotted at the 95% confidence level. Coloured ellipses are included in age calculation.

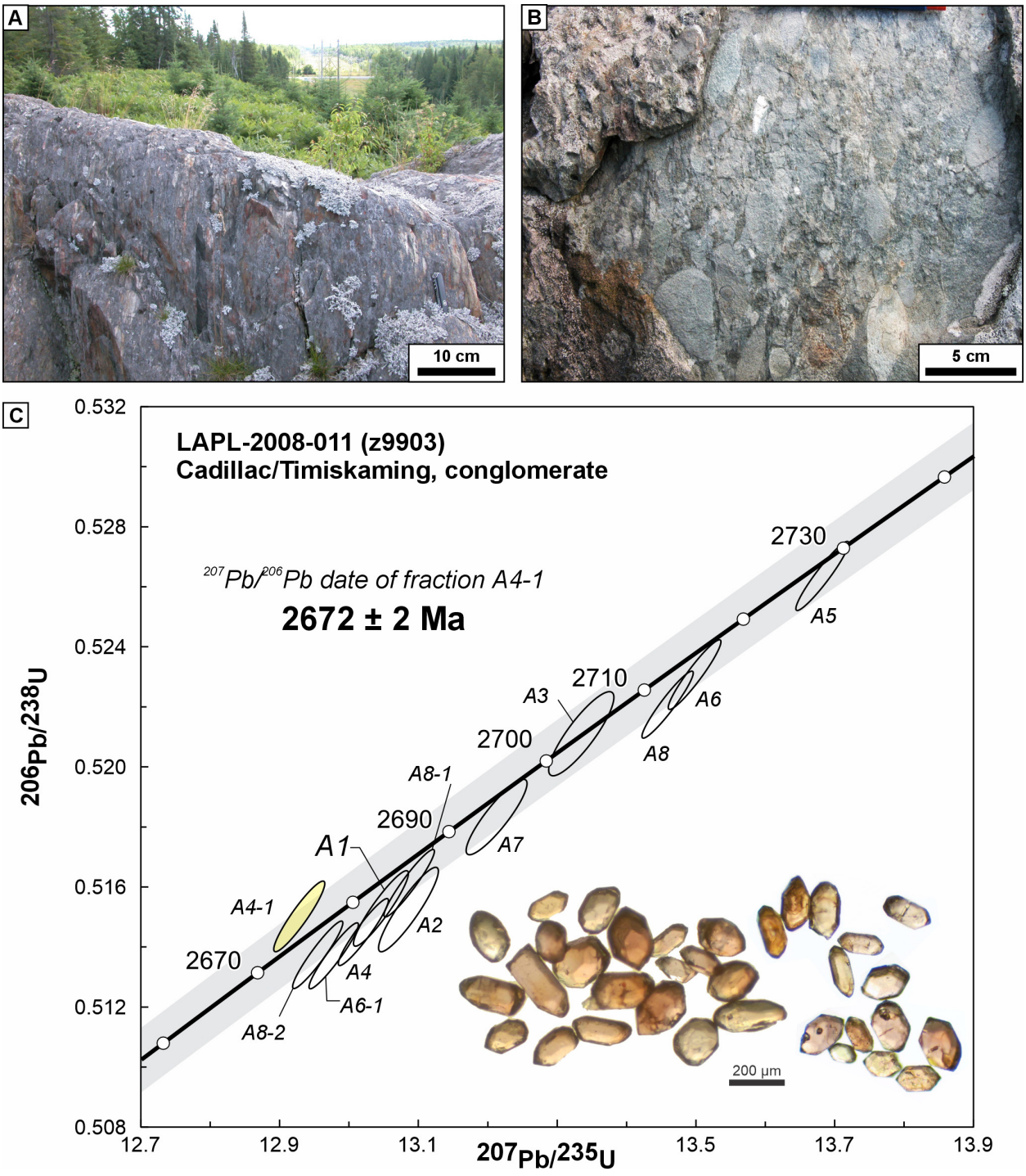


Figure 39. A. LAPL-2008-011 conglomerate sampling site seen in section view perpendicular to the main foliation, with abundant, strongly flattened clasts. Photograph NRCan 2023-732, taken by P. Mercier-Langevin. **B.** Plan view of the polymictic conglomerate in a slightly less foliated area showing well rounded clasts of contrasting texture and composition. Photograph NRCan 2023-733, taken by P. Mercier-Langevin. **C.** U-Pb concordia diagram for ID-TIMS results from sample LAPL-2008-011 (highly discordant analysis A2-1 not plotted; see text for further details). Uncertainties are plotted at the 95% confidence level. The coloured ellipse was used for the age calculation. Inset: Transmitted light image of representative zircon from the sample for ID-TIMS analysis.

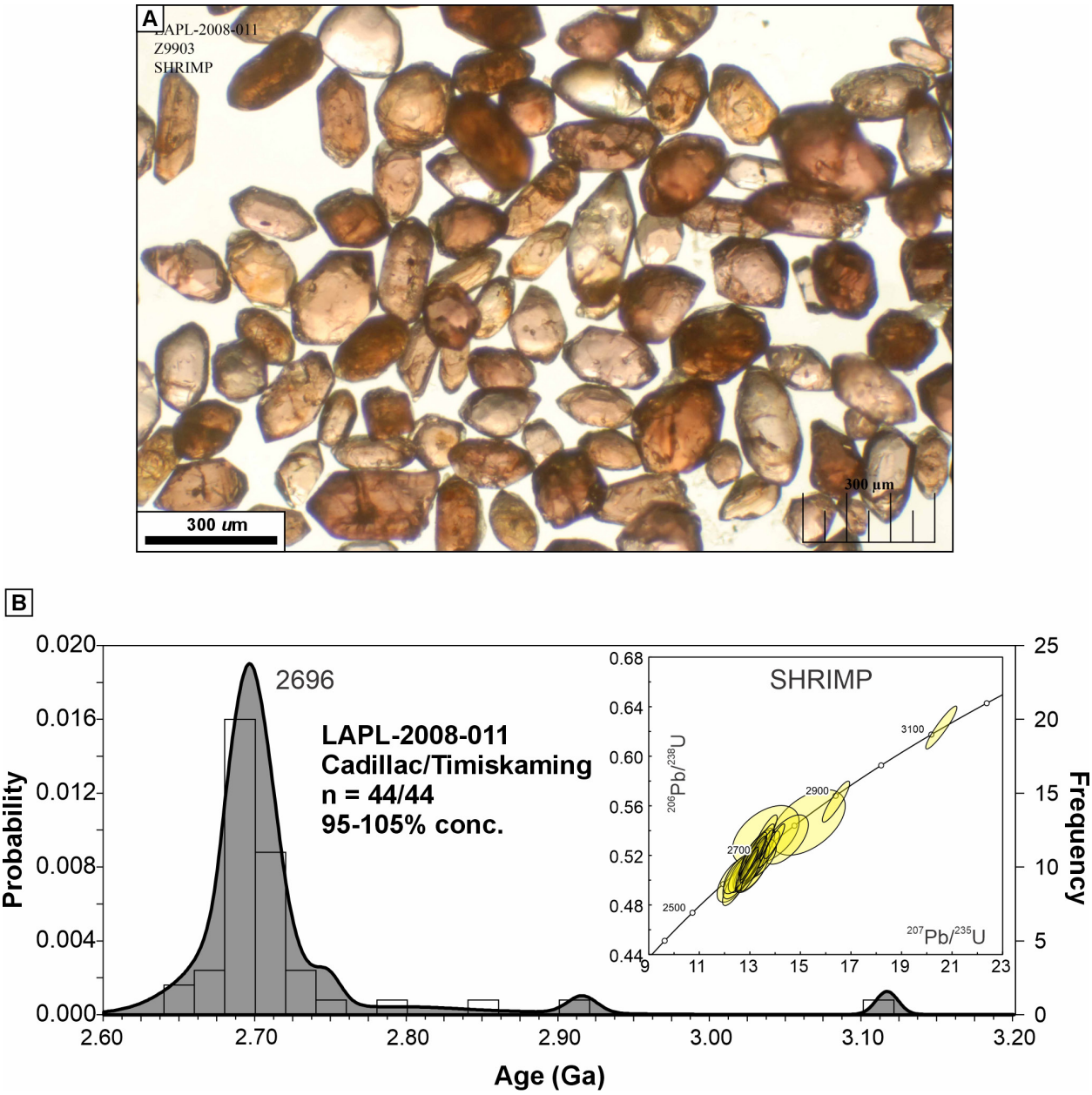


Figure 40. A. Transmitted light image of representative zircon from sample LAPL-2008-011 used for SHRIMP analysis. **B.** Probability density distribution diagram and histogram (20 Ma bins) of $^{207}Pb/^{206}Pb$ dates for SHRIMP spot analyses of detrital zircon from sample LAPL-2008-011. Inset shows the U-Pb concordia diagram with uncertainties plotted at the 95% confidence level.